



**GDAŃSK UNIVERSITY  
OF TECHNOLOGY**

Faculty of Electronics,  
Telecommunications and  
Informatics

Załącznik nr 1/2  
do Zarządzenia Rektora PG nr 5/2015 z 10 lutego 2015 r.



The author of the PhD dissertation: Paulina Listewnik  
Scientific discipline: Electronics

## **DOCTORAL DISSERTATION**

Title of PhD dissertation: Fiber-optic sensors based on microspheres with nanocoatings

Title of PhD dissertation (in Polish): Zastosowanie mikrosfer optycznych z cienkowarstwowymi powłokami w czujnikach światłowodowych

Supervisor
<i>signature</i>
Małgorzata Szczerska, PhD, DSc EE

Gdańsk, 2021



## STATEMENT

The author of the PhD dissertation: Paulina Listewnik

I, the undersigned, agree/~~do not agree~~\* that my PhD dissertation entitled:  
*Fiber-optic sensors based on microspheres with nanocoatings*  
may be used for scientific or didactic purposes.<sup>1</sup>

Gdańsk,.....

.....  
*signature of the PhD student*

Aware of criminal liability for violations of the Act of 4<sup>th</sup> February 1994 on Copyright and Related Rights (Journal of Laws 2006, No. 90, item 631) and disciplinary actions set out in the Law on Higher Education (Journal of Laws 2012, item 572 with later amendments),<sup>2</sup> as well as civil liability, I declare, that the submitted PhD dissertation is my own work.

I declare, that the submitted PhD dissertation is my own work performed under and in cooperation with the supervision of Małgorzata Szczerska, PhD, DSc EE.

This submitted PhD dissertation has never before been the basis of an official procedure associated with the awarding of a PhD degree.

All the information contained in the above thesis which is derived from written and electronic sources is documented in a list of relevant literature in accordance with art. 34 of the Copyright and Related Rights Act.

I confirm that this PhD dissertation is identical to the attached electronic version.

Gdańsk,.....

.....  
*signature of the PhD student*

I, the undersigned, agree/~~do not agree~~\* to include an electronic version of the above PhD dissertation in the open, institutional, digital repository of Gdańsk University of Technology, Pomeranian Digital Library, and for it to be submitted to the processes of verification and protection against misappropriation of authorship.

Gdańsk,.....

.....  
*signature of the PhD student*

\*) delete where appropriate.

---

<sup>1</sup> Decree of Rector of Gdansk University of Technology No. 34/2009 of 9<sup>th</sup> November 2009, TUG archive instruction addendum No. 8.

<sup>2</sup> Act of 27<sup>th</sup> July 2005, Law on Higher Education: Chapter 7, Criminal responsibility of PhD students, Article 226.

## ABSTRACT

Temperature is one of the most important physical quantities. Temperature measurements are used in every field of life, especially electronics, electrical engineering, energy-related fields, including energy source and storage devices. The goal of this dissertation is to design and optimize the microsphere-based fiber-optic sensors construction for measurement of the sensor surrounding medium temperature, including selection of the optical microsphere optimal geometrical parameters and selection of the parameters of the ZnO (zinc oxide) coatings deposited by Atomic Layer Deposition (ALD) method. A comprehensive state of the art about the significance of temperature measurements and measurement methods was performed as well. In the dissertation, the fabrication and the characterization of the designed sensors are described. Experimental results of the measurements validating a proper operation of the sensors are presented. Applications of the microsphere-based fiber-optic sensors, firstly as a device for *in situ* monitoring of the temperature of the supercapacitors and secondly for investigation of the optical and thermal properties of the few-layer black phosphorus coating was proposed.

## STRESZCZENIE

Temperatura jest jedną z najważniejszych wielkości fizycznych. Pomiary temperatury są wykonywane w każdej dziedzinie życia, zwłaszcza w elektronice, elektrotechnice, dziedzinach związanych z energią, w tym w źródłach energii i urządzeniach magazynujących. Celem rozprawy jest zaprojektowanie i optymalizacja konstrukcji mikrosfer światłowodowych do pomiaru temperatury otoczenia czujnika, w tym dobór optymalnych parametrów geometrycznych mikrosfery optycznej oraz selekcja parametrów warstwy ZnO (tlenek cynku) osadzonej metodą powłok atomowych (ALD – Atomic Layer Deposition). Dokonano również kompleksowego przeglądu stanu wiedzy na temat znaczenia pomiarów temperatury i metod pomiarowych. W rozprawie opisano wytwarzanie i charakterystykę zaprojektowanych czujników. Przedstawiono eksperymentalne wyniki pomiarów potwierdzające poprawność działania czujników. Zaproponowano przykładowe zastosowania czujników światłowodowych opartych na mikrosferach: jako urządzenie do monitorowania temperatury superkondensatorów *in situ*, a także do badania właściwości optycznych i termicznych kilkuwarstwowej powłoki z czarnego fosforu.



## TABLE OF CONTENTS

Abstract .....	3
Streszczenie .....	3
Table of contents.....	4
List of important symbols and abbreviations.....	5
1. Introduction, theses .....	7
2. Temperature measurement methods.....	11
3. Microsphere-based fiber-optic sensors .....	21
3.1. Fabrication of the microsphere-based fiber -optic sensor.....	25
4. Microsphere-based sensor for temperature measurements .....	30
4.1. Optical power analysis of the microsphere-based sensors.....	31
4.1.1. Microsphere-based sensor with a 200 nm coating .....	31
4.1.2. Microsphere-based sensor with a 100 nm coating .....	33
4.1.3. Comparison of the microsphere-based sensors with 200 nm and 100 nm coatings .....	34
4.2. Spectral shift analysis of microsphere-based sensor .....	37
4.2.2. Comparison between a optical power and a spectral shift analysis of a temperature sensor with 100 nm ZnO ALD coating. ....	38
5. Applications.....	40
5.1. <i>In situ</i> supercapacitor temperature monitoring.....	42
5.2. Measurement method of optical and thermal properties of nanomaterials .....	47
6. Discussion.....	50
7. Conclusions.....	54
8. List of published papers .....	57
References.....	59



## LIST OF IMPORTANT SYMBOLS AND ABBREVIATIONS

ZnO	–	Zinc Oxide
ALD	–	Atomic Layer Deposition
RTD	–	Resistive Temperature Detector
SLD	–	Superluminescent Diode
OSA	–	Optical Spectrum Analyzer
$\partial\phi, \Delta\phi$	–	phase difference
$\partial T, \Delta T$	–	temperature difference
$\lambda$	–	wavelength
L	–	cavity length
$\beta$	–	normalized propagation constant
$\alpha$	–	thermal expansion coefficient
$\partial n$	–	refractive index difference
$\Delta L$	–	cavity length difference
P	–	optical power
$S(\nu)$	–	spectral distribution of the light source
n	–	refractive index
SEM	–	Scanning Electron Microscopy
STED	–	Stimulated Emission Depletion microscopy
S	–	sensitivity
$\Delta P$	–	optical power of the reflected signal difference
$U_{\text{sensitivity}}$	–	sensitivity error
$S_{\text{theor}}$	–	theoretical fitting sensitivity
$U_{\text{linearity}}$	–	linearity error
P	–	optical power of the reflected signal
$P_{\text{theor}}$	–	theoretical fitting optical power
$\delta$	–	approximation error
$U_M$	–	obtained data
$U_R$	–	linear fit

- RIU – Refractive Index Unit
- NDS – Nanocrystalline Diamond Sheet
- FLBP – Few-Layer Black Phosphorus

## 1. INTRODUCTION, THESES

Temperature is one of the most important physical quantities. Temperature measurements are used in every field of life, especially electronics [1], electrical engineering [2], energy related fields [3], including energy source and storage devices.

In electronics, monitoring of the temperature is used to determine the thermal stability of the substrate, which can cause deformation and disturb the conductivity of the circuit [4]. It also applies during manufacturing of the microelectronic devices. As shown by Schmitz [5] and Mitic *et al.* [6], the deposition temperature of microchips thin films is an important aspect, which can negatively influence surrounding layers, when it is improperly chosen and change parameters of the device as well as affect the bonding of the circuits.

Moreover, temperature monitoring and thermal cycling are great ways to bias test either blocks of device, devices or even entire systems. By submitting the device to the extreme temperatures in the environmental chamber, in which the conditions can be strictly controlled, faulty components, design deficiencies, improperly mounted elements and cooling inefficiencies can be found, before implementation of the device [7]. One of the examples of using such chamber is presented in [8], where it was applied to evaluate the proper operation of the fabricated device.

Temperature monitoring is also crucial during the soldering and bonding of electronic elements. The temperature has to be appropriately selected to the size and the material of the soldered object. If it is too high, there is a danger of damaging the element or the substrate, if the temperature is too low, the bond can be faulty – either too weak or its conductive parameters become impaired. The study on degradation of wire bonded contacts depending on temperature is demonstrated by Rongen *et al.* in [9]. An example of insulated gate bipolar transistor degradation depending on temperature is shown by Dagrenne *et al.* [10]. Furthermore, examination of heating of wires and cables may provide information, which in turn improve the safety of the systems and their operators. Increased temperature of the wire may indicate an improper connection, incorrectly selected diameter or density, as well as ill-suited settings of electrical parameters, such as conductivity. Lu *et al.* [11] demonstrate monitoring of the temperature distribution during high frequency induction heating of the titanium wire.

Temperature measurement is of particular importance in energy source and storage devices, e.g., supercapacitors [12] and batteries [13]. By observation of the internal temperature of the devices, it is possible to gather knowledge of their internal processes occurring over cycle states during repeat charging and discharging [14], as well as the behavior of the components, of which

the devices are made off. Depending on the construction, the device may be composed of various types of electrolyte, each able to operate within a different temperature range [15]. It can be observed in electrode materials and storage mechanisms. In case of an electrolyte, exceeding the temperature limit can cause crystallization of the electrolyte and electrochemical processes disturbance, which leads to damaging and rupturing of the device [16]. Accumulation of the heat on the electrodes may cause degradation of the material, which in turn affects electrolyte. In each case, the consequences of overheated device influence charging and discharging cycles and accelerate its aging [13].

Deviation of the baseline temperature can provide information about defective devices [17], which can lead to a better understanding of their operation, which in turn translates to the possibility of improvement of the technology. Temperature monitoring allows to take steps necessary to cease the function of the devices, in cases when their internal temperature exceeds the critical limit of operation. A situation like that can potentially lead to damaging of the device, melting of elements, starting a fire or explosion. Preventive actions, such as optimization of operating conditions results in the increased safety of the operators as well as equipment, extended lifetime of the devices and reduced costs of operation.

In this work the research related to microsphere-based fiber-optic sensors with a zinc oxide (ZnO) coating applied using Atomic Layer Deposition (ALD) method is described. The design of the sensors, the fabrication process, their modification and its influence on the metrological parameters of the sensor are included in the dissertation. The main research and engineering tasks that have been established in this work consist of the following steps:

- design and optimization of the microsphere-based fiber-optic sensors construction for measurement of the temperature of the sensor surrounding medium:
  - selection of the optical microsphere optimal geometrical parameters,
  - selection of the parameters of the ZnO coatings deposited by ALD method;
- fabrication and characterization of the fiber-optic sensors integrating of the optical microsphere with ZnO ALD coatings,
- application of the designed sensors with modified parameters of microsphere geometry and coating for measurements of the temperature.

Based on the extensive theoretical analysis and preliminary experimental results, it has been assumed that application of the ZnO ALD coating of optimal parameters, on the surface of an optical

microsphere would allow to create an intensity-modulated fiber-optic sensor for measurement of the temperature. Simultaneously, the microsphere would make monitoring of sensor structure integrity possible.

Consequently, the following theses have been formulated:

- T1: Deposition of the nanocoatings on the surface of an optical microsphere integrated with a fiber-optic sensor allows to perform temperature measurements.
- T2: Application of optical microspheres of a certain geometry, allows to identify the damage sustained by the sensor during measurement execution.

In order to verify theses, considerable research and engineering tasks have been executed. Performed tasks included, among others, the development and optimization of the microsphere-based sensors with ALD ZnO coating, the establishment of the research methods and instruments, analysis and interpretation of obtained data. Acquired results were presented in 6 publications in international journals (5 in JCR) – in 4 of them as a first author – and during scientific conferences.

In chapter 1, the significance of the temperature measurements in electronics, electric and energy related fields as well as the dissertation goals and theses are presented. In chapter 2 temperature measurement methods are described, including comprehensive literature review in regard of fiber-optic and non-fiber-optic temperature sensing. Presented methods are accompanied by examples of their utilization. Methods of optimization of the fiber-optic sensors are also demonstrated in this chapter.

In chapter 3 the design, fabrication and characterization of the intensity-modulated microsphere-based fiber-optic sensors are described. The principle of the operation of the sensor is presented as well as the general experimental setup, used to validate the proper functioning of the sensors. The chapter also discusses challenges the author encountered during the fabrication of the optical microspheres. In the following chapter results of the preliminary research of temperature measurements using microsphere-based sensors with ZnO ALD with both optical power and spectral shift analysis are shown (chapter 4). In chapter 5, applications of the designed microsphere-based sensors are presented. Firstly, as an *in situ* device for temperature monitoring of the supercapacitors. Secondly, as a method for measurement of optical and thermal properties of nanomaterials.

Towards the end of the dissertation, in chapter 6, a discussion about the metrological parameters of the temperature sensors is presented. A comparative study of the designed

microsphere-based fiber-optic sensors with the temperature sensors presented during the last few years in the literature is also included.

The dissertation is concluded in chapter 7, followed by the list of published papers, which are the most related to the discussed research (chapter 8) and the list of references cited in this work.

## 2. TEMPERATURE MEASUREMENT METHODS

Given the significance of temperature monitoring, there are many methods for its measurement, each designed to best serve investigated subject. Based on their principle of operation, several basic types of devices can be listed.

Thermocouples are the type of temperature measuring devices, which provide mean temperature measurement at the point of their contact with a measured object. The changes in temperature are indicated by the changes in voltage [18]. Therefore, they should not be used in environments sensitive to electric surges. Moreover, thermocouples are highly sensitive to the changes in temperature and have to be completely immersed in the measured medium, otherwise, environmental factors have a substantial influence on the measurement results, increasing their uncertainties [19]. The miniaturization trend causes the technology of the devices to be constantly improved. Several new solutions in recent years allowed the development of the thermocouple fabricated from thin films, screen printed silver-nickel thermocouple [20], micro-thermocouple [21]. In the paper [22], Tang *et al.* describe a real-time measurement of the proton exchange membrane fuel cell with a thermocouple repeatability of about 4% and high linearity,  $R^2$  of 0.99.

Resistive Temperature Detector (RTDs) is another contact type sensor, which principle of operation is based on the Seebeck effect [23]. This device shows the shift in temperature based on resistance changes [24]. Whereas in thermocouples, the dependence of temperature on measured parameters variation is not specified, the dependence in RTDs is linear [25]. Hence, the RTDs are characterized by high linearity and stability. And while those devices can also operate in a wide temperature range, their production cost is higher, and the response time is slower than that of a thermocouple. Even so, during recent years, RTDs found application as a diagnostic tool, providing solutions to challenging tasks. The authors [26] explain the role of RTD to deal with obstacles during the melting of metals. The utilized meter was operating up to 640°C. Furthermore, Jemaa *et al.* present the application of the RTD sensor chip for maintaining thermal uniformity during thermocompression bonding process [27].

Infrared sensors are contactless devices, which detect infrared radiation of the object [17]. The accuracy of this method is dependent on numerous factors, like the distance of the device from the investigated object or atmospheric conditions, including humidity. At times it is advantageous to perform measurements without having to embed the sensor in the measured medium. Infrared sensing provides the results gathered at the surface of the object, so the accuracy can substantially deviate from the element contained underneath it. Additionally, the material of which the surface

is made of can influence the measurement. Current research related to infrared temperature measurements focuses mostly on improvements of device parameters by modifying the algorithms responsible for data processing [28], or their optimization to reduce manufacturing costs [29] and allowing for easier and wider availability [30]. Infrared thermography can be used, among others, for medical applications, for example to detect an illness based on abnormal body temperature [31].

Among all the methods of temperature measurement, fiber-optic sensing techniques are especially worth mentioning. Fiber-optic sensors are optoelectronics devices, which because of their advantages, such as: small size, compact construction, resistance to external influences, i.e., electromagnetic interference [32], are constantly developed and redesigned. They are used for measurements of various physical quantities, such as: temperature [33], pressure [34], vibration [35]. Furthermore, their structure allows to use them in places, in which common electric sensors cannot be inset, e.g.: remote [36] and hard to access locations, hazardous, potentially explosive areas (ATEX directives) [37], places endangered by fire, severe climatic and corrosive conditions [38].

In general, fiber-optic temperature sensors may be divided into few categories: point, quasi-distributed, distributed sensors [39,40]. Classification of the sensors based on sensing area distribution is presented in Figure 2.1.

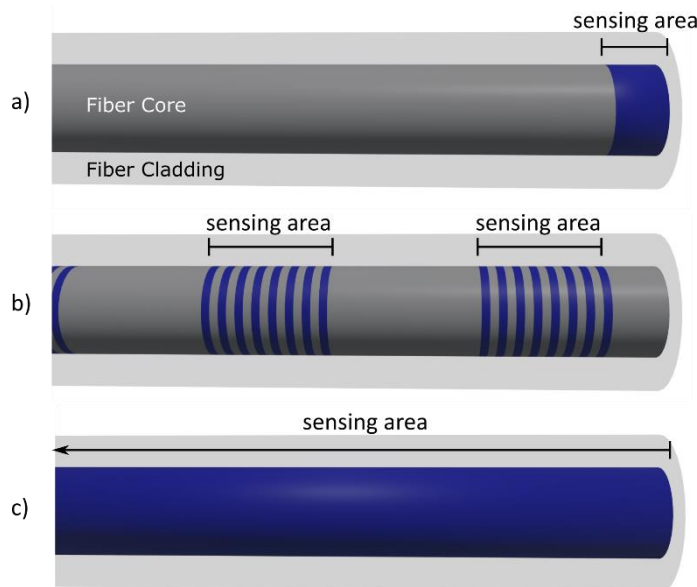


Figure 2.1. Classification of the fiber-optic sensors according to the distribution of sensing area, where: a) point sensor, b) quasi-distributed sensor, c) distributed sensor.

Quasi-distributed sensors are mostly based on the Fiber Bragg Gratings [41,42]. The grating pattern, of a different refractive index than the rest of the core, is embedded into the fiber. During the measurements, incident light propagates through the grating, part of the spectrum (Bragg





wavelength) is reflected back and the rest is transmitted. Increased temperature affects the structure of the fiber, causing alterations in the interface of core-grating, therefore providing information about changing temperature, by observing a shift in the Bragg wavelength. The principle of operation of the Fiber Bragg Grating sensor is presented in Figure 2.2.

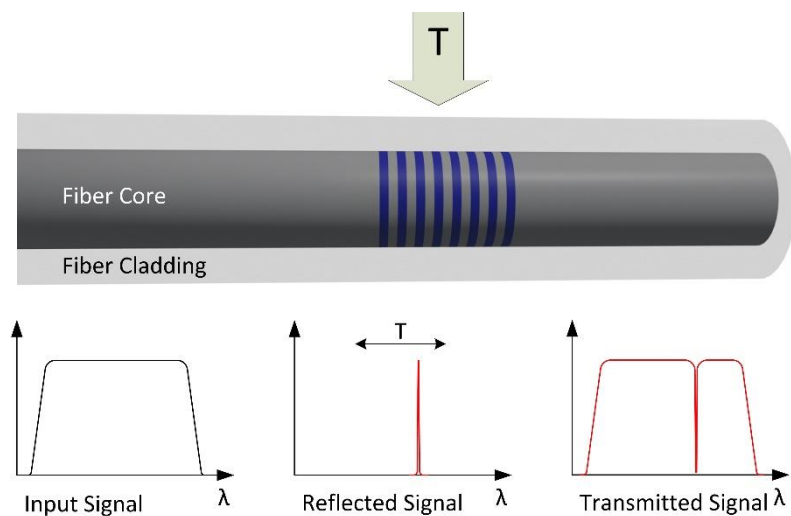


Figure 2.2. Principle of operation of the Fiber Bragg Gratings sensors, where:  $T$  – temperature.

The grating can be imprinted multiple times over the entire length of the fiber, which is a basis of quasi-distributed sensing [43]. Fiber Bragg gratings can also be used for simultaneous measurement of multiple parameters, such as: temperature and strain, as it is presented by Gao *et al.* [44], They demonstrated the capabilities of such sensor, using different sensitivities for each parameter. Fiber Bragg grating temperature sensors can be used in a variety of applications via additional modifications, including deposition of a coating, which provides a protective layer for the Bragg grating; altered structure of the fiber or packaging preventing or delaying the occurrence of unwanted phenomena [45–47]. Not all quasi-distributed sensors are constructed from Fiber Bragg Gratings. Kim *et al.* propose using a V-grooved single-mode fiber along with optical time domain reflectometry [48]. Quasi-distributed sensors are used for instance, for down-hole monitoring. Zhou *et al.* [49] present a sensor with a resolution of 0.06% and long-term stability of 0.11%.

The principle of operation of the distributed sensors is based on the scattering phenomena and allows to simultaneously measure the continuous temperature profile along utilized fiber [50]. Part of the incident light, which propagates through an optical fiber, is absorbed and reemitted in directions varying from the one of incident radiation. The change of direction is accompanied by the change of wavelength. Depending on the wavelength of the scattered light, three types of scattering can be noted: Raman Scattering, Brillouin Scattering and Rayleigh Backscattering.



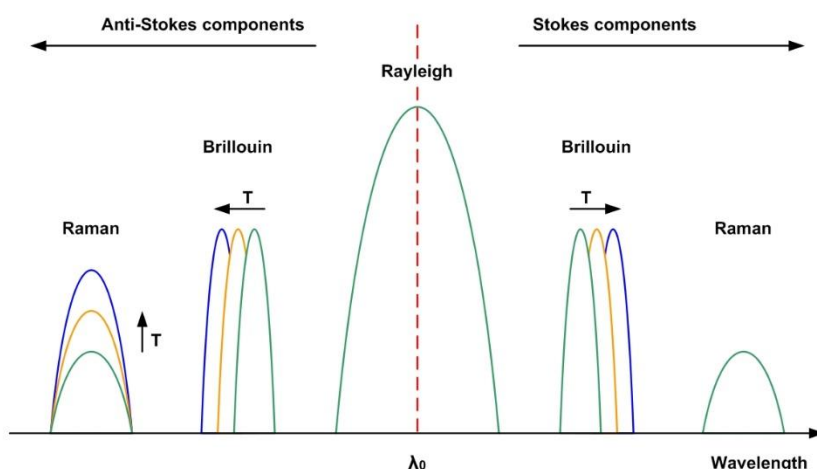


Figure 2.3. Light scattering spectrum during distributed temperature sensing.

The reasons behind Raman scattering are rotational and vibrational molecular transitions based on the energy states of photons. The light is scattered at wavelengths higher and lower (called Stokes and Anti-Stokes components, respectively) than the original one and they occur symmetrically on both sides of a central wavelength, which is presented Figure 2.3. In case of Raman scattering, during the temperature measurement, the lower wavelengths serve as a direct sensing mechanism. While the position of the peak is constant, the amplitude changes with the temperature, whereas the higher wavelengths remain unaffected [51,52]. Calculation of the ratio of Stokes to Anti-Stokes components allows to determine the local temperature of the measured medium. Distributed Raman Temperature Sensors [53] are used for long-distance measurements, especially civil engineering structures and industrial facilities [54–56], for example, tunnel fire detection as it is presented by Yan *et al.* [57]. The authors used distributed Raman Temperature Sensor for monitoring of the tunnel temperature at a distance of about 18 km. In the paper, a method for improvement of the sensor accuracy from 7°C to 1.9°C is also presented.

Brillouin scattering also appears in the form of the symmetrical peaks on both sides of the original wavelength, but their location is relative and acts as a sensing mechanism. Wavelength shift directly correlates to the temperature change. It is caused by the vibration excitation of a lattice of atoms. Similarly to distributed Raman temperature sensors, Brillouin Distributed Temperature Sensors are utilized for a long-distance applications. In [58], the author reviews current advancements in the distributed Brillouin sensing techniques and improvements upon spatial resolution of a conventional method – 2 m at the end of 100 km sensing fiber. Various designs are used for enhanced temperature sensing. Rossi *et al.* [59] present utilization of Brillouin ring laser to



decrease relative intensity noise, therefore improving temperature resolution up to 5.5 dB over traditional design. Moreover, constructions of the sensing system vary to implement different types of fibers in order to increase its metrological parameters. One of such improvements is described by Zhang *et al.* in [60]. The authors used large effective area fiber to achieve decreased measurement uncertainties up to 0.4°C.

If the wavelength of the backscattered signal is equal to this of the incident light, the Rayleigh scattering occurs, due to elastically scattered photons. This kind of scattering is quite restrictive when it comes to temperature sensing. Contrary to the Raman and Brillouin scattering, Rayleigh scattering is not directly dependent on temperature changes, therefore this method is not ideal for temperature measurements [61]. There are solutions, to improve the Rayleigh scattering temperature sensing, but it requires the use of specialty fibers or modification of the fiber, as is presented in [62–64]. Unfortunately, despite achieving decent metrological parameters, the modifications of the method also result in increased cost of production.

The point method of fiber-optic temperature measurement consists of interferometric sensors. Several types of such sensors can be noted: Mach-Zehnder, Michelson, Sagnac and Fabry-Pérot. Detailed descriptions and applications of each type of sensor can be found in numerous reviews e.g., [65,66]. In Mach-Zehnder interferometer sensors, incident light propagates through a splitter, where it is separated into two arms. One of them acts as a reference and the signal traveling through it remains unaffected throughout the measurements. The other – a sensing arm – is influenced by the changes in the measured medium (i.e., temperature). The signals from both arms are then combined, creating interference dependent on the optical path difference [67]. The optical path of the reference arm is always constant, while the path of the sensing arm varies according to the introduced changes, therefore influencing the optical path difference and resulting interference signal. The principle of operation of the Mach-Zehnder interferometric sensor is presented in Figure 2.4.

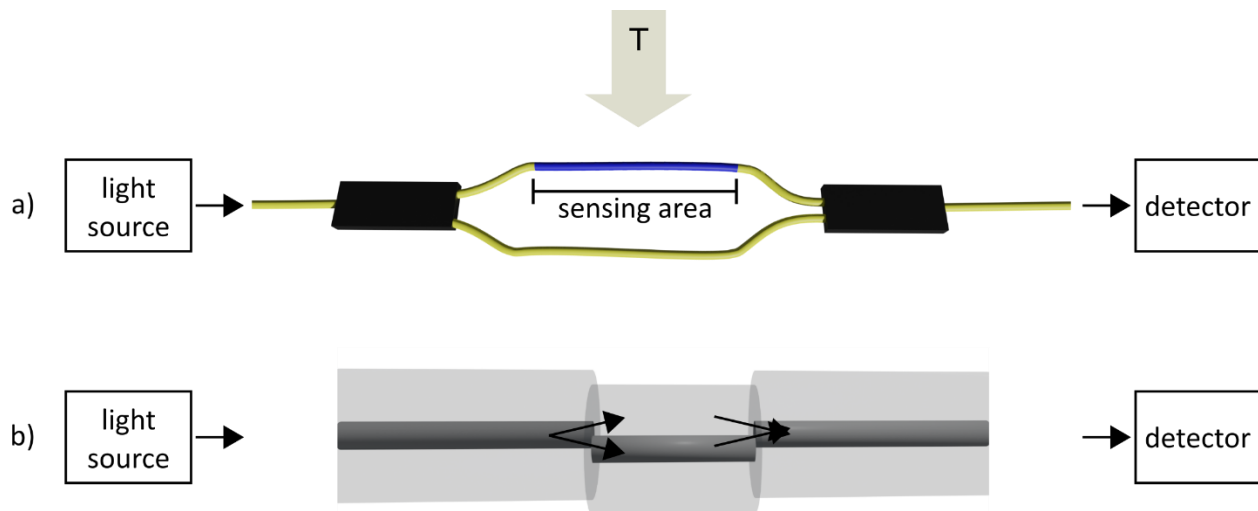


Figure 2.4. Principle of operation of Mach-Zehnder interferometer sensor, where: a) fiber-optic configuration, b) in-line waveguide scheme, where:  $T$  - temperature

Over time, progressing miniaturization forced the conversion of two separate arms into an in-line waveguide scheme. Such construction for high-temperature measurements was demonstrated by Jiang *et al.* [68], while Geng *et al.* [69] propose different configuration of the sensor. Both solutions are high-sensitivity sensors of  $70\text{pm}/^\circ\text{C}$  and  $109\text{pm}/^\circ\text{C}$ , respectively.

The principle of operation of the Michelson Interferometer sensor is also based on an incident light, which is split into two paths. At the end of the path, there is a reflective surface redirecting the beams back onto the same splitter they were separated at. The output interference is a difference of the two optical paths recombined [70]. Michelson interferometer principle of the operation is presented in Figure 2.5.

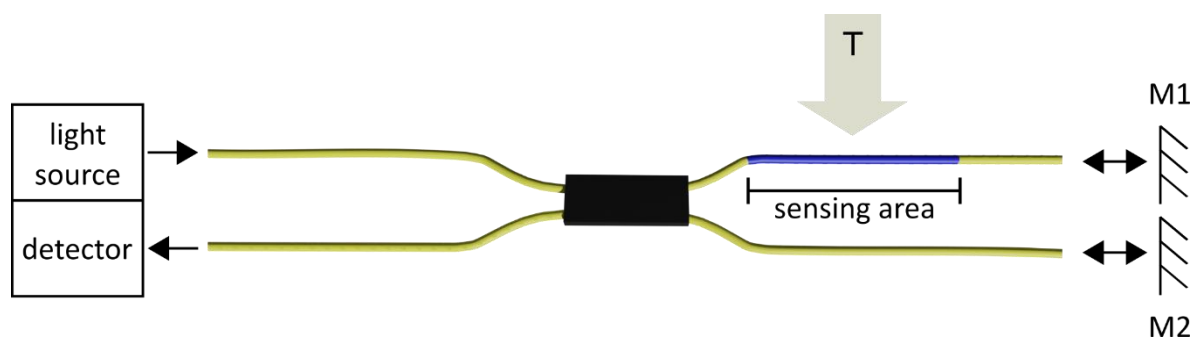


Figure 2.5. Principle of operation of Michelson interferometer sensor, where:  $T$  - temperature,  $M1$ ,  $M2$  - reflective surfaces.

Similarly to Mach-Zehnder interferometer, one of the paths serves as a reference, while the other is subjected to the changes in the investigated medium. In case of Michelson interferometer sensors, new constructions are still developed and improved upon. This year alone, Zhao *et al.* [71]

demonstrated an ultrasensitive Michelson temperature sensor with a sensitivity of  $78.984 \text{ nm}/^\circ\text{C}$ . Han *et al.* [72] used an array of microspheres to fabricate the sensor with a sensitivity of  $166 \text{ pm}/^\circ\text{C}$ .

The principle of operation of the Sagnac interferometer sensor is based on a loop made of an optical fiber. The incident light is split at the beginning of the loop and it is propagated along one path, in opposite directions. Split beams are of a different polarization [73]. After traversing the length of the loop, the beams are recombined and superposed, creating interference. The operation principle is illustrated in Figure 2.6.

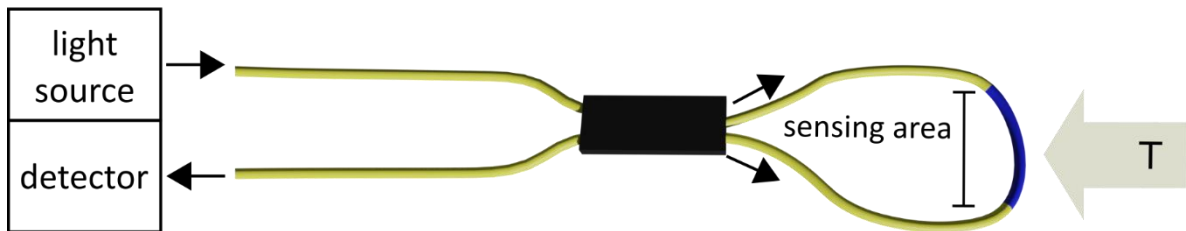


Figure 2.6. Principle of operation of Sagnac interferometer sensor, where:  $T$  – temperature.

Sagnac interferometers are often fabricated from specialty fibers, like: photonic crystal fibers [74], polarization-maintaining fibers [75]. The sensors have some more limitations than the other interferometers, because of space, which the loop takes. The high sensitivities of Sagnac interferometers are still obtainable. Sagnac temperature sensor presented in [76] reached a sensitivity of  $79.2 \text{ nm}/^\circ\text{C}$ .

Fabry-Pérot interferometer sensors, consist of at least two reflective surfaces, positioned in parallel, with a cavity maintained between them [77]. A wave, which propagates along an optical fiber is in part reflected on the surface, while the rest is transmitted through. Multiple superpositions of reflected and transmitted components of the wave in the cavity create an interferometric signal. The principle of operation of the Fabry-Pérot sensor is presented in Figure 2.7.

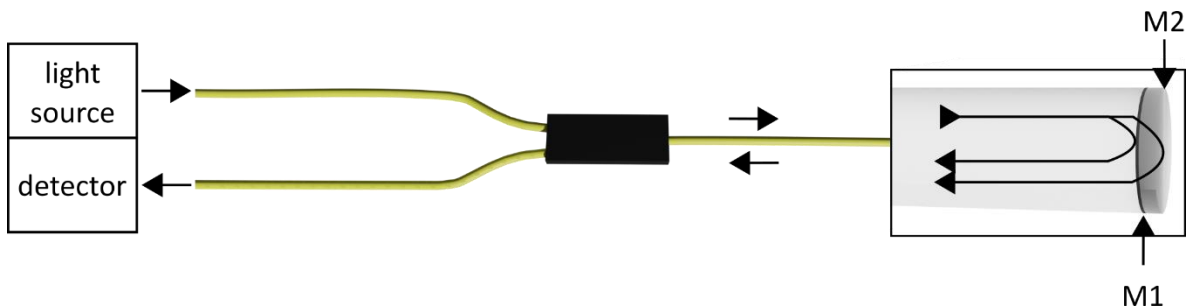


Figure 2.7. Principle of operation of Fabry-Pérot sensor, where:  $M1, M2$  – deposited reflective surfaces.

Modification of any element of the Fabry-Pérot construction (reflective surface, utilized fiber, cavity), allows to easily adjust measurement method and optimize metrological parameters to the desired application. Because of its simplicity and relatively low manufacturing cost, Fabry-Pérot temperature sensors are still actively and rapidly developed. From increasing temperature tolerance up to 1000°C, like proposed by Zhu *et al.* [78], to modification of cavity in order to improve sensor sensitivity, presented by Chen *et al.* [79] – 2.7 nm/°C, the sensors find many applications, including harsh environmental conditions or high temperatures [80,81].

The optimal design of the fiber-optic sensor is crucial when planning measurements. Based on the intended application of the device, the construction of the sensor has to be carefully thought out. Each individual case should be fine-tuned to obtain the best suited parameters. Depending on the allocation of the sensor and the surrounding medium properties, the device may be inadequate for its purpose. There are several ways, in which the fiber-optic sensors can be optimized:

- physical phenomena,
- selection of the type of the fiber,
- modification of the sensor head structure,
- deposition of the coating,
- method of deposition of selected material

The design of the sensor should begin with deciding which physical phenomena will be the basis of its operation. The selection of components for the construction of the sensing system or their modification depends on whether the interference, light scattering, Whispering Mode Gallery or any other phenomenon, will be used. For each phenomenon, the set of unique requirements, have to be fulfilled.

The selection of the right type of an optical fiber is already a huge step toward the optimization of a sensor. Specialty fibers help amplify their optical parameters, stabilize specific parameter or provide protection against harsh operation environment. There are many types of specialty fibers and depending on their application, they can enhance one or more parameters of the fiber-optic temperature sensor. Some of the fibers can be doped with rare earth elements. Wang *et al.* [82] investigate the noise figure characteristic of temperature-dependent bismuth-doped fibers. Then there are photonic crystal fibers, which allow to confine light in the hollow core areas of the fiber. They were used to increase the sensitivity of the temperature sensor by Wang *et al.* [83]. Sensors based on hollow-core can provide a wider range of measured temperature, which is

demonstrated by Zhang *et al.* [84]. Standard telecommunication fibers have advantages on their own. Because they are extensively used, they are easily accessible, therefore do not necessitate any specialty accessories, while on the other hand, they provide numerous possibilities of customization. Polarization maintaining fibers are often applied in Brillouin scattering sensors to limit measurement errors [85,86].

The metrological properties of the sensor can be optimized by selecting the geometry of its measuring head. Advancements in technology and fabrication techniques allow to obtain a multitude of fiber-optic structures. Laser splicing system and fusion splicing allow to modify the structure under the influence of laser or electrodes as a heat source, respectively [87,88]. Femtosecond lasers enable microstructuring and micropatterning of the optical fibers, both on the end-face and the length of the fiber [89–91]. Chemical etching is used to remove or modify the cladding of the fiber and to decrease its core [92,93]. Techniques can also be combined to obtain more complex structures [94,95].

Using modern techniques, a variety of structures can be fabricated. Each of them can be fabricated in multiple ways and used in system configurations of various complexity. The majority of them operate as a resonator, based on Whispering Mode Gallery phenomenon. A signal from a high-coherence light source (e.g., tunable laser) is propagated into an optical microstructure in order to excite a resonance within the structure. This measurement method often requires additional fiber acting as a probe or a waveguide to deliver optical radiation. Examples of utilizing microstructures for temperature sensing are widely presented in the literature. Ma *et al.* [96] describe the performance of the microdisk optical resonator used for simultaneous measurement of both refractive index and temperature, while Luo *et al.* [97] present a lithium niobate resonator for self-reference sensing. Microrings are used in a similar manner. As shown by Wang *et al.* [98] the device utilizes thermal properties of nematic liquid crystal, which is incorporated as a cladding, and during alteration to the ambient temperature the refractive index of nematic liquid crystal changes, therefore shifting the resonance wavelength. Another kind of the fiber-optic structures are tapers. Mainly, they serve as a coupling mechanism between other microstructures and a light source, as it is presented in [99,100]. They can operate on their own as well. Kou *et al.* [101] demonstrate tapered optical fiber with microcavity etched near the tip, which acts as a Fabry-Pérot modal interferometer.

Optical microspheres constitute a large portion of the structures used for temperature sensing. They are fabricated in various forms. Microspheres can also be used as a microresonator,

coupled through a separate taper with a high-coherent light source, as it is demonstrated by Rahman [102]. They can be fabricated in the middle of the fiber and act as an interferometer. Such a solution is presented by Tan *et al.* in [103] or by Zhang *et al.* in [104]. Other solutions can also be found. The review on microsphere geometries was written by Gomes *et al.* [105], where the authors consider multiple optimization techniques of the sensor and propose an application of microsphere array. Although the fiber-optic sensors with microspheres occur in a variety of forms and applications, none of those presented in the literature are capable of simultaneous monitoring of the integrity of their structure.

Measurement properties of the sensor can be enhanced by applying a coating to the measuring area of the device. The coatings consist of a variety of materials, which can be deposited in different forms. There are many reasons, why applying an additional layer may be beneficial during the designing of the sensor. While selecting the suitable material, its properties, as well as compatibility with a measured medium should be considered. It is also important to evaluate whether the material has to be prepared for the deposition purpose and if it will dissolve due to processes occurring during measurements, i.e., chemical process, electric charge. Based on their properties, they are used for specific applications. For example, strontium titanate ( $\text{SrTiO}_3$ ) coating, deposited by pulse laser technique was used by Cheng *et al.* [45] to enhance sensitivity range and decrease system noise. Mishra *et al.* [106] consider coatings of different metals, including copper, lead and aluminum. Because each of the materials differs in thermal expansion coefficient, therefore shifting transmission point as a function of wavelength, which in turn allows to tune the sensor for a specific application.

The deposition method is an important part of the design of a sensing device. The selection of improper deposition method can damage the substrate or deposited material. When choosing the method, the material of which the substrate is made, must be taken under consideration, to ensure deposition of stable and uniform coating. Whether the materials are deposited by dip-coating method [107], Atomic Layer Deposition [108] or magnetron sputtering [109], the coatings adopt different geometry, shading and uniformity [110]. Furthermore, deposition of the same material by a variety of methods may influence the material to exhibit different behavior in contact with a measured medium.



### 3. MICROSPHERE-BASED FIBER-OPTIC SENSORS

In this chapter the design, fabrication, characterization and the principle of operation of the microsphere-based fiber-optic sensors are described. The sensor was developed at the end of a standard, telecommunication optical fiber as an integrated structure. The optical microsphere was formed using an optical fiber fusion splicer. Subjecting the fiber to the electric arc of the fusion splicer incites melting in the exposed part. The surface tension of the liquid glass in combination with performing a pulling motion causes the end-face of the fiber to form spherical shape. The process enables the development of the structure exhibiting a boundary between the core and the cladding, each of different refractive index. Parameters of the obtained microsphere, e.g., size or shape may be modified by adjusting the type of utilized fiber, process type, number of pulls, their fusion current and time as well as pre-fuse current and time. The design of the presented sensor was based on a standard telecommunication optical fiber. Their accessibility makes them ideal for a wide range of applications, lowering the cost of production and ease of replacement in case of sensor damage or failure.

Preparation, characterization and principle of operation of the proposed microsphere-based fiber-optic sensors were presented in the following papers:

- publication [PL1], titled *“Preparation and Characterization of Microsphere ZnO ALD Coating Dedicated for the Fiber-Optic Refractive Index Sensor”*, describes a manufacturing method of a fiber-optic sensor, as well as characterization of the sensor head without coating and with a ZnO ALD coating of 200 nm thickness. The author’s contribution during the research included conceiving, designing and performing the experiments, formal analysis of the experimental results, writing of the original draft of the manuscript.
- publication [PL2] titled *“ZnO coated fiber optic microsphere sensor for the enhanced refractive index sensing”*, describes fabrication and characterization of the microsphere-based fiber-optic sensor with ZnO ALD coatings of 50 nm and 100 nm thickness and the analysis of the results obtained from an experimental investigation of the refractive index. The author’s contribution during the research included conceiving, designing and performing the experiments, formal analysis of the experimental results, writing of the original draft of the manuscript.

Generally, the microsphere-based fiber-optic sensor is used in an experimental setup consisting of a broadband light source, an optical coupler and a detector. A schematic of such a system is presented in Figure 3.1.

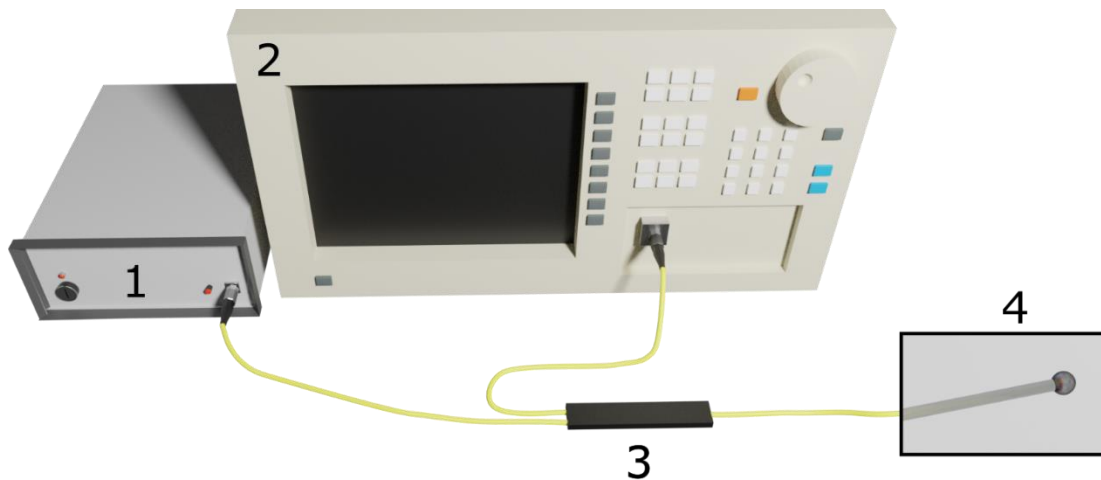


Figure 3.1. Schematic of an experimental setup for validation of a microsphere-based fiber-optic sensor, where: 1 – broadband light source (SLD), 2 – Optical Spectrum Analyzer, 3 – optical coupler, 4 – microsphere-based fiber-optic sensor

The broadband light source – superluminescent diode (SLD) – generates the signal, which is propagated through an optical coupler to the sensor where it is reflected to the Optical Signal Analyzer (OSA). Obtained data is then gathered, processed and analyzed using a data analysis and graphing software. Low-coherence interferometry is a measurement method, which benefits from high sensitivity [111], high stability and reduced coherent noise, and high resolution [112]. Application of the low-coherence interferometry provides absolute measurements [113].

The microsphere-based fiber-optic sensor is composed of two spheres – the inner sphere is made out of fiber's core and is embedded in the outer sphere, made out of fiber's cladding. When a signal reaches a sensor, part of it is reflected from the boundary of the optical fiber core and cladding, while the rest is transmitted through and reflects from the interface between the cladding and the investigated medium, surrounding the sensor. As a result, reflected waves superpose exciting interference. The principle of operation of the microsphere-based fiber-optic sensor is shown in Figure 3.2.

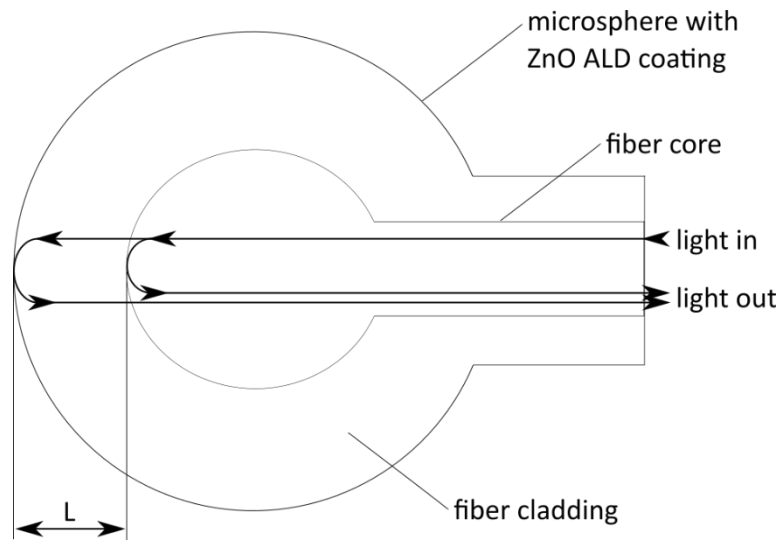


Figure 3.2. Principle of operation of the microsphere-based fiber-optic sensor.

The reflection obtained on the core-cladding boundary is always constant, while the reflection on the surface of the microsphere is highly dependent on the properties of an examined medium.

While designing fiber-optic sensors for temperature measurements it is important to consider how the changing temperature will affect the stability of the sensor parameters, i.e.: signal phase, refractive index of the fiber material, birefringence and thermal expansion of the fiber. To preserve the stability of birefringence, all utilized light sources are equipped with polarization-insensitive fiber-optic isolators, whereas the total length of the optical fiber in the measurement system makes polarization influence negligible. The table with parameters of the light sources, used during the research is presented below (Table 3.1).

Table 3.1. Parameters of light sources utilized during research.

Light source	FiberLabs SLD-1310-18-W	Superlum S1300-G-I-20	ThorLabs SLD830S-A20
Central wavelength ( $\lambda$ ) [nm]	1310	1290	830
Spectrum width [nm]	52	50	50
Total output power [mW]	18	20	22

Considering the change of phase with temperature, it can be described by the following formula (3.1) [114]:

$$\frac{\partial \phi}{\partial T} = \frac{2\pi}{\lambda} \left[ L \frac{\partial \beta}{\partial T} + \beta \frac{\partial L}{\partial T} \right] = \frac{2\pi L}{\lambda} \left[ \frac{\partial \beta}{\partial T} + \beta \alpha \right] \quad (3.1)$$

where:  $\partial\phi$  – phase difference,  $\partial T$  – temperature difference,  $\lambda$  – wavelength,  $L$  – cavity length,  $\beta$  – normalized propagation constant,  $\alpha$  - thermal expansion coefficient.

$\frac{\partial\beta}{\partial T}$  can be approximated as the change in the refractive index with temperature, which for silica  $\frac{\partial n}{\partial T} = 9.7 * 10^{-6}/^{\circ}C$ .

Theoretical calculations were performed to estimate the sensitivity of the clean, uncoated microsphere-based sensor to the temperature. Because the sensor would not have an additional layer, it would not be able to exploit any thermal properties except its own thermal expansion coefficient, which is defined as a gain ratio of the material over its initial length. For the purpose of the calculations, the thermal expansion coefficient of pure silica was assumed –  $4.1 * 10^{-7}/^{\circ}C$  at  $20^{\circ}C$  [115]. Therefore, the following formula (3.2) was utilized [116]:

$$\alpha = \frac{\Delta L}{L\Delta T} \quad (3.2)$$

where:  $\Delta L$  – cavity length difference,  $L$  – initial cavity length,  $\Delta T$  – temperature difference.

Based on the formula, for an optical microsphere with a diameter of  $250 \mu m$ , the gain of length is equal to  $102.5 \text{ pm}/^{\circ}C$ . Considering the temperature range of  $275^{\circ}C$  – the range of the performed experiment – the total expansion of the microsphere is  $28.1 \text{ nm}$ . Given the rate of expansion of the uncoated structure, it was concluded, the sensor has to be coated with an additional layer to obtain satisfactory results.

The output signal of the fiber-optic sensor measured by Optical Signal Analyzer is influenced by effects of the temperature on parameters of the coating, such as the thermal expansion of the coating and its change of the refractive index. The parameters of the OSA used during research is presented are Table 3.2.

Table 3.2. Parameters of Optical Spectrum Analyzer – Ando AQ6319

Optical Spectrum Analyzer	Ando AQ6319
Measurement wavelength range [nm]	600 to 1700
Wavelength accuracy [pm]	$\pm 50 \text{ pm}$ (Full range, after calibration with built-in source)
Resolution bandwidth [nm]	0.01, 0.02, 0.05, 0.1, 0.2, 0.5 and 1
Maximum input power [dBm]	23
Sweep time	3 sec. (any 100nm, SMPL.: 1001, SENS.: HIGH 1)* <ul style="list-style-type: none"> <li>*For wavelength resolution 0.2nm</li> </ul>

During the design of the microsphere-based fiber-optic sensor, zinc oxide coating was chosen, due to its optical properties, numerous deposition techniques and applicability for a broad range of sensing devices. Zinc oxide nanomaterials have a thermal expansion coefficient greater by two orders of magnitude over pure silica – about  $4.7 * 10^{-5}/^{\circ}C$  [117]. The exact value is dependent on the method of its deposition. Moreover, while the temperature increases the refractive index of the ZnO coating also increases [118]. A similar situation occurs with the growth of coating thickness [119]. Taking it into consideration, the optical power density change can be calculated, according to the change difference formula (3.3) [120]:

$$P = S(\nu)\cos(\Delta\phi) \quad (3.3)$$

where:  $P$  – optical power density,  $S(\nu)$  – spectral distribution of the light source,  $\Delta\phi$  – change of phase,

while  $\Delta\phi$  is expressed by (3.4):

$$\Delta\phi = 2\pi * \frac{n\Delta L}{\lambda} \quad (3.4)$$

where:  $n$  – refractive index.

Based on the presented formula, it can be concluded, the optical power of the reflected signal increases, the more the refractive index grows.

### 3.1. *Fabrication of the microsphere-based fiber -optic sensor*

While opting to implement an optical microsphere into the fiber-optic sensor, the goal is to create a clean and perfectly round structure, which would allow for highly precise results. By paying close attention to all details during a manufacture of a microsphere, the sensors will be reproducible, which translates to an easy modification to tune them to the selected measurements.

In the quest for a perfect microsphere, there are many obstacles along the way. It is important to pay attention to every element to ensure the production of the best microstructure possible.

During the process of manufacturing an optical microsphere on the end-face of the fiber, there are a lot of issues, that can occur, including:

- deformity of the microsphere,
- offset between the center of a microsphere and the core of a fiber,
- obtaining an inconsistent diameter of the microsphere,
- damage to the inner structure integrity,
- appearance of defects in the material structure,

- improper application of the coating.

Each of the mentioned issues introduces uncertainty on its own. However, any combination of those cases invalidates the measurements completely.

The most common problem during the manufacturing of the microsphere, visible at first glance, is obtaining the structure, which will be round and centered vis-à-vis the fiber propagating the signal. Each deformity, whether it is an elongation of the microsphere or a gravitational drop, like the ones shown in Figure 3.3, causes a considerable alteration of an optical spectrum. The image was obtained by an optical microscope (Olympus CX31, Japan).

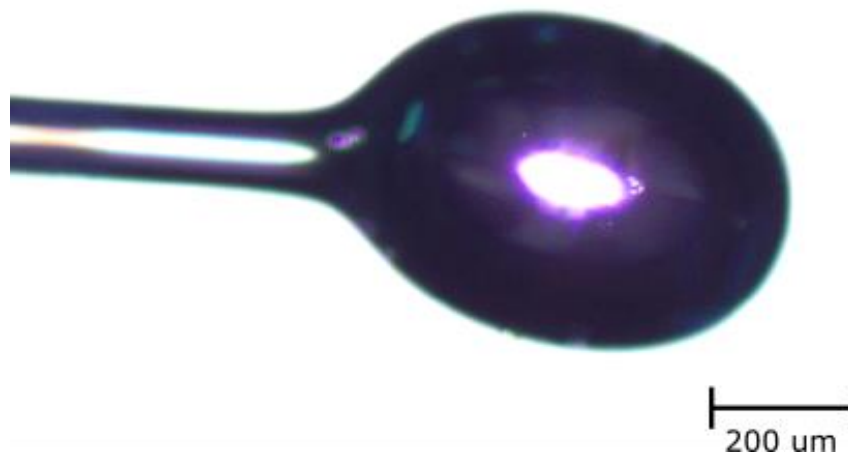


Figure 3.3. *Elongation or offset of the microsphere during manufacturing are the easiest mistakes to spot.*

Secondly, obtaining a selected diameter of the microsphere is of utmost importance. One of the features of microsphere-based fiber-optic sensors is the presence of an intrinsic fixed cavity. Changing the diameter of the microstructure influences the length of the cavity, therefore utilizing a microsphere of diameter varying from the one specifically selected, results in obtaining a spectrum of the measured signals vastly different than expected which in turn causes erroneous data analysis. In Figure 3.4, microspheres with 253  $\mu\text{m}$  and 477  $\mu\text{m}$  in diameter are presented, including their cavity length, where  $L_1 \neq L_2$ .

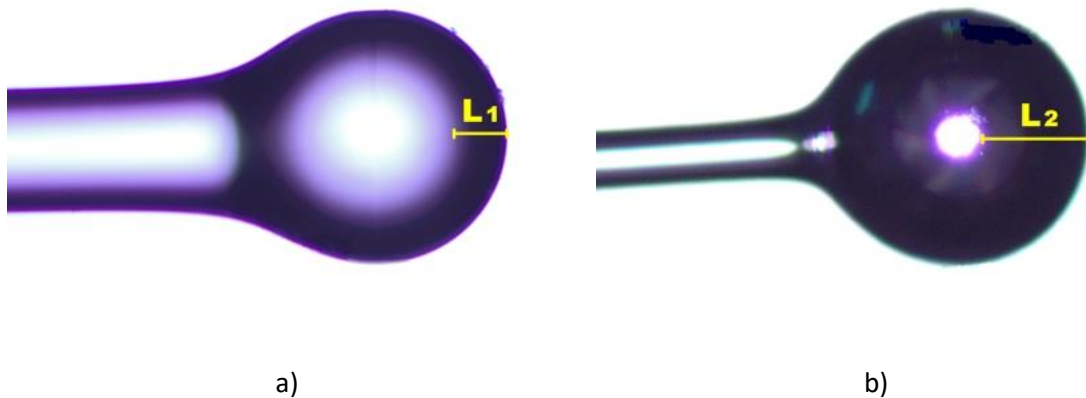


Figure 3.4. Altering the diameter of the microsphere results in changing of cavity dimensions. Example of a variety of microspheres: a) 253  $\mu\text{m}$  and b) 477  $\mu\text{m}$ .  $L_1$ ,  $L_2$  – cavity lengths.

Another issue shown in Figure 3.5 is the preservation of the inner structure of the microsphere. It can be observed, the core of a fiber was disturbed during production. A microsphere made of a core of an optical fiber was detached, which resulted in the rest of the core to form a taper. Figure 3.5 and Figure 3.6 were obtained by a Stimulated Emission Depletion microscopy (Leica TCS SP8 STED, Germany).

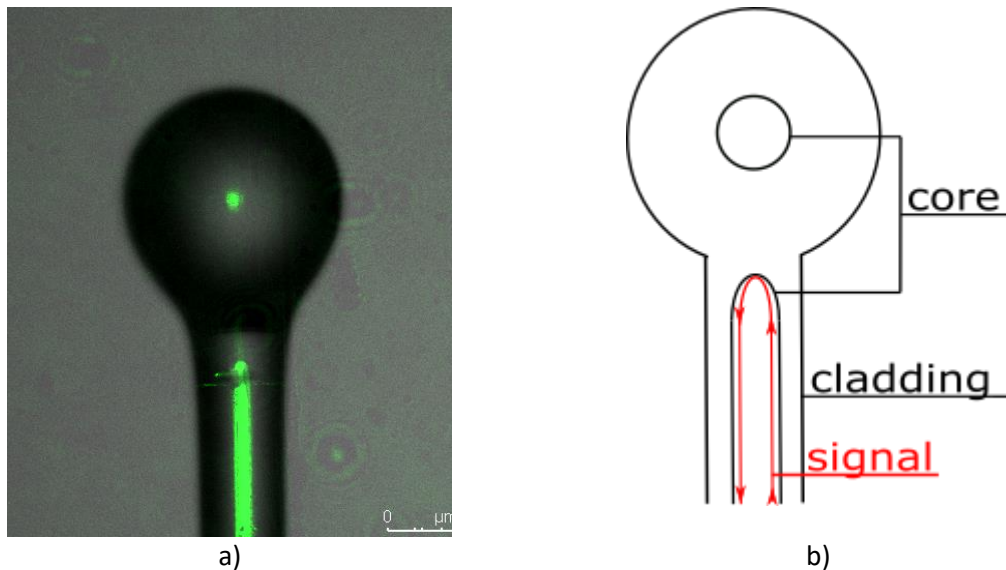


Figure 3.5. Impaired inner structure integrity of the microsphere: a) STED microscopy image, b) schematic explanation of the issue.

Magnification of the microsphere surface, presented in Figure 3.6, shows damage to the fiber structure. Parameters of the splicer during the production of the microspheres were

improperly set, therefore causing the emergence of air bubbles within the material of an optical fiber. Such damage distorts the signal during measurement.

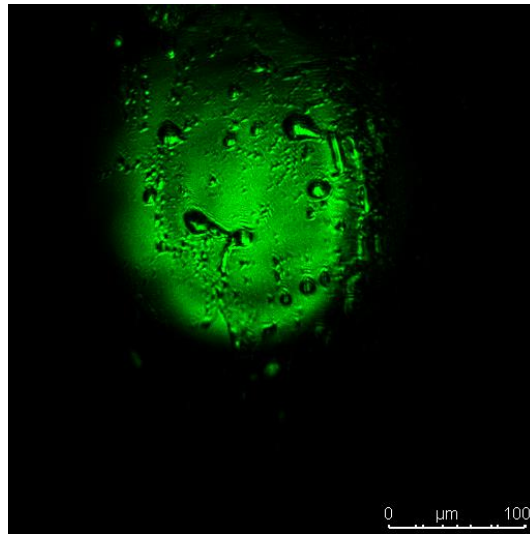


Figure 3.6. *Magnification of the microsphere surface with affected material structure.*

The coating was applied to the surface of the microsphere by Atomic Layer Deposition method. This technology is used to synthesize thin films on challenging substrates, e.g., optical fibers and is extremely controllable in respect to the thickness of the coating. Depending on the number of deposition cycles, the thickness of the coating can be estimated. ALD method is also ideal for deposition on uneven or curved surfaces, because it allows to apply a uniform coating on the entire sample.

Besides the quality and geometry of the optical microsphere, the metrological parameters of the sensor are dependent on the quality of the ZnO ALD coating. The thickness of the coatings was calculated and because of the limited resources, their deposition was commissioned to the Institut Européen des Membranes in Montpellier (France). Each fabricated sensor was subjected to the characterization using Scanning Electron Microscopy (SEM, FEI S50, Hillsboro, OR, USA) to verify the accuracy of the geometrical design as well as the topography and morphology of the deposited ZnO coating. SEM images of uncoated sensor and sensors with 50 nm, 100 nm and 200 nm ZnO ALD coatings were included in Figure 3.7. The images were taken with 500x magnification.



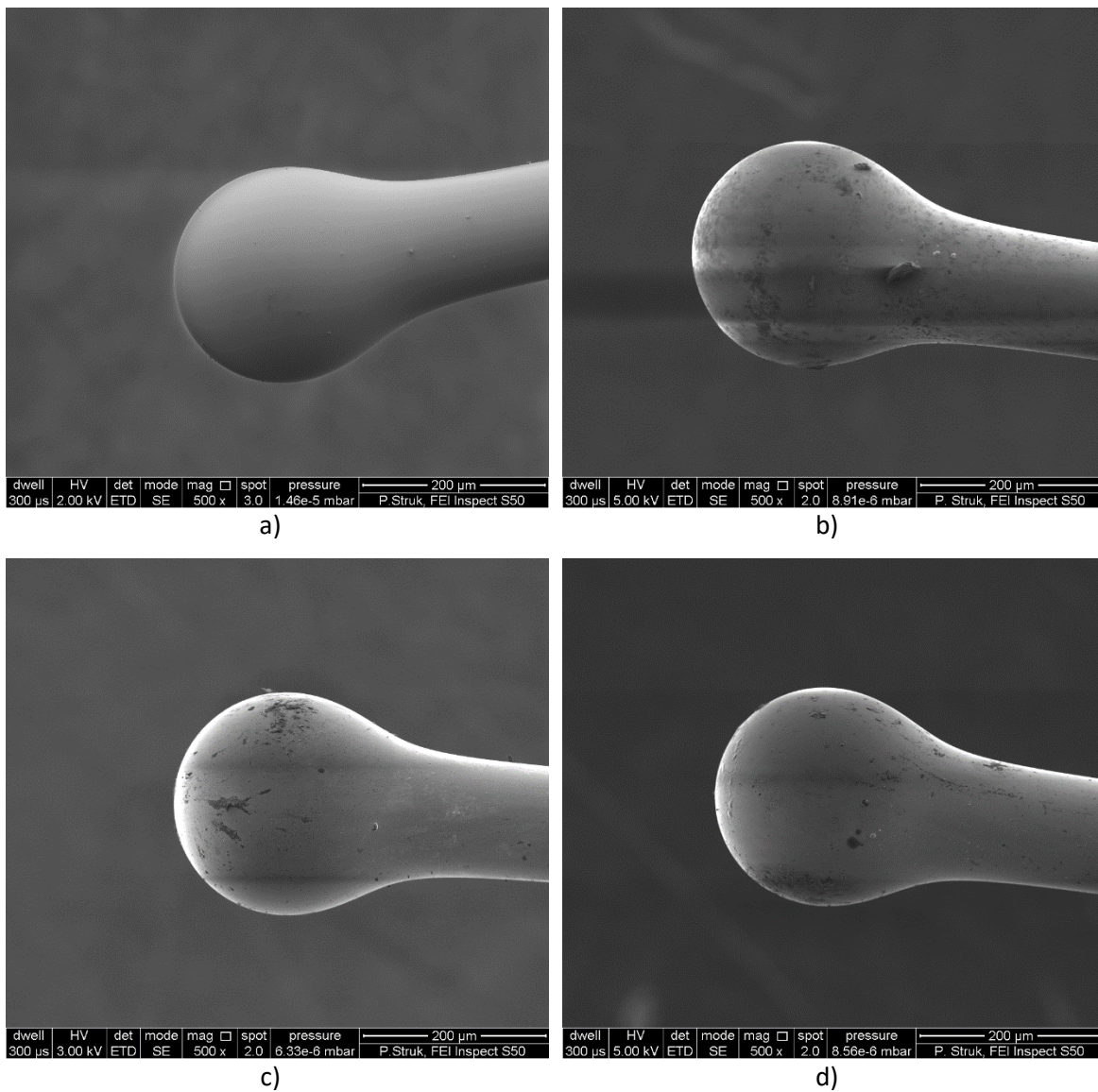


Figure 3.7. SEM images of designed microsphere-based fiber-optic sensors with their respective ZnO ALD coatings: a) uncoated, b) 50 nm, c) 100 nm, d) 200nm

As can be observed all presented sensors demonstrate consistent spherical shape. Moreover, the coating is visible on the surface of the sensor's structure. Images seen in Figure 3.7. indicate high repeatability of the fabrication process of the sensor.

#### 4. MICROSPHERE-BASED SENSOR FOR TEMPERATURE MEASUREMENTS

In order to validate a microsphere-based fiber-optic sensor, temperature measurements were performed. The investigation was executed using the sensors with a coating thickness of 100 nm and 200 nm. The setup was following the general configuration for this sensor and it is presented in Figure 4.1.

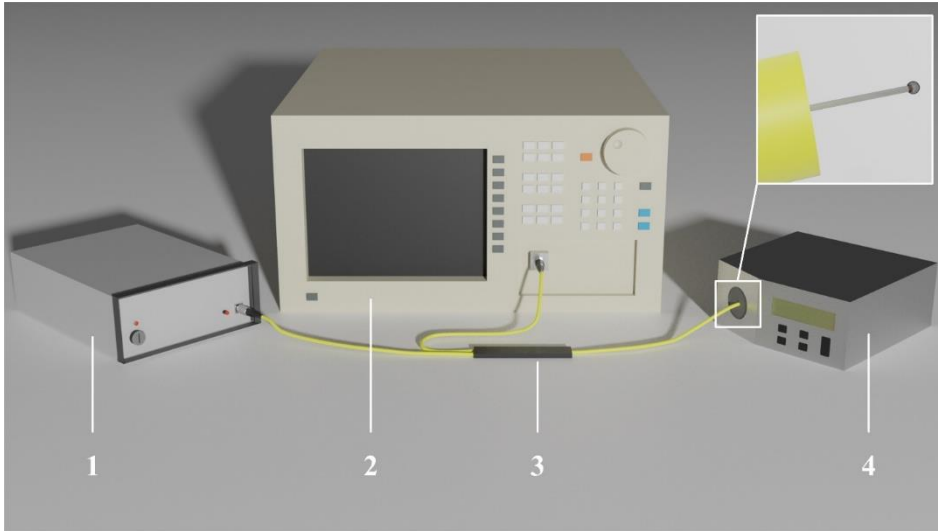


Figure 4.1. The experimental setup for temperature measurements, where: 1 – SLD light source, 2 – OSA, 3 – optical coupler, 4 – temperature calibrator.

The light source used in this setup had a central wavelength of  $1310 \text{ nm} \pm 10 \text{ nm}$  (SLD-1310-18-W, FiberLabs Inc., Fujimino, Japan). The microsphere-based fiber-optic sensor was placed in the temperature calibrator (ETC-400A, Ametek, Berwyn, PA, USA) during the measurements. While adjusting the temperature in a range of  $100^\circ\text{C}$  -  $300^\circ\text{C}$ , the reflected signal was observed on the Optical Spectrum Analyzer with an increase of every  $10^\circ\text{C}$ . While the temperature was measured in the  $100^\circ\text{C}$  to  $300^\circ\text{C}$ , the working range is limited by operating temperature of the utilized fiber, as well as that of the coating. The latter depends on parameters of the selected material and its deposition method. The measurements exploited the thermal properties of a ZnO ALD coating, which allowed to observe spectral changes while the temperature was being adjusted.

Experimental results of the microsphere-based fiber-optic sensor for temperature measurements are included in the following publications:

- publication [PL3], titled “ZnO ALD-Coated Microsphere-Based Sensors for Temperature Measurements”, demonstrates experimental results of the temperature measured in the range of  $100^\circ\text{C}$  -  $300^\circ\text{C}$  using a microsphere-based fiber-optic sensor with a 200 nm ZnO ALD coating. The author’s contribution during the research included conceiving,

designing and performing the experiments, formal analysis of the experimental results, writing of the original draft of the manuscript.

- publication [PL4] titled “*Temperature Fiber-Optic Sensor with ZnO ALD Coating*”, demonstrates experimental results of the temperature measured in the range of 100°C to 300°C using a microsphere-based fiber-optic sensor with a 100 nm ZnO ALD coating. The author’s contribution during the research included conceiving, designing and performing the experiments, formal analysis of the experimental results, writing of the original draft of the manuscript.

The datasets obtained during the research are available in the *MOST Wiedzy* repository, Open Research Data - *Measurement spectrum obtained with the use of ALD coated microsphere-based fiber-optic sensor*. In subsection 4.1, the optical power analysis for sensors with 200 nm and 100 nm coatings is presented. In subsection 4.2, the data of the sensor with a 100 nm ZnO ALD coating with spectral shift analysis is included.

#### 4.1. *Optical power analysis of the microsphere-based sensors*

The results of the temperature measurements utilizing the sensors with ZnO ALD coatings of 200 nm [PL3] and 100 nm [PL4] are presented. Optical power analysis was performed. The comparison of both sensors is presented at the end of the subsection.

##### 4.1.1. *Microsphere-based sensor with a 200 nm coating*

Figure 4.2 shows the measured response of the sensor with a 200 nm ZnO ALD coating.

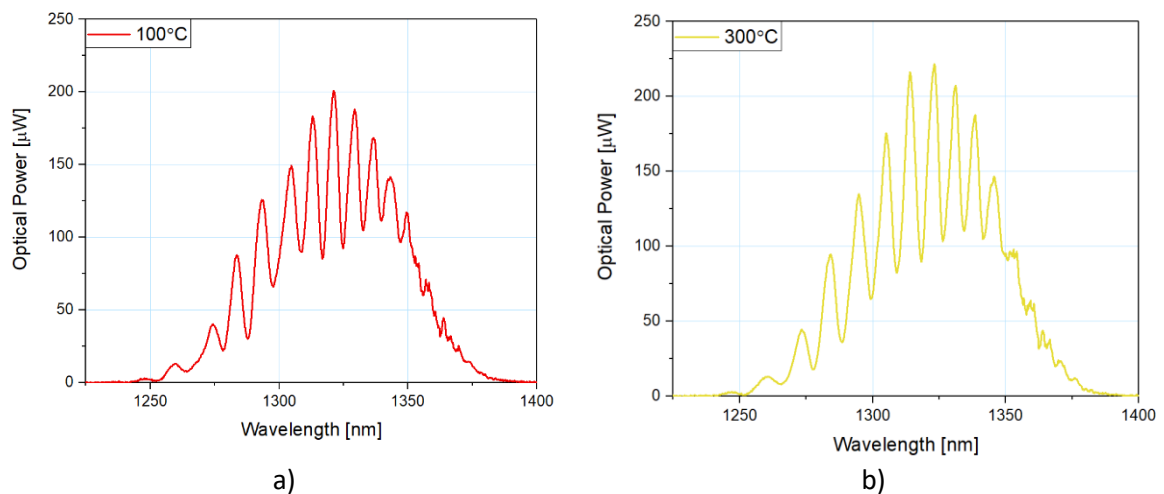


Figure 4.2. *Measured response of the microsphere-based fiber-optic sensor with a ZnO ALD coating of 200 nm thickness during the temperature investigation at: a) 100°C, b) 300°C.*

As can be seen, the optical power of the reflected signal rises, the more temperature grows. The envelope of the spectrum and the distribution of the modulation are consistent throughout the measurements. That, along with the presence of the modulation provides the information about the proper functioning of the sensor, while the optical power level indicates the changes in the measured temperature. The increase of the power between 100°C and 300°C is about 10%.

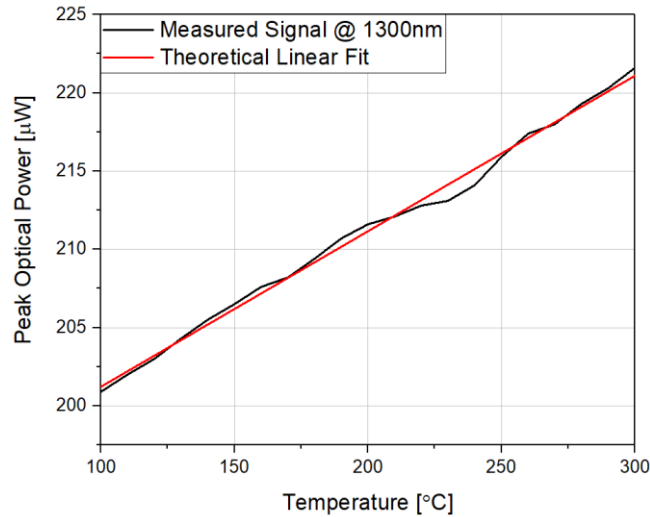


Figure 4.3. Dependence of the reflected signal peak optical power on the rising temperature.

In Figure 4.3, the dependency of the optical power of the reflected signal is presented. Moreover, a theoretical linear fitting was calculated to determine the metrological parameters of the designed sensor. Based on acquired data, the sensitivity of the sensor can be calculated from the following formula (4.1) [121]:

$$S = \frac{\Delta P}{\Delta T} \quad (4.1)$$

where:  $S$  – sensitivity of the sensor,  $\Delta P$  – optical power of the reflected signal difference,  $\Delta T$  – temperature range.

The sensitivity of the temperature sensor with a 200 nm ZnO ALD coating equals 103.5 nW/°C. The coefficient of determination  $R^2$ , which determines the deviation of the data obtained during measurements from the regression line, was also calculated and it is 0.995. Thanks to the  $R^2$  coefficient linearity of the sensor can be concluded. In this case, obtained data retains close fit to the theoretical data, except in the range between 225°C and 250°C, where it deviates the most.

#### 4.1.2. Microsphere-based sensor with a 100 nm coating

A similar situation can be observed for a sensor with a 100 nm ZnO ALD coating. Figure 4.4 illustrates the measured response of the reflected signal optical power.

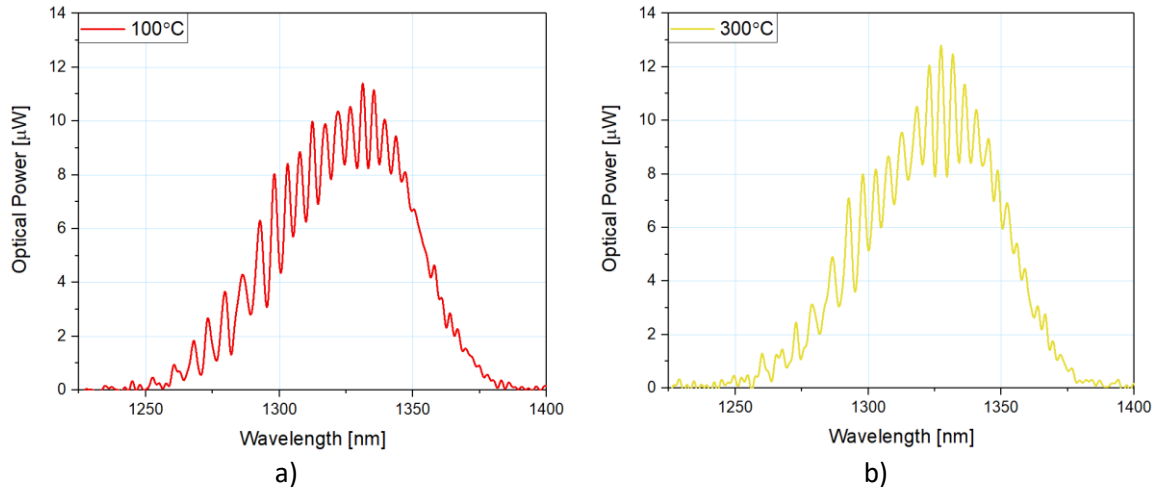


Figure 4.4. Measured response of the reflected signal optical power for the microsphere-based fiber-optic temperature sensor at: a) 100°C, b) 300°C.

In this case, the similarities of the spectra can be observed, while the optical power of the reflected signal rises as a function of temperature.

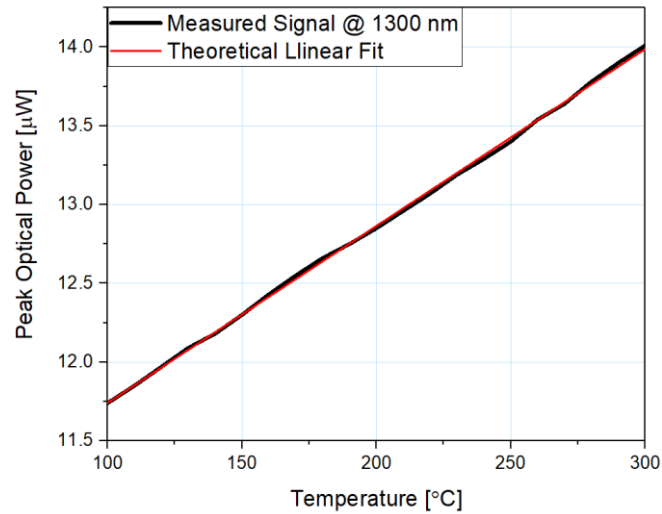


Figure 4.5. Reflected signal optical power dependence on the changing temperature and its theoretical linear fit, measured at a wavelength of 1300 nm, using the microsphere-based sensor with 100 nm ZnO ALD coating.

The results presented in Figure 4.5 allowed to calculate that the increase of the signal throughout the examined range is 16%. The sensitivity of the microsphere-based sensor with 100

nm ZnO ALD coating was also calculated and it equals 11.35 nW/°C. A theoretical linear fit was included in the presented graph.

#### 4.1.3. Comparison of the microsphere-based sensors with 200 nm and 100 nm coatings

Figure 4.6. presents a comparison of the reflected signal optical power of both sensors: the one with a 100 nm ZnO ALD coating and with a 200 nm coating. As can be observed, the optical power of a reflected signal of the sensor with a thicker coating was 10 times higher than the other one. The values on the graph were normalized to the highest quantity of optical power as to comparison would be clear.

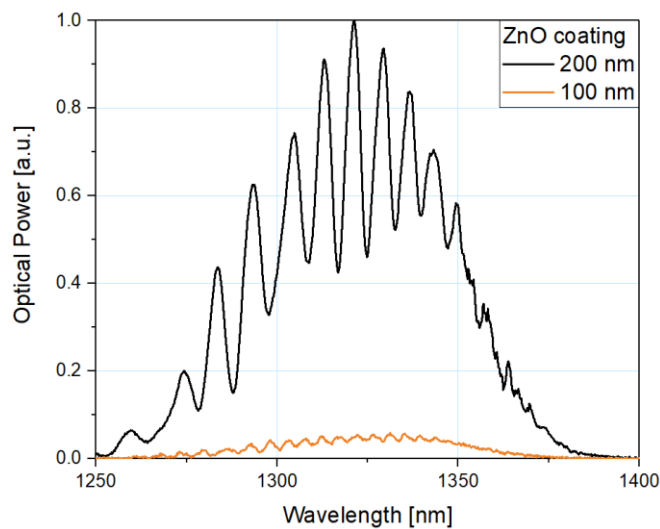


Figure 4.6. Normalized reflected spectra measured at 100°C with microsphere-based sensors with a 200 nm (black line) and a 100 nm (orange line) ZnO ALD coating.

Furthermore, dependencies of the peak optical power of the reflected signals on the changing temperature were plotted, combined with the equations of theoretical linear fitting characteristics.

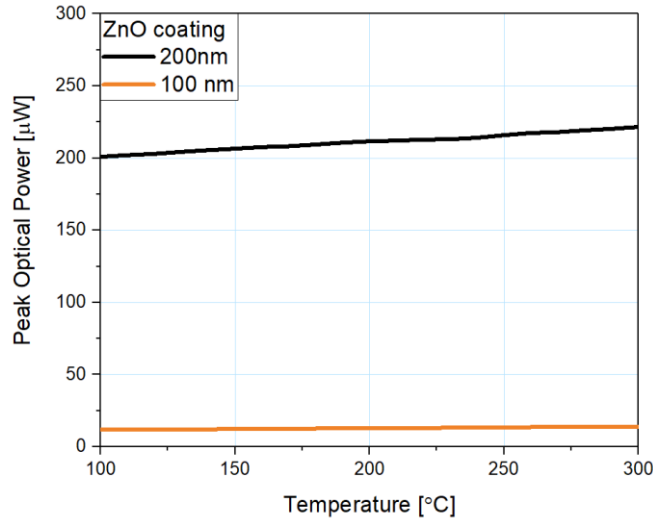


Figure 4.7. Comparison of the obtained peak optical power of the reflected signal for each sensor.

Figure 4.7 shows the dependency of the peak optical power on temperature for microsphere fiber-optic sensors and their difference while using 200 nm and 100 nm ZnO ALD coating. Because the linear fit is a close match to the obtained data, by following linear regression, it is possible to accurately predict metrological properties of the sensor at a temperature beyond the investigated range and to forecast the behavior of the sensor with any other thickness of a ZnO ALD coating.

In addition, the values of linearity error, sensitivity error and approximation error were calculated. The parameters are presented in Table 4.1.

Table 4.1. List of metrological parameters of the microsphere-based fiber-optic temperature sensors – optical power analysis.

Parameter	100 nm coating	200 nm coating
Investigated range [°C]	100-300	
Characteristics	linear	
Analysis type	optical power	
Sensitivity [nW/°C]	11.35	103.5
Sensitivity error [%]	0.99	3.97
Theoretical sensitivity [nW/°C]	11.24	99.39
Linearity error [%]	1.15	5
Approximation error [%]	0.2	0.49
R <sup>2</sup>	0.999	0.995

As observed, the sensitivity of the sensor with a 200 nm ZnO ALD coating is almost 10 times higher than the sensor with a 100 nm coating. The sensitivity error, determining a deviation of this parameter from the one fitted from the theoretical zero-deviation slope, was calculated from the formula (4.2) [121]:

$$u_{sensitivity} = \left(1 - \frac{S_{theor}}{S}\right) * 100\% \quad (4.2)$$

where:  $u_{sensitivity}$  – sensitivity error,  $S_{theor}$  – theoretical fitting sensitivity.

While the sensitivity error of the sensor with a 100 nm coating is 1%, the sensor with a 200 nm coating errs by 3.97%. Throughout measurement planning, it is worth to consider the sensitivity needed to accomplish a task. For investigations requiring lower sensitivity, the sensor with thinner ZnO ALD coating may still provide sufficient metrological parameters, whereas in terms of time and cost of its production, it will be more beneficial. On the other hand, the sensor with a 200 nm coating will be more suitable for high-sensitivity needs.

The dependence of the optical power changes occurring in the spectra on increasing temperature during measurements with each sensor is consistent with linear characteristic and the linear fit was included in the graphs (Figure 4.3 and Figure 4.5). Therefore, the linearity error between obtained data to the theoretical model was calculated (4.3) [122]:

$$u_{linearity} = \frac{\max|P - P_{theor}|}{\Delta P} \quad (4.3)$$

where:  $u_{linearity}$  – linearity error,  $P$  – optical power of the reflected signal,  $P_{theor}$  – theoretical fitting optical power,  $\Delta P$  – optical power difference.

Calculated linearity error in terms of optical power analysis indicates almost 5 times lower error in case of the sensor with a 100 nm coating than the sensor with a 200 nm coating. However, in both instances, the error does not exceed 5%.

The next calculated parameter was approximation error, which indicates divergency between obtained data and its linear fit. For both presented sensors, approximation error is less than 0.5%, while for the sensor with a 100 nm coating the error is 2.5 times lower. Approximation error was calculated from the following formula (4.4) [123]:

$$\delta = \left| \frac{u_M - u_R}{u_R} \right| * 100\% \quad (4.4)$$

where:  $\delta$  – approximation error,  $u_M$  – obtained data,  $u_R$  – linear fit.

By comparing  $R^2$  coefficients of both sensors, it is shown, the value for the microsphere-based fiber-optic sensor with a 100 nm ZnO ALD coating equals 0.999, which indicates a closer match



of the obtained data to the theoretical fit, therefore its measured characteristic exhibits higher linearity than the sensor with a 200 nm coating, where  $R^2=0.995$ .

#### 4.2. Spectral shift analysis of microsphere-based sensor

Performing measurement with a sensor coated by 100 nm ZnO ALD, besides optical power analysis, spectral shift is also available. Figure 4.8 shows normalized values of the measured signal response for the microsphere-based sensor with a 100 nm ZnO ALD coating, at 100°C and 300°C to preserve the readability of the plot. By rising the temperature, the spectral peak of the reflected signal shifts toward lower values of the wavelength. The envelope remains similar for each temperature.

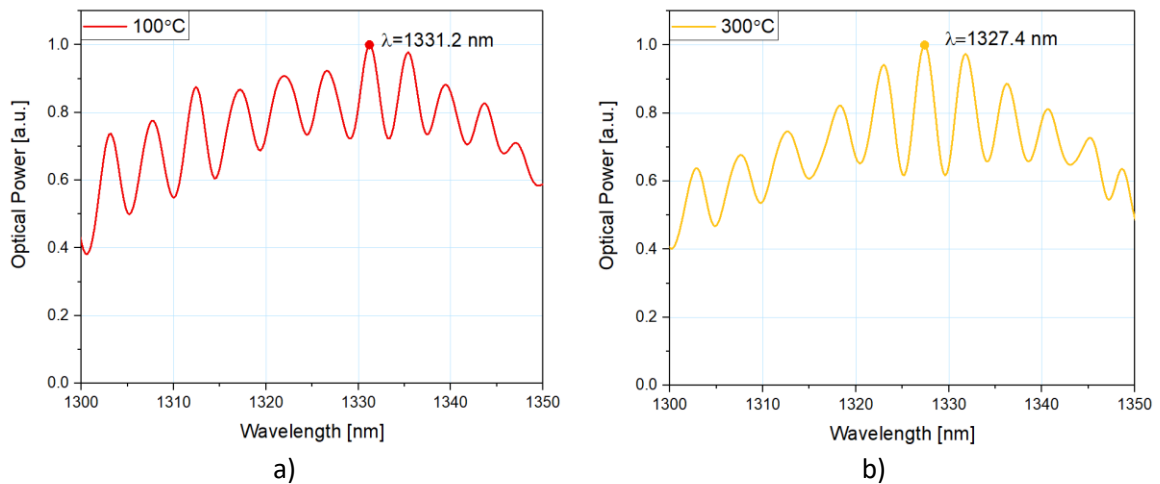


Figure 4.8. Normalized measured response of the reflected signal for the microsphere-based sensor with 100 nm ZnO ALD coating at a) 100°C and b) 300°C.

The dependence of the peak wavelength position on the temperature can be observed in Figure 4.9.

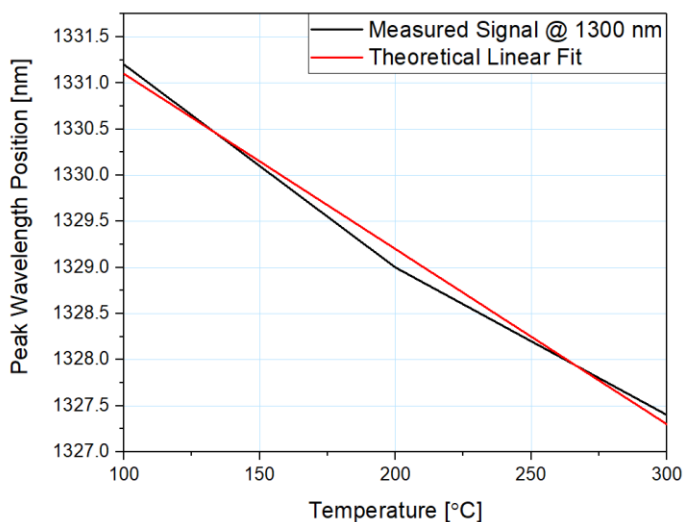


Figure 4.9. Dependence of the spectral shift of a reflected signal on the temperature.

The spectrum changes its peak wavelength position when the temperature is altered. As the temperature rises, the spectrum shifts by a constant value throughout the whole range of roughly 2 nm per 100°C. By following linear regression, it is possible to determine the position of the reflected signal peak for each measured temperature.

#### 4.2.2. Comparison between a optical power and a spectral shift analysis of a temperature sensor with 100 nm ZnO ALD coating.

As mentioned before the results of a microsphere-based fiber-optic sensor can be analyzed using optical power and spectral shift. In Table 4.2, the parameters of the sensor are listed.

Table 4.2. Comparison between optical power and spectral shift analysis of parameters of the microsphere-based sensor with a 100 nm coating.

Parameter	100 nm coating	
Investigated range [°C]	100-300	
Characteristics	linear	
Analysis type	spectral shift	optical power
Sensitivity	19 pm/°C	11.35 nW/°C
Sensitivity error [%]	0	0.99
Theoretical sensitivity [%]	19 pm/°C	11.24 nW/°C
Linearity error [%]	5.2	1.15
Approximation error [%]	0.02	0.2
R <sup>2</sup>	0.992	0.999

The sensitivity of the sensor with optical power analysis cannot be compared to the one with spectral shift, however the parameters of both analysis methods are shown to provide metrological possibilities of the sensor. Depending on the nature of designed measurements, the

required sensitivity can differ. As observed, in spectral shift analysis sensitivity error equals 0%. The offset of the values is present, but the relative deviation takes the same values on both sides of the range. The sensitivity error in optical power analysis is close to 1%. On the other hand, the linearity error is almost 5 times lower, while analyzing the data of optical power, in comparison to those analyzed in the spectral shift analysis. Approximation error, while in both instances remains below 0.2%, its value is 10 times lower (0.02%) with spectral shift analysis. Microsphere-based sensor with optical power analysis exhibits higher linearity.

As presented in chapter 4, the microsphere-based fiber-optic temperature sensor with a ZnO ALD coating allows to perform temperature measurements, therefore concurring **Thesis 1**. The presence of the modulation in the measured signal allows to monitor the sensor microstructure, which substantiate **Thesis 2**.

## 5. APPLICATIONS

In the previous chapter validation of the designed sensors was shown. Knowing the sensors are operational and their metrological parameters depend on properties of the deposited ZnO ALD coating, it is time to move to their applications, which is *in situ* monitoring of the supercapacitors. Besides internal temperature changes, the electrolyte used in the construction of the supercapacitor, can also change its other properties, i.e., refractive index [124]. Therefore, comprehensive study on the metrological parameters of the sensor depending on the changing refractive index are presented in [PL1, PL2].

The investigation was executed on the uncoated microsphere, as well as coated with a ZnO of various thicknesses: 50 nm, 100 nm and 200 nm. The setup used for this experiment is presented in Figure 5.1.

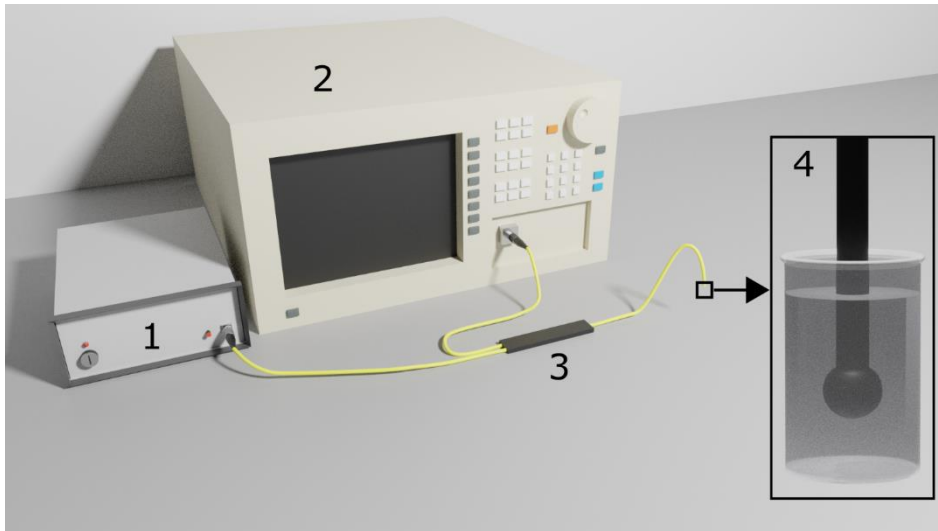


Figure 5.1. *Experimental setup for measurements of refractive index, where: 1 – broadband light source, 2 – Optical Spectrum Analyzer, 3 – optical coupler, 4 – sensor immersed in refractive index liquid.*

The setup is consistent with previously shown general configuration. The light source used for those measurements was a superluminescent diode with a central wavelength of (S1300-G-I-20, SUPERLUM, Ireland). During the experiment, the sensors were immersed in Cargille Refractive Index Liquids (Series A, AA, AAA, Cargille Laboratories, Cedar Grove, NJ, USA). The refractive indices of examined liquids were of standardized series, between a range of 1.4-1.6 at 589.3 nm, with a resolution of 0.1. Because of dispersion, at the utilized wavelength refractive index values of the liquids alter. Therefore, at a wavelength of 1300 nm, the indices were respectively: 1.390, 1.487, 1.576. The sensors were also validated without immersion to establish reference baseline. When

performing measurements of a medium, which the value of a refractive index is close to the this of an optical fiber cladding, the reflection of this interface drops toward zero. To prevent it, a microsphere-based fiber-optic sensor can be additionally modified by depositing a coating on the surface of an operational sensor. The coating made out of highly reflective and transparent material, with a refractive index different than those of fiber allows to shift the transition point of the reflection minimum to a higher value of refractive index. The results of the validation of the sensor are presented below.

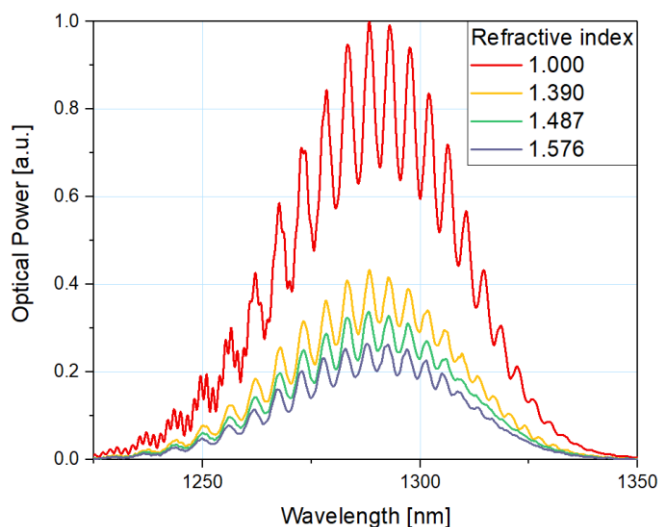


Figure 5.2. Normalized measured reflected spectra for a microsphere-based fiber-optic sensor, with a 200 nm ZnO ALD coating, immersed in refractive indices liquids of 1.000, 1.390, 1.487, 1.576.

Interferogram in Figure 5.2. shows the spectrum retains its envelope as well as the spacing of the modulation. The presence of the modulation proves, the sensor's structure is intact, whereas the increase of the optical power of the reflected signal indicates changes occurring at the cladding-investigated medium interface, which proves, the microsphere-based fiber-optic sensor can be successfully used for measurements of the refractive index.

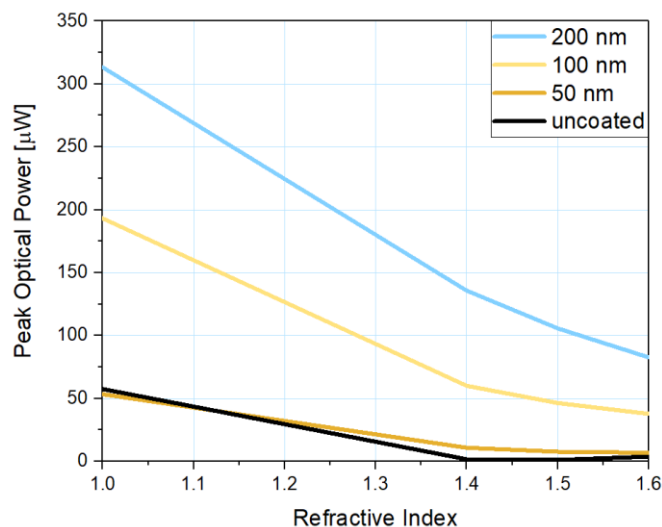


Figure 5.3. The dependencies of the reflected signal peak optical power on the refractive index measured using microsphere-based sensor with coating thickness of 200 nm, 100 nm, 50 nm, and with uncoated sensor.

Based on the plots shown in Figure 5.3, the sensitivity of the sensor has been calculated. It equals: 89  $\mu\text{W}/\text{RIU}$  for the uncoated device, 78  $\mu\text{W}/\text{RIU}$  for the sensor with 50 nm coating, 259  $\mu\text{W}/\text{RIU}$  for 100 nm and 384  $\mu\text{W}/\text{RIU}$  for 200 nm. It can be also observed the optical power was much higher – up to 6 times – for the sensor with ZnO ALD coating of 200 nm over the uncoated sensor or the one with a coating of 50 nm thickness. In general, the coating with 50 nm thickness is too thin to improve metrological parameters of the sensor, however, the optical power marginally increases, around 1.4-1.5 refractive index – the value exhibited by a standard telecommunication optical fiber cladding.

### 5.1. *In situ* supercapacitor temperature monitoring

Microsphere-based fiber-optic temperature sensor was embedded inside the supercapacitor. By doing this, it is possible to constantly monitor *in situ* temperature of the device during its operation.

The general setup described in chapter 5 was used for the experiment, which is presented in Figure 5.4.



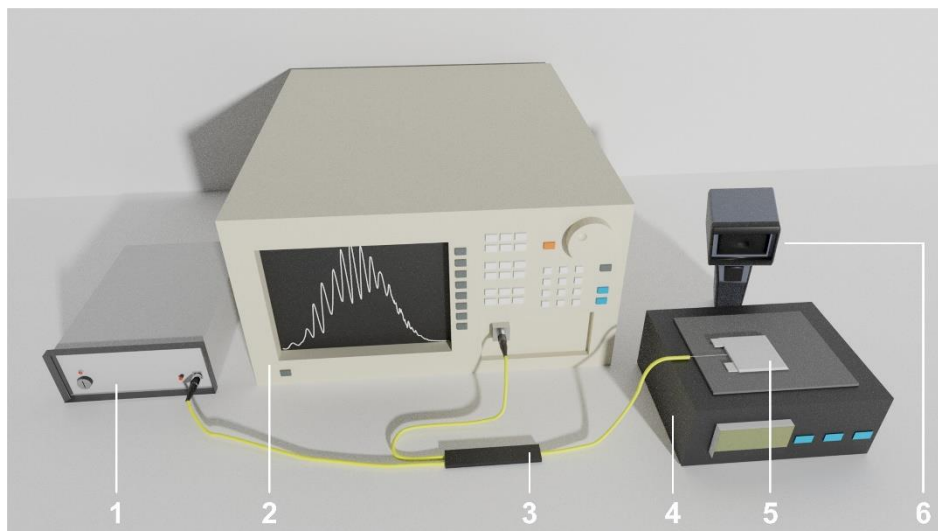


Figure 5.4. The experimental setup for in situ monitoring of the supercapacitor temperature, where: 1 – broadband light source, 2 – OSA, 3 – optical coupler, 4 – hot plate, 5 – investigated supercapacitor, 6 – thermal camera.

The superluminescent light source with a central wavelength of  $1310 \text{ nm} \pm 10 \text{ nm}$  (SLD-1310-18-W, FiberLabs Inc., Fujimino, Japan) was used, while the sensor was placed inside the supercapacitor between the electrode and the cover as to not intervene in the chemical process. The exact placement of the sensor is shown in Figure 5.5.

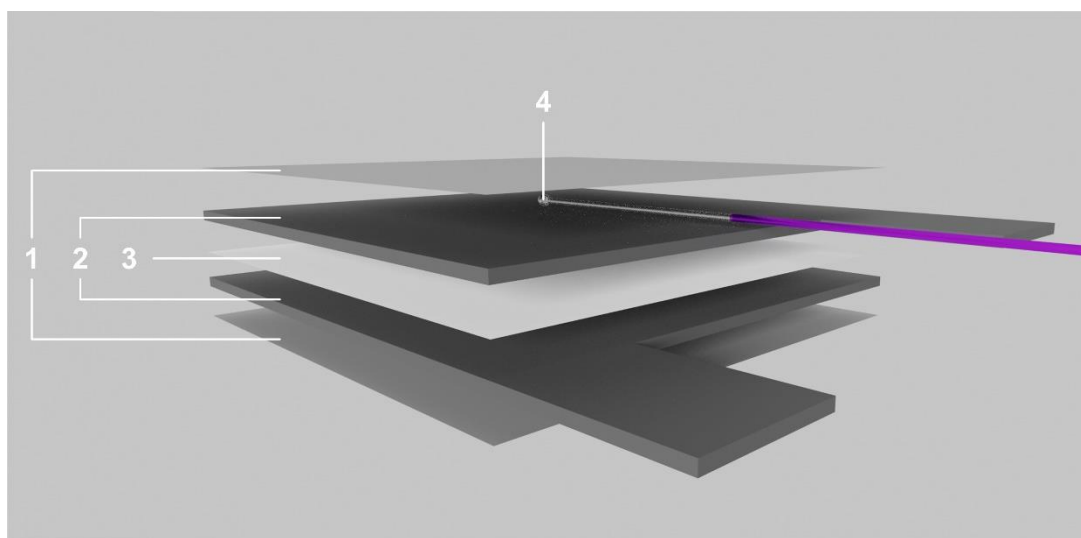


Figure 5.5. Placement of the microsphere-based fiber-optic sensor embedded in the supercapacitor in schematic cross-section, where: 1 – covers, 2 – electrodes, 3 – separator, 4 – microsphere-based fiber-optic sensor.

The construction of the investigated supercapacitor is described in [125]. Additionally, the supercapacitor temperature was measured by a thermal camera (i7, FLIR, Wilsonville, OR, USA) as a reference to control temperature distribution during the measurements. The pictures were taken

at an emissivity setting of  $\epsilon=0.6$ , due to the semi-glossy properties of the supercapacitor enclosure. Representative images taken at the lowest and the highest temperature are presented in Figure 5.6 below.

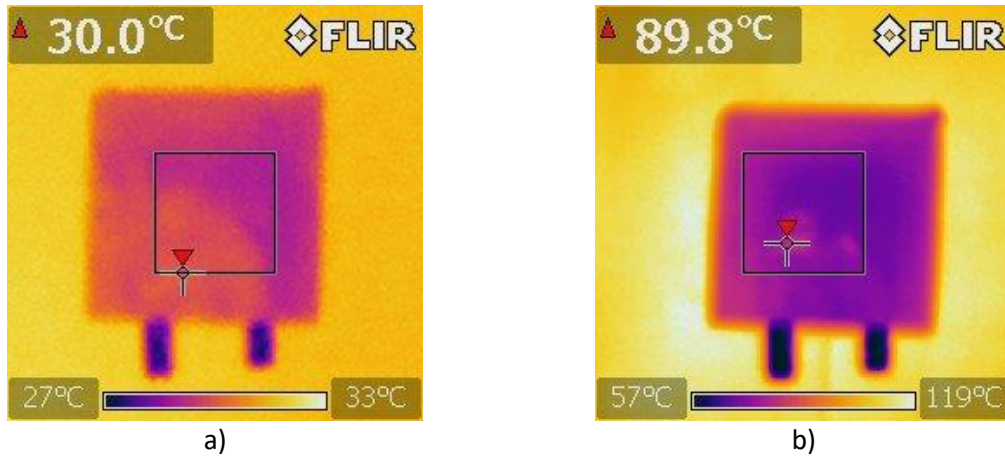


Figure 5.6. Images of the supercapacitor with the in situ fiber optic temperature sensor obtained by thermal camera for the lowest a) 30°C and highest b) 89.8°C value of investigated temperature range.

Because of the aqueous electrolyte (1 M  $K_2SO_4$ ), used for conductivity, the measurements were executed in a range of 30°C - 90°C with a step of 5°C. The data was obtained at about 80% state of charge of supercapacitor. All measurements were taken 5 minutes after the temperature was stabilized. Only selected spectra are included in Figure 5.7 to retain clarity of the graph and they show the correlation of the optical power of the reflected signal to the changing temperature.

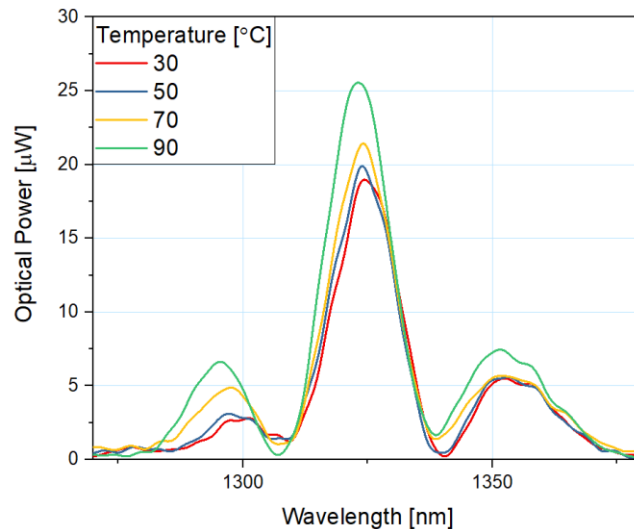


Figure 5.7. Changes in the optical power of the reflected signal with rising temperature.

As can be seen, an increase in the temperature also causes a rise in the optical power of the reflected signal. Characteristics of the spectra remain similar, demonstrating the proper operation



of the sensor. The entire range of the measurements and the dependence of the peak optical power on the temperature can be observed in Figure 5.8.

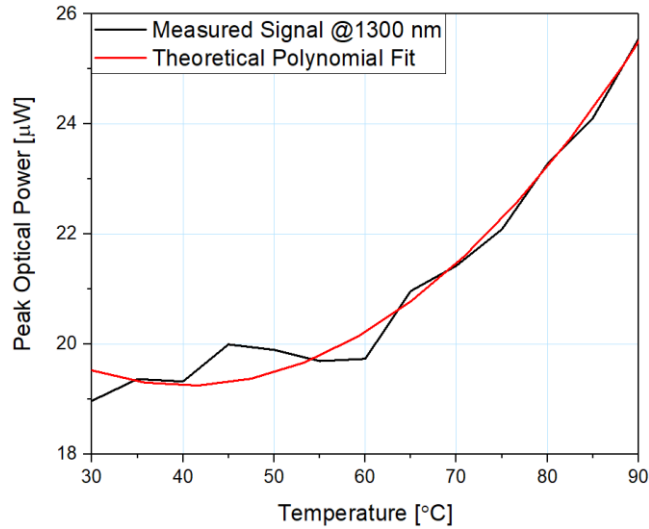


Figure 5.8. Reflected signal peak optical power dependence in the changing temperature.

The plot exhibits a polynomial characteristic, unlike the measurement of the temperature performed for the range of over 100°C. This behavior repeats throughout multiple series of measurement, therefore allowing to use it as the basis of the sensing mechanism. Having repeatable, reference characteristics of the spectrum, any deviation is noticeable, which serves as an indicator about the significance of the changes. If the characteristics are altered completely, it shows critical problem, and the device should be immediately shut down. Smaller changes serve as a warning, which if unattended, could lead to further damage.

Table 5.1. List of metrological parameters of the microsphere-based fiber-optic sensor for *in situ* temperature monitoring.

Parameter	<i>In situ</i> sensor with a 200 nm coating
Investigated range [°C]	30 – 90
Characteristics	2 <sup>nd</sup> order polynomial
Analysis type	optical power
Sensitivity [nW/°C]	109.59
Sensitivity error [%]	10.16
Theoretical sensitivity [nW/°C]	98.45
Linearity error [%]	9.92
Approximation error [%]	3.26
R <sup>2</sup>	0.97

In the range of 30°C - 90°C, presented plot assumes linear characteristic with a sensitivity of 109.6 nW/°C and the sensitivity error between the theoretical calculations and the one obtained

from the measurements is 10.16%. Approximation error at this temperature range equals 3.26%, while the linearity error is just below 10%. The  $R^2$  coefficient assumes 0.97.

Based on the results presented in this chapter, both theses were confirmed. The dependence of changing optical power of the reflected signal on the temperature changes corroborates **Thesis 1**, while the stability of the modulation during the measurements supports **Thesis 2**.

Because of the ZnO incompatibility in certain environments [126], the idea of protecting the sensor and the medium arose. A preliminary study was conducted, which investigates the possibility to protect the deposited coating with a nanocrystalline diamond sheet (NDS). The results are presented in the following publication:

- publication [PL5], titled “*Microscale diamond protection for a ZnO coated fiber optic sensor*”, demonstrates the application of the nanocrystalline diamond sheet, synthesized in a Microwave Plasma Assisted Chemical Vapor Deposition System, on the end-face of an optical fiber coated by ZnO ALD. The author’s contribution during the research included conceiving and designing the experiments, formal analysis of the experimental results, writing of the original draft of the manuscript.

During the research, a nanocrystalline diamond sheet was attached to the sensor head made of an end-face of an optical fiber with deposited ZnO ALD coating. NDS works as a protective layer to prevent the ZnO coating from mechanical and chemical damage. The experimental investigation considers how the NDS influences the output signal of the sensor. Sensing parameters of both layers were measured using Fabry-Pérot interferometer operating in the reflective mode – the setup similar to the one shown in Figure 2.7. The measurements were taken firstly, with a sensor with just ZnO coating deposited on the end-face of an optical fiber, and secondly with NDS attached over the coating. The results of the experiment are presented in Figure 5.9. While validating the sensor, the distance was measured by changing the cavity length between the sensor head and the additional reflective surface placed directly underneath. The results shown in figure below, were taken while the cavity was set to 140  $\mu\text{m}$ .

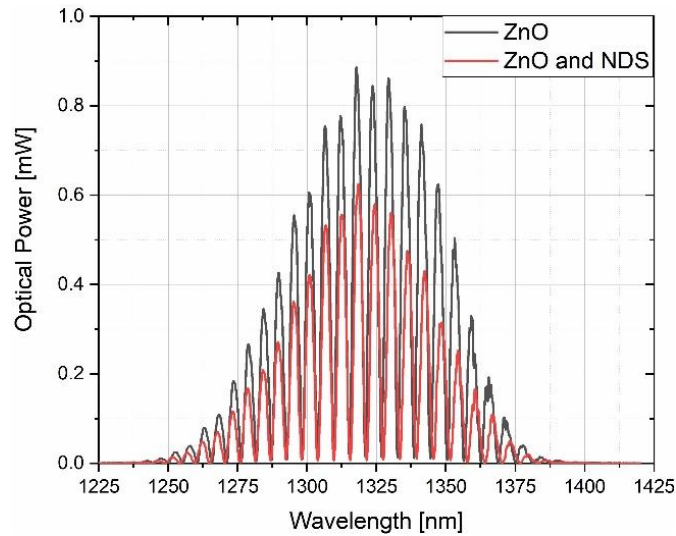


Figure 5.9. Measurement signals obtained for the measurement head with ZnO coating, and ZnO coating and nanocrystalline diamond sheet. The Fabry–Pérot cavity length was set to 140  $\mu\text{m}$ .

As observed, application of the nanocrystalline diamond sheet over the sensor head with ZnO coating causes the optical power to decrease about 30%, while the envelope and modulation distribution of the spectra remains similar. Presented results suggest it is possible to apply a nanocrystalline diamond sheet on the surface of the microsphere-based fiber-optic sensor with ZnO ALD coating. The decline of the optical power with an additional protective layer is acceptable, considering it would allow the longer lifetime of the sensor and immunity against unforeseen reactions between a ZnO and an investigated medium.

## 5.2. Measurement method of optical and thermal properties of nanomaterials

Microsphere-based fiber-optic sensor can be utilized for the investigation of 2D nanomaterials, such as: optical and thermal properties of black phosphorus. For the purpose of the study, Few-Layer Black Phosphorus (FLBP) was deposited as a coating on the surface of the optical microsphere, which allows for rapid and accurate measurements. The coating was investigated after 2, 3, and 5 deposition cycles. Black phosphorus is a 2D material, which properties are still being discovered, therefore the acquisition of any new data is a substantial information leading to better understanding of the material.

The results of the study of optical and thermal properties of FLBP using microsphere-based fiber-optic sensor are included in the following publication:

- publication [PL6], titled “*Measurements of the optical and thermal properties of the 2D black phosphorus coating*”, demonstrates optical and thermal properties measured in

the range of 50°C to 300°C using a microsphere-based fiber-optic sensor before deposition of the coating and after deposition of 2, 3 and 5 cycles of FLBP coating. The author's contribution during the research included conceiving, designing and performing the experiments, formal analysis of the experimental results, writing of the original draft of the manuscript.

The experimental measurements were performed using the setup shown in chapter 3 (Figure 3.1), using a broadband light source with a central wavelength of 830 nm (SLD830S-A20, Thorlabs Inc., Newton, NJ, USA), for investigation of optical properties and of 1310 nm (SLD-1310-18-W, FiberLabs Inc., Fujimi), for investigation of thermal properties. Optical properties of the FLBP coating were examined after 2, 3 and 5 deposition cycles. The spectrum of the uncoated sensor is also presented as a reference. The measured spectra obtained after each deposition cycle are included in Figure 5.10a and the dependence of the deposition cycles on the peak optical power is shown in Figure 5.10b.

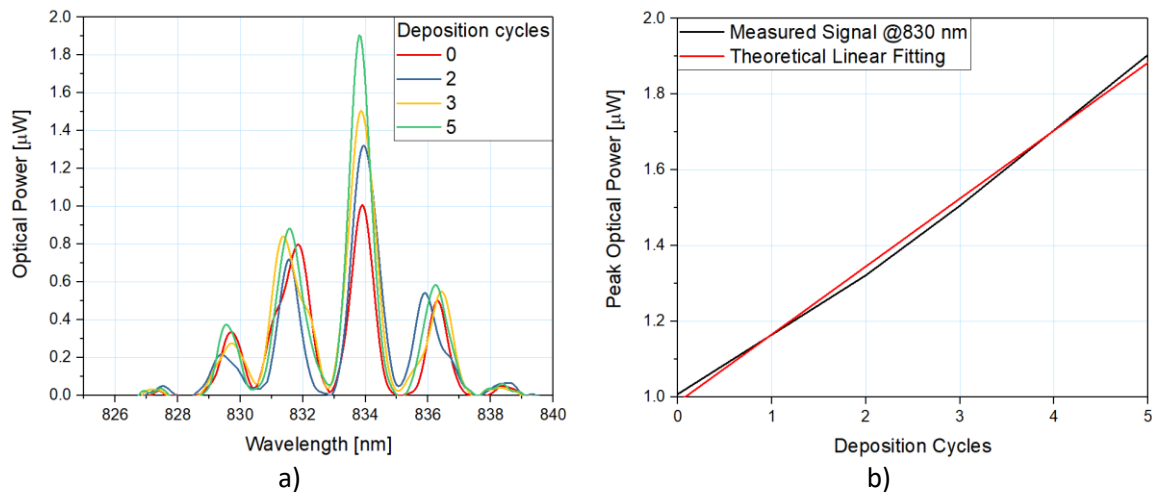


Figure 5.10. The measured reflected signal from the fiber-optic microsphere-based structure coated with 2D black phosphorus, where: a) spectra before deposition of FLBP and for coatings of 2, 3 and 5 deposition cycles, b) the dependence of the peak intensity on the number of deposition cycles.

As observed, optical power increases after each measured deposition cycle, which is a result of tightening of the material on the surface of the microsphere with each layer, therefore increasing its thickness. With increasing thickness of the coating, optical path difference also changed. The dependency of the intensity of the reflected light on the thickness of the layer was demonstrated by Yang *et al.* [127]. The  $R^2$  coefficient was also calculated based on the theoretical linear fit, which equals 0.995.

Furthermore, the coating sensitivity on the changing temperature was investigated, in the range of 50°C to 300°C. To retain the clarity of the plot, only the spectra obtained at 50°C, 150°C and 200°C are included in Figure 5.11. The dependency of the peak optical power on the temperature is also illustrated in the figure below.

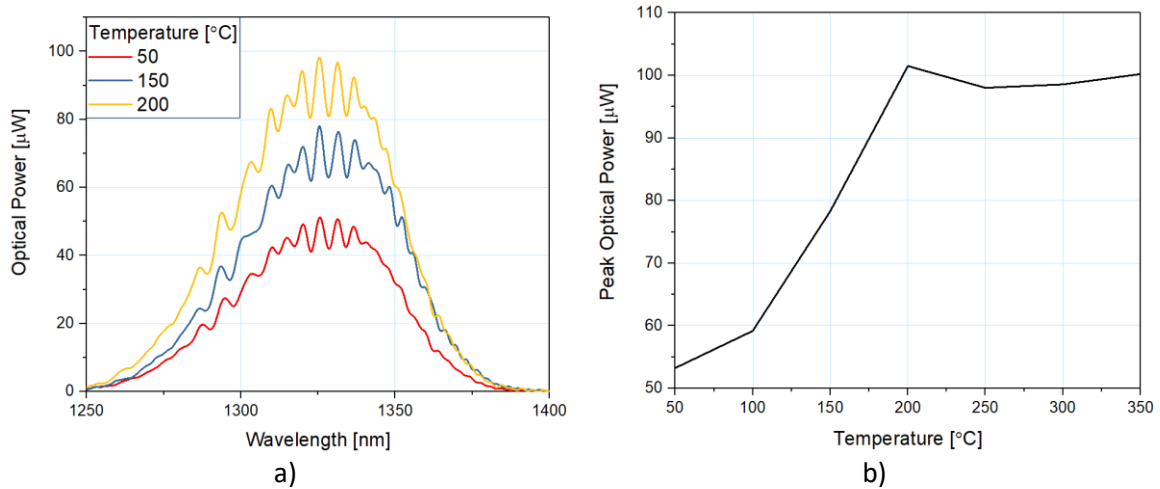


Figure 5.11. The measured reflected signal from the fiber-optic microsphere-based sensor during the temperature measurements, where: a) representative spectra measured at 50°C, 100°C, 200°C for the sensor with a coating of 5 deposition cycles; and reflected signal peak intensity dependence on changing temperature, measured for a coating of 5 deposition cycles in the range of 50°C - 350°C.

As can be seen, the optical power increases with rising temperature up to 200°C, at which point it stabilizes. The growth of the temperature causes softening of atomic bonds and higher phonon velocity, resulting in a higher refractive index, which in turn leads to an increase of the reflected signal optical power. Stabilization of the signal at temperatures over 200°C may be a result of the anharmonicity of phonons and further the phonon-phonon scattering. A similar dependence on temperature is in the case of the thermal conductivity of phosphorene [128,129].

The results presented in this chapter, prove both theses. The dependence of changing optical power of the reflected signal on the temperature changes corroborates **Thesis 1**, while the stability of the signal modulation during the measurements supports **Thesis 2**.

## 6. DISCUSSION

In the dissertation, the microsphere-based fiber-optic intensity-modulated sensors are discussed. In general, intensity-modulated sensors provide low-complexity systems and rapid response time, however most fiber-optic sensors without microsphere structure are susceptible to the changes of their cavity, low robustness and accuracy due to external influences, therefore when the reflected signal cannot be detected, the reason for it is uncertain e.g., whether the sensor head is damaged, the sensor is out of alignment. The proposed design exhibits a number of advantages over traditional intensity-modulated fiber-optic sensors. The application of an optical microsphere provides a fixed cavity within the sensor head, which desensitizes the sensor to the cavity changes and provides a monitoring mechanism for the integrity of the sensor structure.

By modifying the parameters of the structure as well as the coating, the metrological parameters can be tuned. While the changes occurring in the investigated medium are determined by observing the optical power of the reflected signal, the presence of modulation provides information about the integrity of the structure. When the modulation in the spectrum recedes, it may indicate the microstructure of the sensor sustained damage or was completely broken off. Constant, real-time monitoring of the sensor operation allows for immediate feedback, which in turn allows to take appropriate steps to mend the situation. The sensors are ideal for application in remote and hard-to-reach places because they limit inaccuracies related to the uncertainties about the proper operation of the sensor.

Implementation of the coating thickness of 200  $\mu\text{m}$  on the surface of the microsphere allows to obtain the sensitivity of 103.5  $\text{nW}/^\circ\text{C}$ . The results presented in this dissertation revealed it is possible to perform the temperature measurements with thinner coating, while retaining high sensitivity – 11.35  $\text{nW}/^\circ\text{C}$ . Application of the thinner coating requires fewer deposition cycles, therefore saving time and reducing the cost of production.

The microsphere-based sensor was directly made of the end of an optical fiber, so it does not require additional steps during the fabrication process. To date, other solutions involved the preparation of the microsphere separate from the fiber, and then connecting both by fusion splicing. The sensor using optical microspheres can also be fabricated and left unattached, in which case, the signal has to be guided by an independent probe, e.g., a tapered optical fiber, which may cause losses of the input light optical power. Not only, the method presented in the dissertation allows to create repeatable structures, but also the microsphere always keeps in alignment with the waveguide fiber.

The simplicity of the sensor design subsequently benefits the entire system because it does not require supplementary elements or components (e.g., external reflective surfaces). Thanks to the structure is fabricated from the standard, telecommunication, single-mode optical fiber, it is not necessary to combine them with specialty fibers.

When selecting the best method for specific temperature measurement, several factors should be considered, especially investigated environment. Consideration of the working environment is crucial, while choosing the measurement method and the type of instrument [130]. Based on their construction and materials used during manufacturing, the sensors differ in terms of measurement parameters, such as:

- temperature range – defines the minimum and maximum temperatures, in which the device can operate. Microsphere-based sensors with a ZnO ALD coating were validated in the temperature range of 30°C to 300°C due to the limitation of available resources. The range can be broadened depending on the optical fiber, of which the sensor will be fabricated, the material of the coating and the method of its deposition. based on previous investigation [131] and further research [132], stands to reason the sensor would be fully functional, upon appropriate optimization of its parameters, at the temperature of at least 600°C.
- invasiveness – explores if the sensor utilized during the measurements can cause damage to the measured environment, e.g.: electric sensor can be a potential risk, while surrounded by combustible materials or improperly selected instrument can contaminate the environment. Because the designed sensor is made of optical fiber it is resistant to external influences, such as electromagnetic interference. While due to its small size (250 μm), the sensor will not distort the measured medium, the deposited ZnO coating depending on the type of the medium may have an unwitting chemical reaction.
- sensitivity – the temperature sensitivity determines the capability of the sensor to detect changes of the investigated environment, while the sensor temperature also changes. As presented in the dissertation, by selecting the suitable thickness of the ZnO ALD coating, the sensitivity of the designed sensor can be tuned according to the measurement needs. The sensitivities of designed sensors range from 103.5 nW/°C to 11.35 nW/°C, or in case of spectral analysis: 19 pm/°C.
- replicability – indicates the ability to reconstruct the sensor, while preserving its full range of parameters. The microsphere-based sensor is fully replicable. Choosing the

same equipment for structure manipulation and the exact same set of modification parameters (e.g., fusion current and time), ensures obtaining optical microspheres of matching metrological parameters.

- reusability – considers whether the sensor can be used again after the measurements and additionally, if it can be further utilized in modified conditions, e.g., different type of investigated environment. The presented sensor is fully reusable, until the structure or the coating will sustain damage.
- stability – specifies retention of the parameters over time. The drift of stability can provide information about the sensor's state and changes in the measured signal. The stability of the presented sensors largely depends on the stability of the light source, used to generate the signal. The measures were taken to limit the instability of the utilized system. The light sources are equipped in polarization-insensitive insulators.
- compatibility – specifies whether used sensor is suitable for a measured environment. Improper instrument can cause unforeseen reactions, causing damage to both the sensor and to the investigated medium. Considering the designed sensor, the ZnO coating can react with certain environments, however, the preliminary results indicate, negative reactions can be neutralized by applying nanocrystalline diamond sheet in addition to ZnO coating as a protective layer.
- response time – is a time lapse between the temperature change and the reading of the value [39]. Response time is dependent on multiple factors, e.g., the type of the measured medium, utilized detector. The Optical Spectrum Analyzer, which served as the detector during this research allowed to gather data every 3 s, as can be seen in Table 3.2.
- linearity – specifies consistency of the measured parameter along over the measurement range. Presented temperature sensors demonstrate high linearity from 70°C to 300°C, with a fitting coefficient of over 0.99.
- repeatability – refers to the ability to reproduce the same results during multiple measurement series, while retaining the same measurement conditions. Because of the implemented fixed cavity, the problems with allocation and displacement of the sensor are eliminated. Therefore, measurements with the designed sensor are highly repeatable.



In the literature, several solutions of the fiber-optic sensor using microsphere can be found, however none of them offer the possibility to monitor the state of their structure during the measurements. For example, He *et al.* [133] propose the application of the microsphere for measurement of the temperature, using Whispering Mode Gallery phenomenon as a basis of sensing. The authors investigate temperature change in the range of 25°C to 80°C. The sensor described in this dissertation is capable of measurements in the range of at least 30°C to 300°C. The sensor was not tested in a wider range, because of limited resources, i.e., validated measurement method.

Monteiro *et al.* [134] presents a microsphere structure, which requires to splice two fiber beforehand, then fabricate microsphere and at the end splice another optical fiber to the structure. The sensitivity of such sensor for the temperature measurements is 1.17 pm/°C. In comparison, the microsphere-based sensor with a 100 nm coating presented in this dissertation has sensitivity of almost 10000 times higher. A similar solution was proposed by Yan *et al.* [135], who utilize two tapered optical fibers to propagate light through a microsphere. Obtained sensitivity demonstrated in the paper equals 13.37pm/°C.

Chen *et al.* [79] demonstrate an air-microbubble Fabry-Pérot interferometer from the hollow core fiber. The sensitivity of such sensor reaches 2.7 nm/°C. The microsphere-based fiber-optic sensor is made from standard telecommunications, single-mode fiber and its lowest sensitivity is about 5 times higher.

## 7. CONCLUSIONS

The subject of the dissertation is “*fiber-optic sensors based on microspheres with nanocoatings*”. In the first chapter, the significance of the research is presented, as well as goals and theses, that are being proven throughout the dissertation. Temperature measurement methods, and to optimize performance of the fiber-optic sensors are described in chapter 2.

In chapter 3, the principle of operation of the microsphere-based fiber-optic sensor with ZnO ALD coatings, its fabrication, characterization is demonstrated. The validation of the microsphere-based fiber-optic sensor was executed, by performing temperature measurements. The results of the measurements are presented in chapter 4. Proposed applications of microsphere-based fiber-optic sensor are demonstrated in chapter 5.

Based on conducted research (chapter 3) as well as the results presented in chapter 4 and chapter 5, it can be concluded the following thesis was proven:

T1: Deposition of the nanocoatings on the surface of an optical microsphere integrated with a fiber-optic sensor allows to perform temperature measurements.

By depositing the ZnO ALD coating of at least 100 nm thickness on the microsphere, which forms the fiber-optic head, the temperature measurements in the temperature range of 30°C - 300°C were successfully executed.

Based on the experimental results presented in chapter 4 and chapter 5, it can be concluded the thesis T2 was proven:

T2: Application of optical microspheres of a certain geometry, allows to identify the damage sustained by the sensor during measurement execution.

Fabrication of the microsphere allowed to obtain intensity-modulated sensor, with a fixed cavity. When performing the temperature measurements, the optical power of the reflected signal provides information about the changes in the temperature occurring in the investigated medium. Simultaneously, the presence of the modulation allows to monitor the integrity of the microsphere structure in real-time.

The results of conducted research were published in many peer-reviewed international journals and they were presented at an international conferences. During doctoral studies, the author participated in international scholarship exchange program, which provided additional data to improve the quality of the study. The author has published 12 papers, of which 8 are the journals

indexed in the JCR. 6 publications, which validate the theses have been included in the dissertation. Their list is presented in chapter 8 of this work. Over the duration of doctoral studies, the author co-submitted 2 patent applications and she is participating in 2 research grants: „*Fiber-optic biosensors with metal-oxide ALD coatings*” financed by the Polish National Agency of for Academic Exchange and “*Functionalized fiber-optic sensor – optical detection method of SARS-CoV-2*” financed by Gdańsk University of Technology under the ‘Excellence Initiative - Research University’ program.

Author’s achievements include:

- Devising a method of fabrication of the optical microsphere from the end-face of the optical fiber.
- Conceiving, designing and fabricating the microsphere-based temperature sensors with a ZnO coating applied by Atomic Layer Deposition method.
- Validation of the sensors by performing experimental measurements in representative media, using representative constructions of the sensor.
- Successful application of the sensor for an *in situ* temperature monitoring of the supercapacitors
- Successful application of the sensor for measurement of the optical and thermal properties of the few-layer black phosphorus coating.

The microsphere-based fiber-optic sensors can be further developed as well as they can find many new applications. Future tasks will focus on the following issues:

1. Application of the nanocrystalline diamond sheet on the surface of the optical microsphere with a ZnO coating.

As mentioned before, ZnO coating is not compatible with all investigated media. Therefore, application of the nanocrystalline diamond sheet may be crucial, in order to protect both the construction of the sensor and the investigated medium from possible contamination by leftover particles, which can break off of the sensor. The next study will concentrate on possible methods of applying the nanocrystalline diamond sheet to the surface of the microsphere structure.



2. *In situ* simultaneous measurements of both temperature and electrochemical changes of the supercapacitors.

Simultaneous measurement of two parameters will allow to study not only influence of the changing temperature of the supercapacitor, but also other processes occurring inside the device, which will allow to better understand it, therefore providing basis for further enhancement of the technology.

## 8. LIST OF PUBLISHED PAPERS

This chapter contains the list of papers, that was decided to relate the most to the subject of this dissertation. A brief description of its content was provided for each paper.

*Description of the fabrication and characterization of the uncoated microsphere-based fiber-optic sensor and with a ZnO ALD coating thickness of 200 nm. Analysis of the results obtained from an experimental investigation of the refractive index.*

**[PL1]** Listewnik, P.; Hirsch, M.; Struk, P.; Weber, M.; Bechelany, M.; Jędrzejewska-Szczerska, M. Preparation and Characterization of Microsphere ZnO ALD Coating Dedicated for the Fiber-Optic Refractive Index Sensor. *Nanomaterials* 2019, 9, doi:10.3390/nano9020306.

*Description of the fabrication and characterization of the microsphere-based fiber-optic sensor and with ZnO ALD coatings thickness of 50 nm and 100 nm. Analysis of the results obtained from an experimental investigation of the refractive index.*

**[PL2]** Hirsch, M.; Listewnik, P.; Struk, P.; Weber, M.; Bechelany, M.; Szczerska, M. ZnO coated fiber optic microsphere sensor for the enhanced refractive index sensing. *Sensors Actuators, A Phys.* 2019, 298, doi:10.1016/j.sna.2019.111594.

*Analysis of the results from an experimental investigation of the temperature obtained with a microsphere-based fiber-optic sensor with a 200 nm ZnO ALD coating.*

**[PL3]** Listewnik, P.; Bechelany, M.; Jasinski, J.B.; Szczerska, M. ZnO ALD-coated Microsphere-Based Sensors for Temperature Measurements. *Sensors (Switzerland)* 2020, 20, 1–8, doi:10.3390/s20174689.

*Analysis of the results from an experimental investigation of the temperature obtained with a microsphere-based fiber-optic sensor with a 100 nm ZnO ALD coating.*

**[PL4]** Listewnik, P. Temperature Fiber-Optic Sensor with ZnO ALD Coating. *Eng. Proc.* 2021, 2, 99, doi:10.3390/engproc2020002099.

*Analysis of the preliminary results of the influence of nanocrystalline diamond sheet on the measured response of the Fabry-Pérot fiber-optic sensor.*

**[PL5]** Kosowska, M.; **Listewnik, P.**; Majchrowicz, D.; Rycewicz, M.; Bechelany, M.; Fleger, Y.; Chen, M.; Fixler, D.; Dholakia, K.; Szczerska, M. Microscale diamond protection for a ZnO coated fiber optic sensor. *Sci. Rep.* 2020, 10, doi:10.1038/s41598-020-76253-5.

*Analysis of the results of the optical and thermal properties of the few-layer black phosphorus coating measured with a microsphere-based fiber-optic sensor.*

**[PL6]** **Listewnik P.**; Szczerska M.; Jakóbczyk P. Measurements of the optical and thermal properties of the 2D black phosphorus coating. *Mater. Res. Express* 2021, 8, doi: 10.1088/2053-1591/ac07e2

## REFERENCES

1. Jiang, Q.; Rogez, B.; Claude, J.-B.; Baffou, G.; Wenger, J. Temperature Measurement in Plasmonic Nanoapertures Used for Optical Trapping. *ACS Photonics* **2019**, *6*, 1763–1773, doi:10.1021/acsp Photonics.9b00519.
2. Likitchatchawankun, A.; Whang, G.; Lau, J.; Munteshari, O.; Dunn, B.; Pilon, L. Effect of Temperature on Irreversible and Reversible Heat Generation Rates in Ionic Liquid-Based Electric Double Layer Capacitors. *Electrochimica Acta* **2020**, *338*, 135802, doi:10.1016/j.electacta.2020.135802.
3. Tao, P.; Chang, C.; Tong, Z.; Bao, H.; Song, C.; Wu, J.; Shang, W.; Deng, T. Magnetically-Accelerated Large-Capacity Solar-Thermal Energy Storage within High-Temperature Phase-Change Materials. *Energy Environ. Sci.* **2019**, *12*, 1613–1621, doi:10.1039/C9EE00542K.
4. Zardetto, V.; Brown, T.M.; Reale, A.; Carlo, A.D. Substrates for Flexible Electronics: A Practical Investigation on the Electrical, Film Flexibility, Optical, Temperature, and Solvent Resistance Properties. *Journal of Polymer Science Part B: Polymer Physics* **2011**, *49*, 638–648, doi:https://doi.org/10.1002/polb.22227.
5. Schmitz, J. Low Temperature Thin Films for Next-Generation Microelectronics (Invited). *Surface and Coatings Technology* **2018**, *343*, 83–88, doi:10.1016/j.surfcoat.2017.11.013.
6. Mitic, V.V.; Ribar, S.; Randjelovic, B.; Lu, C.-A.; Radovic, I.; Stajcic, A.; Novakovic, I.; Vlahovic, B. Neural Networks and Microelectronics Parameters Distribution Measurements Depending on Sintering Temperature and Applied Voltage. *Mod. Phys. Lett. B* **2020**, *34*, 2150172, doi:10.1142/S0217984921501724.
7. Hook, M.D.; Mayer, M. Miniature Environmental Chambers for Temperature Humidity Bias Testing of Microelectronics. *Review of Scientific Instruments* **2017**, *88*, 034707, doi:10.1063/1.4978916.
8. Mahadeva, S.K.; Yun, S.; Kim, J. Flexible Humidity and Temperature Sensor Based on Cellulose–Polypyrrole Nanocomposite. *Sensors and Actuators A: Physical* **2011**, *165*, 194–199, doi:10.1016/j.sna.2010.10.018.
9. Rongen, R.; van IJzerloo, A.; Mavinkurve, A.; O’Halloran, G.M. Degradation of Cu-Al Wire Bonded Contacts under High Current and High Temperature Conditions Using in-Situ Resistance Monitoring. In Proceedings of the 2015 IEEE 65th Electronic Components and Technology Conference (ECTC); May **2015**; pp. 1396–1402.
10. Degrenne, N.; Mollov, S. On-Line Health Monitoring of Wire-Bonded IGBT Power Modules Using On-State Voltage at Zero-Temperature-Coefficient. In Proceedings of the PCIM Europe 2018; International Exhibition and Conference for Power Electronics, Intelligent Motion, Renewable Energy and Energy Management; June **2018**; pp. 1–7.
11. Lu, L.; Zhang, S.; Xu, J.; He, H.; Zhao, X. Numerical Study of Titanium Melting by High Frequency Inductive Heating. *International Journal of Heat and Mass Transfer* **2017**, *108*, 2021–2028, doi:10.1016/j.ijheatmasstransfer.2017.01.062.

12. Kreczanik, P.; Venet, P.; Hijazi, A.; Clerc, G. Study of Supercapacitor Aging and Lifetime Estimation According to Voltage, Temperature, and RMS Current. *IEEE Transactions on Industrial Electronics* **2014**, *61*, 4895–4902, doi:10.1109/TIE.2013.2293695.
13. Zhang, X.; Chang, X.; Shen, Y.; Xiang, Y. Electrochemical-Electrical-Thermal Modeling of a Pouch-Type Lithium Ion Battery: An Application to Optimize Temperature Distribution. *Journal of Energy Storage* **2017**, *11*, 249–257, doi:10.1016/j.est.2017.03.008.
14. Yang, H. Effects of Aging and Temperature on Supercapacitor Charge Capacity. In Proceedings of the 2020 IEEE Power Energy Society General Meeting (PESGM); August **2020**; pp. 1–5.
15. Ruiz, V.; Huynh, T.; R. Sivakkumar, S.; G. Pandolfo, A. Ionic Liquid – Solvent Mixtures as Supercapacitor Electrolytes for Extreme Temperature Operation. *RSC Advances* **2012**, *2*, 5591–5598, doi:10.1039/C2RA20177A.
16. Xiong, G.; Kundu, A.; Fisher, T.S. Influence of Temperature on Supercapacitor Performance. In *Thermal Effects in Supercapacitors*; SpringerBriefs in Applied Sciences and Technology; Springer International Publishing: Cham, **2015**; pp. 71–114 ISBN 978-3-319-20241-9.
17. Usamentiaga, R.; Venegas, P.; Guerediaga, J.; Vega, L.; Molleda, J.; Bulnes, F.G. Infrared Thermography for Temperature Measurement and Non-Destructive Testing. *Sensors* **2014**, *14*, 12305–12348, doi:10.3390/s140712305.
18. Liu, H.; Sun, W.; Xu, S. An Extremely Simple Thermocouple Made of a Single Layer of Metal. *Advanced Materials* **2012**, *24*, 3275–3279, doi:https://doi.org/10.1002/adma.201200644.
19. Kus, A.; Isik, Y.; Cakir, M.C.; Coşkun, S.; Özdemir, K. Thermocouple and Infrared Sensor-Based Measurement of Temperature Distribution in Metal Cutting. *Sensors* **2015**, *15*, 1274–1291, doi:10.3390/s150101274.
20. Thermoelectric Response of a Screen Printed Silver-Nickel Thermocouple. *Materials Science and Engineering: B* **2021**, *264*, 114929, doi:10.1016/j.mseb.2020.114929.
21. Wang, Q.; Gao, M.; Zhang, L.; Deng, Z.; Gui, L. A Handy Flexible Micro-Thermocouple Using Low-Melting-Point Metal Alloys. *Sensors* **2019**, *19*, 314, doi:10.3390/s19020314.
22. Tang, Y.-Q.; Fang, W.-Z.; Lin, H.; Tao, W.-Q. Thin Film Thermocouple Fabrication and Its Application for Real-Time Temperature Measurement inside PEMFC. *International Journal of Heat and Mass Transfer* **2019**, *141*, 1152–1158, doi:10.1016/j.ijheatmasstransfer.2019.07.048.
23. Turkani, V.S.; Maddipatla, D.; Narakathu, B.B.; Altay, B.N.; Fleming, P.D.; Bazuin, B.J.; Atashbar, M.Z. Nickel Based RTD Fabricated via Additive Screen Printing Process for Flexible Electronics. *IEEE Access* **2019**, *7*, 37518–37527, doi:10.1109/ACCESS.2019.2904970.
24. Chauhan, J.; Neelakantan, U. An Experimental Approach for Precise Temperature Measurement Using Platinum RTD PT1000. In Proceedings of the 2016 International Conference on Electrical, Electronics, and Optimization Techniques (ICEEOT); March **2016**; pp. 3213–3215.
25. Blasdel, N.J.; Wujcik, E.K.; Carletta, J.E.; Lee, K.-S.; Monty, C.N. Fabric Nanocomposite Resistance Temperature Detector. *IEEE Sensors Journal* **2015**, *15*, 300–306, doi:10.1109/JSEN.2014.2341915.



26. Malini, T.; Sudha, R.; Anantha Christu Raj, P.; Stalin, B. The Role of RTD and Liquid Sensors in Electric Arc Furnace for Melting of Aluminium. *Materials Today: Proceedings* **2020**, *33*, 4793–4796, doi:10.1016/j.matpr.2020.08.371.
27. Jemaa, S.B.; Sylvestre, J.; Gagnon, P. Integrated RTD Sensors for Maintaining Thermal Uniformity During TCB Process. In Proceedings of the 2019 IEEE 69th Electronic Components and Technology Conference (ECTC); May **2019**; pp. 1744–1750.
28. Wei, S.; Qin, W.; Han, L.; Cheng, F. The Research on Compensation Algorithm of Infrared Temperature Measurement Based on Intelligent Sensors. *Cluster Comput* **2019**, *22*, 6091–6100, doi:10.1007/s10586-018-1828-5.
29. Wildermuth, S.; Szasz, P.; Gebhardt, J.; Kaul, H.; Koenig, K. Infrared Temperature Sensing in Electrical Equipment by Low-Cost IR Cameras. In Proceedings of the VDE High Voltage Technology 2018; ETG-Symposium; November **2018**; pp. 1–5.
30. aan de Stegge, W.B.; Mejaiti, N.; van Netten, J.J.; Dijkgraaf, M.G.W.; van Baal, J.G.; Busch-Westbroek, T.E.; Bus, S.A. The Cost-Effectiveness and Cost-Utility of at-Home Infrared Temperature Monitoring in Reducing the Incidence of Foot Ulcer Recurrence in Patients with Diabetes (DIATEMP): Study Protocol for a Randomized Controlled Trial. *Trials* **2018**, *19*, 520, doi:10.1186/s13063-018-2890-2.
31. Lahiri, B.B.; Bagavathiappan, S.; Jayakumar, T.; Philip, J. Medical Applications of Infrared Thermography: A Review. *Infrared Physics & Technology* **2012**, *55*, 221–235, doi:10.1016/j.infrared.2012.03.007.
32. Chiavaioli, F.; Gouveia, C.A.J.; Jorge, P.A.S.; Baldini, F. Towards a Uniform Metrological Assessment of Grating-Based Optical Fiber Sensors: From Refractometers to Biosensors. *Biosensors (Basel)* **2017**, *7*, doi:10.3390/bios7020023.
33. Hromadka, J.; Mohd Hazlan, N.N.; Hernandez, F.U.; Correia, R.; Norris, A.; Morgan, S.P.; Korposh, S. Simultaneous in Situ Temperature and Relative Humidity Monitoring in Mechanical Ventilators Using an Array of Functionalised Optical Fibre Long Period Grating Sensors. *Sensors and Actuators B: Chemical* **2019**, *286*, 306–314, doi:10.1016/j.snb.2019.01.124.
34. Yu, Q.; Zhou, X. Pressure Sensor Based on the Fiber-Optic Extrinsic Fabry-Perot Interferometer. *Photonic Sens* **2011**, *1*, 72–83, doi:10.1007/s13320-010-0017-9.
35. García, Y.R.; Corres, J.M.; Goicoechea, J. Vibration Detection Using Optical Fiber Sensors. *Journal of Sensors* **2010**, *2010*, e936487, doi:10.1155/2010/936487.
36. Fernandez-Vallejo, M.; Lopez-Amo, M. Optical Fiber Networks for Remote Fiber Optic Sensors. *Sensors* **2012**, *12*, 3929–3951, doi:10.3390/s120403929.
37. Aliyu, F.; Sheltami, T. Development of an Energy-Harvesting Toxic and Combustible Gas Sensor for Oil and Gas Industries. *Sensors and Actuators B: Chemical* **2016**, *231*, 265–275, doi:10.1016/j.snb.2016.03.037.

38. Ren, L.; Jiang, T.; Jia, Z.; Li, D.; Yuan, C.; Li, H. Pipeline Corrosion and Leakage Monitoring Based on the Distributed Optical Fiber Sensing Technology. *Measurement* **2018**, *122*, 57–65, doi:10.1016/j.measurement.2018.03.018.
39. Izawa, K.; Ulmer, H.; Staerz, A.; Weimar, U.; Barsan, N. 5 - Application of SMOX-based sensors. In *Gas Sensors Based on Conducting Metal Oxides*; Barsan, N., Schierbaum, K., Eds.; Metal Oxides; Elsevier, **2019**; pp. 217–257 ISBN 978-0-12-811224-3.
40. Mikolajek, M.; Martinek, R.; Koziorek, J.; Hejduk, S.; Vitasek, J.; Vanderka, A.; Poboril, R.; Vasinek, V.; Hercik, R. Temperature Measurement Using Optical Fiber Methods: Overview and Evaluation. *Journal of Sensors* **2020**, *2020*, e8831332, doi:10.1155/2020/8831332.
41. Wilson, B.A.; Blue, T.E. Quasi-Distributed Temperature Sensing Using Type-II Fiber Bragg Gratings in Sapphire Optical Fiber to Temperatures up to 1300°C. *IEEE Sensors Journal* **2018**, *18*, 8345–8351, doi:10.1109/JSEN.2018.2865910.
42. Wang, P.; Liu, J.; Song, F.; Zhao, H. Quasi-Distributed Temperature Measurement for Stator Bars in Large Generator via Use of Fiber Bragg Gratings. In Proceedings of the Proceedings of 2011 6th International Forum on Strategic Technology; August **2011**; Vol. 2, pp. 810–813.
43. Giurgiutiu, V. 17 - Structural health monitoring (SHM) of aerospace composites. In *Polymer Composites in the Aerospace Industry (Second Edition)*; Irving, P., Soutis, C., Eds.; Woodhead Publishing Series in Composites Science and Engineering; Woodhead Publishing, **2020**; pp. 491–558 ISBN 978-0-08-102679-3.
44. Gao, X.; Ning, T.; Zhang, C.; Xu, J.; Zheng, J.; Lin, H.; Li, J.; Pei, L.; You, H. A Dual-Parameter Fiber Sensor Based on Few-Mode Fiber and Fiber Bragg Grating for Strain and Temperature Sensing. *Optics Communications* **2020**, *454*, 124441, doi:10.1016/j.optcom.2019.124441.
45. Cheng, P.; Wang, L.; Pan, Y.; Yan, H.; Gao, D.; Wang, J.; Zhang, H. Fiber Bragg Grating Temperature Sensor of Cladding with SrTiO<sub>3</sub> Thin Film by Pulsed Laser Deposition. *Laser Phys.* **2019**, *29*, 025107, doi:10.1088/1555-6611/aaf635.
46. Dong, Y.; Xiao, S.; Wu, B.; Xiao, H.; Jian, S. Refractive Index and Temperature Sensor Based on D-Shaped Fiber Combined With a Fiber Bragg Grating. *IEEE Sensors Journal* **2019**, *19*, 1362–1367, doi:10.1109/JSEN.2018.2880305.
47. Feng, Y.; Zhang, H.; Li, Y.; Rao, C. Temperature Sensing of Metal-Coated Fiber Bragg Grating. *IEEE/ASME Transactions on Mechatronics* **2010**, *15*, 511–519, doi:10.1109/TMECH.2010.2047111.
48. Kim, Kwang Taek Quasi-Distributed Temperature Sensor Based on a V-Grooved Single-Mode Optical Fiber Covered with Ethylene Vinyl Acetate. *센서학회지* **2014**, *23*, 229–233, doi:10.5369/JSST.2014.23.4.229.
49. Zhou, X.; Li, L.; Yu, Q. Fiber Bragg Grating-Based Quasi-Distributed Temperature Sensor for Down-Hole Monitoring. *Sensor Letters* **2012**, *10*, 1486–1490, doi:10.1166/sl.2012.2486.
50. Pelegrin, J. de; Bazzo, J.P.; Vieira da Costa, I.B.; Martelli, C.; Pipa, D.R.; Cardozo da Silva, J.C. Total Variation Deconvolution of Raman Distributed Temperature Sensing Signals. In Proceedings of the



2019 SBMO/IEEE MTT-S International Microwave and Optoelectronics Conference (IMOC); November **2019**; pp. 1–3.

51. Ukil, A.; Braendle, H.; Krippner, P. Distributed Temperature Sensing: Review of Technology and Applications. *IEEE Sensors Journal* **2012**, *12*, 885–892, doi:10.1109/JSEN.2011.2162060.

52. Liu, Y.; Ma, L.; Yang, C.; Tong, W.; He, Z. Long-Range Raman Distributed Temperature Sensor with High Spatial and Temperature Resolution Using Graded-Index Few-Mode Fiber. *Opt. Express* **2018**, *26*, 20562, doi:10.1364/OE.26.020562.

53. Failleau, G.; Beaumont, O.; Razouk, R.; Delepine-Lesoille, S.; Landolt, M.; Courthial, B.; Hénault, J.M.; Martinot, F.; Bertrand, J.; Hay, B. A Metrological Comparison of Raman-Distributed Temperature Sensors. *Measurement* **2018**, *116*, 18–24, doi:10.1016/j.measurement.2017.10.041.

54. Amira, Z.; Bouyahi, M.; Ezzedine, T. Measurement of Temperature through Raman Scattering. *Procedia Computer Science* **2015**, *73*, 350–357, doi:10.1016/j.procs.2015.12.003.

55. Toccafondo, I.; Nannipieri, T.; Signorini, A.; Guillermain, E.; Kuhnenn, J.; Brugger, M.; Pasquale, F.D. Raman Distributed Temperature Sensing at CERN. *IEEE Photonics Technology Letters* **2015**, *27*, 2182–2185, doi:10.1109/LPT.2015.2456029.

56. Ouyang, J.; Chen, X.; Huangfu, Z.; Lu, C.; Huang, D.; Li, Y. Application of Distributed Temperature Sensing for Cracking Control of Mass Concrete. *Construction and Building Materials* **2019**, *197*, 778–791, doi:10.1016/j.conbuildmat.2018.11.221.

57. Yan, B.; Li, J.; Zhang, M.; Zhang, J.; Qiao, L.; Wang, T. Raman Distributed Temperature Sensor with Optical Dynamic Difference Compensation and Visual Localization Technology for Tunnel Fire Detection. *Sensors* **2019**, *19*, 2320, doi:10.3390/s19102320.

58. Dong, Y. High-Performance Distributed Brillouin Optical Fiber Sensing. *Photonic Sens* **2021**, *11*, 69–90, doi:10.1007/s13320-021-0616-7.

59. Rossi, L.; Marini, D.; Bastianini, F.; Bolognini, G. Analysis of Enhanced-Performance Fibre Brillouin Ring Laser for Brillouin Sensing Applications. *Opt. Express* **2019**, *27*, 29448, doi:10.1364/OE.27.029448.

60. Zhang, Z.; Lu, Y.; Tanaka, Y.; Peng, J.; Zhuang, Z. Discriminative Sensing of Temperature and Acoustic Impedance by Using Forward Brillouin Scattering in Large Effective Area Fiber. *Appl. Phys. Express* **2021**, *14*, 042004, doi:10.35848/1882-0786/abebb2.

61. Palmieri, L. Distributed Optical Fiber Sensing Based on Rayleigh Scattering. *TOOPTSJ* **2013**, *7*, 104–127, doi:10.2174/1874328501307010104.

62. Wang, M.; Zhao, K.; Huang, S.; Wu, J.; Lu, P.; Ohodnicki, P.R.; Lu, P.; Li, M.-J.; Mihailov, S.J.; Chen, K.P. Reel-to-Reel Fabrication of In-Fiber Low-Loss and High-Temperature Stable Rayleigh Scattering Centers for Distributed Sensing. *IEEE Sensors Journal* **2020**, *20*, 11335–11341, doi:10.1109/JSEN.2020.2995606.

63. Wu, H.; Feder, K.S.; Stolov, A.A.; Shenk, S.D.; Monberg, E.M.; Simoff, D.A. High-Temperature Enhanced Rayleigh Scattering Optical Fiber Sensor for Borehole Applications. In Proceedings of the

Optical Components and Materials XVII; Dignonnet, M.J., Jiang, S., Eds.; SPIE: San Francisco, United States, March 3 **2020**; p. 32.

64. Wu, H.; Stolov, A.; Feder, K. Optical Fiber as Distributed Acoustic Sensing Element with Improved Rayleigh Backscattering Sensitivity and Robustness under Elevated Temperature. In Proceedings of the Optical Fibers and Sensors for Medical Diagnostics, Treatment and Environmental Applications XXI; Gannot, I., Roodenko, K., Eds.; SPIE: Online Only, United States, March 5 **2021**; p. 13.

65. Lee, B.H.; Kim, Y.H.; Park, K.S.; Eom, J.B.; Kim, M.J.; Rho, B.S.; Choi, H.Y. Interferometric Fiber Optic Sensors. *Sensors* **2012**, *12*, 2467–2486, doi:10.3390/s120302467.

66. Zhu, T.; Wu, D.; Liu, M.; Duan, D.-W. In-Line Fiber Optic Interferometric Sensors in Single-Mode Fibers. *Sensors* **2012**, *12*, 10430–10449, doi:10.3390/s120810430.

67. Guha, B.; Gondarenko, A.; Lipson, M. Minimizing Temperature Sensitivity of Silicon Mach-Zehnder Interferometers. *Opt. Express* **2010**, *18*, 1879, doi:10.1364/OE.18.001879.

68. Jiang, L.; Yang, J.; Wang, S.; Li, B.; Wang, M. Fiber Mach-Zehnder Interferometer Based on Microcavities for High-Temperature Sensing with High Sensitivity. *Opt. Lett., OL* **2011**, *36*, 3753–3755, doi:10.1364/OL.36.003753.

69. Geng, Y.; Li, X.; Tan, X.; Deng, Y.; Yu, Y. High-Sensitivity Mach-Zehnder Interferometric Temperature Fiber Sensor Based on a Waist-Enlarged Fusion Bitaper. *IEEE Sensors Journal* **2011**, *11*, 2891–2894, doi:10.1109/JSEN.2011.2146769.

70. Zhang, J.; Sun, H.; Wang, R.; Su, D.; Guo, T.; Feng, Z.; Hu, M.; Qiao, X. Simultaneous Measurement of Refractive Index and Temperature Using a Michelson Fiber Interferometer With a Hi-Bi Fiber Probe. *IEEE Sensors Journal* **2013**, *13*, 2061–2065, doi:10.1109/JSEN.2013.2237898.

71. Zhao, Y.; Dai, M.; Chen, Z.; Liu, X.; Gandhi, M.S.A.; Li, Q.; Fu, H.Y. Ultrasensitive Temperature Sensor with Vernier-Effect Improved Fiber Michelson Interferometer. *Opt. Express* **2021**, *29*, 1090, doi:10.1364/OE.415857.

72. Han, Y.; Liu, B.; Wu, Y.; Mao, Y.; Zhao, L.; Nan, T.; Wang, J.; Zhang, Y.; Tang, R.; Liu, Y.; et al. High-Sensitivity High-Temperature Sensor Based on Multi-Microspheres Improved Michelson Interferometer. *Optics Communications* **2021**, *491*, 126932, doi:10.1016/j.optcom.2021.126932.

73. Shi, J.; Wang, Y.; Xu, D.; Zhang, H.; Su, G.; Duan, L.; Yan, C.; Yan, D.; Fu, S.; Yao, J. Temperature Sensor Based on Fiber Ring Laser With Sagnac Loop. *IEEE Photonics Technology Letters* **2016**, *28*, 794–797, doi:10.1109/LPT.2015.2514105.

74. Cui, Y.; Shum, P.P.; Hu, D.J.J.; Wang, G.; Humbert, G.; Dinh, X.-Q. Temperature Sensor by Using Selectively Filled Photonic Crystal Fiber Sagnac Interferometer. *IEEE Photonics Journal* **2012**, *4*, 1801–1808, doi:10.1109/JPHOT.2012.2217945.

75. Zhang, J.; Qiao, X.; Guo, T.; Weng, Y.; Wang, R.; Ma, Y.; Rong, Q.; Hu, M.; Feng, Z. Highly Sensitive Temperature Sensor Using PANDA Fiber Sagnac Interferometer. *J. Lightwave Technol., JLT* **2011**, *29*, 3640–3644.

76. Liu, Q.; Li, S.-G.; Chen, H. Enhanced Sensitivity of Temperature Sensor by a PCF with a Defect Core Based on Sagnac Interferometer. *Sensors and Actuators B: Chemical* **2018**, *254*, 636–641, doi:10.1016/j.snb.2017.07.120.
77. Mathew, J.; Schneller, O.; Polyzos, D.; Havermann, D.; Carter, R.M.; MacPherson, W.N.; Hand, D.P.; Maier, R.R.J. In-Fiber Fabry–Perot Cavity Sensor for High-Temperature Applications. *Journal of Lightwave Technology* **2015**, *33*, 2419–2425, doi:10.1109/JLT.2015.2397936.
78. Zhu, C.; Zhuang, Y.; Zhang, B.; Muhammad, R.; Wang, P.P.; Huang, J. A Miniaturized Optical Fiber Tip High-Temperature Sensor Based on Concave-Shaped Fabry–Perot Cavity. *IEEE Photonics Technology Letters* **2019**, *31*, 35–38, doi:10.1109/LPT.2018.2881721.
79. Chen, M.; Zhao, Y.; Xia, F.; Peng, Y.; Tong, R. High Sensitivity Temperature Sensor Based on Fiber Air-Microbubble Fabry-Perot Interferometer with PDMS-Filled Hollow-Core Fiber. *Sensors and Actuators A: Physical* **2018**, *275*, 60–66, doi:10.1016/j.sna.2018.03.044.
80. Liang, H.; Jia, P.; Liu, J.; Fang, G.; Li, Z.; Hong, Y.; Liang, T.; Xiong, J. Diaphragm-Free Fiber-Optic Fabry-Perot Interferometric Gas Pressure Sensor for High Temperature Application. *Sensors* **2018**, *18*, 1011, doi:10.3390/s18041011.
81. Wang, M.; Yang, Y.; Yang, Y.; Huang, S.; Wu, J.; Zhao, K.; Li, Y.; Peng, Z.; Zou, R.; Lan, H.; et al. Multiplexable High-Temperature Stable and Low-Loss Intrinsic Fabry-Perot in-Fiber Sensors through Nanograting Engineering. *Opt. Express, OE* **2020**, *28*, 20225–20235, doi:10.1364/OE.395382.
82. Wang, Y.; Thipparapu, N.K.; Wang, S.; Barua, P.; Richardson, D.J.; Sahu, J.K. Study on the Temperature Dependent Characteristics of O-Band Bismuth-Doped Fiber Amplifier. *Opt. Lett., OL* **2019**, *44*, 5650–5653, doi:10.1364/OL.44.005650.
83. Wang, Y.; Yang, M.; Wang, D.N.; Liao, C.R. Selectively Infiltrated Photonic Crystal Fiber With Ultrahigh Temperature Sensitivity. *IEEE Photonics Technology Letters* **2011**, *23*, 1520–1522, doi:10.1109/LPT.2011.2163705.
84. Zhang, Z.; Liao, C.; Tang, J.; Wang, Y.; Bai, Z.; Li, Z.; Guo, K.; Deng, M.; Cao, S.; Wang, Y. Hollow-Core-Fiber-Based Interferometer for High-Temperature Measurements. *IEEE Photonics Journal* **2017**, *9*, 1–9, doi:10.1109/JPHOT.2017.2671437.
85. Zou, W.; He, Z.; Hotate, K. Demonstration of Brillouin Distributed Discrimination of Strain and Temperature Using a Polarization-Maintaining Optical Fiber. *IEEE Photonics Technology Letters* **2010**, *22*, 526–528, doi:10.1109/LPT.2010.2041922.
86. Xing, R.; Dong, C.; Wang, Z.; Wu, Y.; Yang, Y.; Jian, S. Simultaneous Strain and Temperature Sensor Based on Polarization Maintaining Fiber and Multimode Fiber. *Optics & Laser Technology* **2018**, *102*, 17–21, doi:10.1016/j.optlastec.2017.12.013.
87. Zhu, G. High Efficiency Pump Combiner Fabricated by CO2 Laser Splicing System. In Proceedings of the Components and Packaging for Laser Systems IV; Glebov, A.L., Leisher, P.O., Eds.; SPIE: San Francisco, United States, February 20 **2018**; p. 46.

88. Zhou, X.; Chen, Z.; Chen, H.; Hou, J. Fusion Splicing Small-Core Photonic Crystal Fibers and Single-Mode Fibers by Controlled Air Hole Collapse. *Optics Communications* **2012**, *285*, 5283–5286, doi:10.1016/j.optcom.2012.06.090.
89. Zhao, L.; Jiang, L.; Wang, S.; Xiao, H.; Lu, Y.; Tsai, H.-L. A High-Quality Mach-Zehnder Interferometer Fiber Sensor by Femtosecond Laser One-Step Processing. *Sensors* **2011**, *11*, 54–61, doi:10.3390/s110100054.
90. Dai, Y.; Yang, M.; Xu, G.; Yuan, Y. Magnetic Field Sensor Based on Fiber Bragg Grating with a Spiral Microgroove Ablated by Femtosecond Laser. *Opt. Express* **2013**, *21*, 17386, doi:10.1364/OE.21.017386.
91. Liao, C.R.; Wang, D.N.; Wang, M.; Yang, M. Fiber In-Line Michelson Interferometer Tip Sensor Fabricated by Femtosecond Laser. *IEEE Photonics Technology Letters* **2012**, *24*, 2060–2063, doi:10.1109/LPT.2012.2219517.
92. Kbashi, H.J. Fabrication of Submicron-Diameter and Taper Fibers Using Chemical Etching. *Journal of Materials Science & Technology* **2012**, *28*, 308–312, doi:10.1016/S1005-0302(12)60059-0.
93. Sun, X.; Dong, X.; Hu, Y.; Li, H.; Chu, D.; Zhou, J.; Wang, C.; Duan, J. A Robust High Refractive Index Sensitivity Fiber Mach-Zehnder Interferometer Fabricated by Femtosecond Laser Machining and Chemical Etching. *Sensors and Actuators A: Physical* **2015**, *230*, 111–116, doi:10.1016/j.sna.2015.04.006.
94. Liao, C.R.; Hu, T.Y.; Wang, D.N. Optical Fiber Fabry-Perot Interferometer Cavity Fabricated by Femtosecond Laser Micromachining and Fusion Splicing for Refractive Index Sensing. *Opt. Express* **2012**, *20*, 22813, doi:10.1364/OE.20.022813.
95. Yuan, L.; Huang, J.; Lan, X.; Wang, H.; Jiang, L.; Xiao, H. All-in-Fiber Optofluidic Sensor Fabricated by Femtosecond Laser Assisted Chemical Etching. *Opt. Lett., OL* **2014**, *39*, 2358–2361, doi:10.1364/OL.39.002358.
96. Ma, T.; Yuan, J.; Sun, L.; Kang, Z.; Yan, B.; Sang, X.; Wang, K.; Wu, Q.; Liu, H.; Gao, J.; et al. Simultaneous Measurement of the Refractive Index and Temperature Based on Microdisk Resonator With Two Whispering-Gallery Modes. *IEEE Photonics Journal* **2017**, *9*, 1–13, doi:10.1109/JPHOT.2017.2648259.
97. Luo, R.; Jiang, H.; Liang, H.; Chen, Y.; Lin, Q. Self-Referenced Temperature Sensing with a Lithium Niobate Microdisk Resonator. *Opt. Lett., OL* **2017**, *42*, 1281–1284, doi:10.1364/OL.42.001281.
98. Wang, C.-T.; Wang, C.-Y.; Yu, J.-H.; Kuo, I.-T.; Tseng, C.-W.; Jau, H.-C.; Chen, Y.-J.; Lin, T.-H. Highly Sensitive Optical Temperature Sensor Based on a SiN Micro-Ring Resonator with Liquid Crystal Cladding. *Opt. Express* **2016**, *24*, 1002, doi:10.1364/OE.24.001002.
99. Rostami, A.; Ahmadi, H.; Heidarzadeh, H.; Taghipour, A. Microsphere and Fiber Optics based Optical Sensors. In *Optical Sensors - New Developments and Practical Applications*; Yasin, Moh., Ed.; InTech, **2014** ISBN 978-953-51-1233-4.





100. Lei, F.; Murphy, R.M.J.; Ward, J.M.; Yang, Y.; Nic Chormaic, S. Bandpass Transmission Spectra of a Whispering-Gallery Microcavity Coupled to an Ultrathin Fiber. *Photon. Res.* **2017**, *5*, 362, doi:10.1364/PRJ.5.000362.
101. Kou, J.; Feng, J.; Ye, L.; Xu, F.; Lu, Y. Miniaturized Fiber Taper Reflective Interferometer for High Temperature Measurement. *Opt. Express* **2010**, *18*, 14245, doi:10.1364/OE.18.014245.
102. Rahman, A. Temperature Sensor Based on Dielectric Optical Microresonator. *Optical Fiber Technology* **2011**, *17*, 536–540, doi:10.1016/j.yofte.2011.06.014.
103. Tan, X.; Li, X.; Geng, Y.; Yin, Z.; Wang, L.; Wang, W.; Deng, Y. Polymer Microbubble-Based Fabry–Perot Fiber Interferometer and Sensing Applications. *IEEE Photon. Technol. Lett.* **2015**, *27*, 2035–2038, doi:10.1109/LPT.2015.2449654.
104. Zhang, C.-L.; Gong, Y.; Zou, W.-L.; Wu, Y.; Rao, Y.-J.; Peng, G.-D.; Fan, X. Microbubble-Based Fiber Optofluidic Interferometer for Sensing. *Journal of Lightwave Technology* **2017**, *35*, 2514–2519, doi:10.1109/JLT.2017.2696957.
105. Gomes, A.D.; Monteiro, C.S.; Silveira, B.; Frazão, O. A Brief Review of New Fiber Microsphere Geometries. *Fibers* **2018**, *6*, 48, doi:10.3390/fib6030048.
106. Mishra, V.; Lohar, M.; Amphawan, A. Improvement in Temperature Sensitivity of FBG by Coating of Different Materials. *Optik* **2016**, *127*, 825–828, doi:10.1016/j.ijleo.2015.10.014.
107. Grosso, D. How to Exploit the Full Potential of the Dip-Coating Process to Better Control Film Formation. *J. Mater. Chem.* **2011**, *21*, 17033, doi:10.1039/c1jm12837j.
108. Johnson, R.W.; Hultqvist, A.; Bent, S.F. A Brief Review of Atomic Layer Deposition: From Fundamentals to Applications. *Materials Today* **2014**, *17*, 236–246, doi:10.1016/j.mattod.2014.04.026.
109. Sarakinos, K.; Alami, J.; Konstantinidis, S. High Power Pulsed Magnetron Sputtering: A Review on Scientific and Engineering State of the Art. *Surface and Coatings Technology* **2010**, *204*, 1661–1684, doi:10.1016/j.surfcoat.2009.11.013.
110. Barranco, A.; Borrás, A.; Gonzalez-Elipe, A.R.; Palmero, A. Perspectives on Oblique Angle Deposition of Thin Films: From Fundamentals to Devices. *Progress in Materials Science* **2016**, *76*, 59–153, doi:10.1016/j.pmatsci.2015.06.003.
111. Chapeleau, X.; Leduc, D.; Lupi, C.; Gaillard, V.; Boisrobert, C. Low Coherence Interferometry. In *Measurements using Optic and RF Waves*; John Wiley & Sons, Ltd; pp. 81–111 ISBN 978-1-118-58622-8.
112. Benítez, J.; Bolea, M.; Mora, J. High-Performance Low Coherence Interferometry Using SSB Modulation. *IEEE Photonics Technology Letters* **2017**, *29*, 90–93, doi:10.1109/LPT.2016.2628963.
113. Borgetto, N.; Galizzi, C.; André, F.; Escudié, D. A Thickness Measurement Technique Based on Low-Coherence Interferometry Applied to a Liquid Film with Thermal Gradient. *Experimental Thermal and Fluid Science* **2010**, *34*, 1242–1246, doi:10.1016/j.expthermflusci.2010.05.004.

114. Dyott, R.H. *Elliptical Fiber Waveguides*; Artech House Publishers, **1995**; ISBN 978-0-89006-477-1.
115. Li, X.; Lin, S.; Liang, J.; Zhang, Y.; Oigawa, H.; Ueda, T. Fiber-Optic Temperature Sensor Based on Difference of Thermal Expansion Coefficient Between Fused Silica and Metallic Materials. *IEEE Photonics Journal* **2012**, *4*, 155–162, doi:10.1109/JPHOT.2011.2181943.
116. Experimental Study on Thermal Expansion Coefficient of Composite Multi-Layered Flaky Gun Propellants. *Composites Part B: Engineering* **2019**, *166*, 428–435, doi:10.1016/j.compositesb.2019.02.024.
117. Singh, M.; Singh, M. Thermal Expansion in Zinc Oxide Nanomaterials. *Nanoscience and Nanotechnology Research* **2013**, *1*, 27–29, doi:10.12691/nnr-1-2-4.
118. Qiu, K.; Zhao, Y.; Gao, Y.; Liu, X.; Ji, X.; Cao, S.; Tang, J.; Sun, Y.; Zhang, D.; Feng, B.; et al. Refractive Index of a Single ZnO Microwire at High Temperatures. *Appl. Phys. Lett.* **2014**, *104*, 081109, doi:10.1063/1.4866668.
119. Pilz, J.; Perrotta, A.; Christian, P.; Tazreiter, M.; Resel, R.; Leising, G.; Griesser, T.; Coclite, A.M. Tuning of Material Properties of ZnO Thin Films Grown by Plasma-Enhanced Atomic Layer Deposition at Room Temperature. *Journal of Vacuum Science & Technology A* **2017**, *36*, 01A109, doi:10.1116/1.5003334.
120. Boland, M.; Mitsuhashi, T.; Naito, T.; Wootton, K. Intensity Imbalance Optical Interferometer Beam Size Monitor.; **2012**; p. WECC03.
121. Wu, J.; Dhingra, R.; Gambhir, M.; Remais, J.V. Sensitivity Analysis of Infectious Disease Models: Methods, Advances and Their Application. *Journal of The Royal Society Interface* **2013**, *10*, 20121018, doi:10.1098/rsif.2012.1018.
122. Regtien, P.; Dertien, E. 3 - Uncertainty aspects. In *Sensors for Mechatronics (Second Edition)*; Regtien, P., Dertien, E., Eds.; Elsevier, **2018**; pp. 39–60 ISBN 978-0-12-813810-6.
123. Kreinovich, V. How to Define Relative Approximation Error of an Interval Estimate: A Proposal. *ams* **2013**, *7*, 211–216, doi:10.12988/ams.2013.13019.
124. Tan, C.-Y.; Huang, Y.-X. Dependence of Refractive Index on Concentration and Temperature in Electrolyte Solution, Polar Solution, Nonpolar Solution, and Protein Solution. *J. Chem. Eng. Data* **2015**, *60*, 2827–2833, doi:10.1021/acs.jced.5b00018.
125. Bogdanowicz, R.; Dettlaff, A.; Skiba, F.; Trzcinski, K.; Szkoda, M.; Sobaszek, M.; Ficek, M.; Dec, B.; Macewicz, L.; Wyrębski, K.; et al. Enhanced Charge Storage Mechanism and Long-Term Cycling Stability in Diamondized Titania Nanocomposite Supercapacitors Operating in Aqueous Electrolytes. *J. Phys. Chem. C* **2020**, *124*, 15698–15712, doi:10.1021/acs.jpcc.0c02792.
126. Hultqvist, A.; Aitola, K.; Sveinbjörnsson, K.; Saki, Z.; Larsson, F.; Törndahl, T.; Johansson, E.; Boschloo, G.; Edoff, M. Atomic Layer Deposition of Electron Selective SnO<sub>x</sub> and ZnO Films on Mixed Halide Perovskite: Compatibility and Performance. *ACS Appl. Mater. Interfaces* **2017**, *9*, 29707–29716, doi:10.1021/acsami.7b07627.



127. Cai, Y.; Zhang, G.; Zhang, Y.-W. *Phosphorene: Physical Properties, Synthesis, and Fabrication*; 1st ed.; Jenny Stanford Publishing, **2019**; ISBN 978-981-4774-64-2.
128. Qin, G.; Hu, M. Thermal Transport in Phosphorene. *Small* **2018**, *14*, 1702465, doi:10.1002/smll.201702465.
129. Ong, Z.-Y.; Cai, Y.; Zhang, G.; Zhang, Y.-W. Strong Thermal Transport Anisotropy and Strain Modulation in Single-Layer Phosphorene. *J. Phys. Chem. C* **2014**, *118*, 25272–25277, doi:10.1021/jp5079357.
130. Nwaoha, C. Appendix I: Methods for Measuring Process Temperature. In *Process Plant Equipment*; John Wiley & Sons, Ltd, **2012**; pp. 653–657 ISBN 978-1-118-16256-9.
131. Jędrzejewska-Szczerska, M.; Wierzba, P.; Chaaya, A.A.; Bechelany, M.; Miele, P.; Viter, R.; Mazikowski, A.; Karpienko, K.; Wróbel, M. ALD Thin ZnO Layer as an Active Medium in a Fiber-Optic Fabry–Perot Interferometer. *Sensors and Actuators A: Physical* **2015**, *221*, 88–94, doi:10.1016/j.sna.2014.11.001.
132. Wang, H.; Yang, A.; Tang, L. Wide Measurement-Range Fiber-Optic Temperature Sensor Based on ZnO Thin Film. *Optics and Lasers in Engineering* **2014**, *60*, 49–53, doi:10.1016/j.optlaseng.2014.03.008.
133. He, C.; Sun, H.; Mo, J.; Yang, C.; Feng, G.; Zhou, H.; Zhou, S. Temperature Sensor Based on High-Q Polymethylmethacrylate Optical Microbubble. *Laser Phys.* **2018**, *28*, 076202, doi:10.1088/1555-6611/aab452.
134. Monteiro, C.; Silva, S.; Frazão, O. Hollow Microsphere Fabry–Perot Cavity for Sensing Applications. *IEEE Photonics Technology Letters* **2017**, *29*, 1229–1232, doi:10.1109/LPT.2017.2701000.
135. Soria, S.; Berneschi, S.; Brenci, M.; Cosi, F.; Nunzi Conti, G.; Pelli, S.; Righini, G.C. Optical Microspherical Resonators for Biomedical Sensing. *Sensors* **2011**, *11*, 785–805, doi:10.3390/s110100785.





[PL1]

**Listewnik, P.;** Hirsch, M.; Struk, P.; Weber, M.; Bechelany, M.; Jędrzejewska-Szczerska, M. Preparation and Characterization of Microsphere ZnO ALD Coating Dedicated for the Fiber-Optic Refractive Index Sensor. *Nanomaterials* 2019, 9, doi:10.3390/nano9020306.

*Description of the fabrication and characterization of the uncoated microsphere-based fiber-optic sensor and with a ZnO ALD coating thickness of 200 nm. Analysis of the results obtained from an experimental investigation of the refractive index.*



Article

# Preparation and Characterization of Microsphere ZnO ALD Coating Dedicated for the Fiber-Optic Refractive Index Sensor

Paulina Listewnik <sup>1</sup>, Marzena Hirsch <sup>1</sup>, Przemysław Struk <sup>2,\*</sup>, Matthieu Weber <sup>3</sup>,  
Mikhael Bechelany <sup>3</sup> and Małgorzata Jędrzejewska-Szczerska <sup>1,\*</sup>

<sup>1</sup> Department of Metrology and Optoelectronics, Faculty of Electronics, Telecommunications and Informatics, Gdańsk University of Technology, 11/12 Narutowicza Street, 80-233 Gdańsk, Poland; paulist@o2.pl (P.L.); marpluta1@student.pg.gda.pl (M.H.)

<sup>2</sup> Department of Optoelectronics, Faculty of Electrical Engineering, Silesian University of Technology, 2 Krzywoustego Street, 44-100 Gliwice, Poland

<sup>3</sup> Institut Européen des Membranes (ENSCM, UMR CNRS 5635), Univ. Montpellier, Place Eugène Bataillon, 34095 Montpellier, France; matthieu.weber@umontpellier.fr (M.W.); mikhael.bechelany@umontpellier.fr (M.B.)

\* Correspondence: Przemyslaw.Struk@polsl.pl (P.S.); mjedrzej@eti.pg.edu.pl (M.J.-S.); Tel.: +48-32-237-2182 (P.S.); +48-58-347-1361 (M.J.-S.)

Received: 5 January 2019; Accepted: 19 February 2019; Published: 23 February 2019



**Abstract:** We report the fabrication of a novel fiber-optic sensor device, based on the use of a microsphere conformally coated with a thin layer of zinc oxide (ZnO) by atomic layer deposition (ALD), and its use as a refractive index sensor. The microsphere was prepared on the tip of a single-mode optical fiber, on which a conformal ZnO thin film of 200 nm was deposited using an ALD process based on diethyl zinc (DEZ) and water at 100 °C. The modified fiber-optic microsphere was examined using scanning electron microscopy and Raman spectroscopy. Theoretical modeling has been carried out to assess the structure performance, and the performed experimental measurements carried out confirmed the enhanced sensing abilities when the microsphere was coated with a ZnO layer. The fabricated refractive index sensor was operating in a reflective mode of a Fabry–Pérot configuration, using a low coherent measurement system. The application of the ALD ZnO coating enabled for a better measurement of the refractive index of samples in the range of the refractive index allowed by the optical fiber. The proof-of-concept results presented in this work open prospects for the sensing community and will promote the use of fiber-optic sensing technologies.

**Keywords:** ZnO; atomic layer deposition; coating; microsphere; fiber-optic sensors; refractive index

## 1. Introduction

Fiber-optic sensing devices present enormous potential, as they benefit from low-cost manufacturing, while maintaining high sensitivity and robustness. Nowadays, advanced fabrication techniques allow the incorporation of various nanomaterials for the tuning of sensing devices, including fiber-optic sensors [1–4]. Fiber-optic sensing devices can find application in many different fields of science such as chemistry (composition and content of various solutions) [1,2,5,6], biology [7–10] and physics [11–14]. Fiber-optics based sensors present a number of advantages, including high sensitivity, the ability to be used in demanding environments (narrow spaces, hazardous areas), as well as immunity to electromagnetic noise during operation [15,16]. Furthermore, the properties of fiber-optic sensors can easily be tuned by modifying their design with optical coatings.

ZnO is an oxide semiconductor material presenting a wide energy band gap of  $\sim 3.3$  eV [17]. The physical properties of ZnO, including the optical properties, strongly vary with the deposition technology used for its preparation. For sensing applications, ZnO films deposited as continuous layers with low surface roughness and/or in the form of nanoporous structures are morphologies which are particularly desired [18,19]. Concerning the optical properties, the refractive index of ZnO is around 2, and this semiconductor is optically transparent for the light above the absorption edge of 380 nm [20–22]. Due to these physical properties, ZnO coatings can be applied for a wide range of applications in sensing devices, for example for the detection of selected molecules in gases and liquids, and for the measurement of refractive indices [19,23–28].

One upcoming deposition technology that can be applied for the preparation of high quality ZnO nanomaterials is atomic layer deposition (ALD). This vapor phase deposition route is typically used for the synthesis of thin films with a thickness controllable at the (sub)nanometer scale. In fact, ALD enables the preparation of thin films and nanoparticles with controlled dimensions at the nanoscale on high aspect ratio substrates and is thus particularly appropriate for the coating of challenging substrates such as optical fibers [29–33].

Fiber-optic structures, such as microspheres are applied in the sensing systems. Most of them are coupled with fiber tapers and utilize the concept of Whispering Gallery Mode (WGM) in order to incite resonance. Successful applications of those sensors have been shown in biosensing and measurement of physical quantities (like temperature) [10,34]. To the best knowledge of the authors, so far none of the research uses fiber-optic microspheres as a low-coherence standalone refractive index sensor.

In this work, we report for the first time the modification of a fiber-optic microsphere-based sensor with a thin ZnO layer prepared by ALD. We also investigate the application of this ALD modified optical fiber as a refractive index sensor. Theoretical modeling is carried out to assess the structure performance, and experimental measurements are achieved to assess the sensing abilities of the new device.

The refractive index sensing principle is based on the measurement of the light reflected from the external surface of the fiber-optic microsphere (Figure 1). In the case of the microsphere, there is also a weak reflection originating from the boundary between the core and the cladding material. The reflected beams interfere, creating a low finesse intrinsic Fabry–Pérot interferometer with a fixed cavity. The reflection of the core–cladding interface is constant, but the value of the reflection coefficient of the sphere surface is highly dependent on the refractive index of the external medium. As its value is close to the refractive index value of the fiber cladding, the reflection decreases toward zero. The coating of the sphere surface by a thin film of transparent, high refractive index material like ZnO allows modification of the reflection function and shifts that transition point to the higher value of the surrounding refractive index [35,36]. Graphical visualization of the sensor structure is presented in Figure 1.

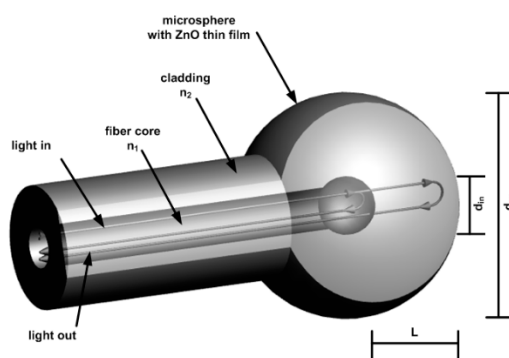


**Figure 1.** Schematic model of the microsphere with 200 nm ZnO thin film deposited on the surface, where:  $d_{in}$ —internal diameter of the sphere,  $d_{ex}$ —external diameter of the sphere,  $L$ —cavity length,  $n_i$ —refractive index.

## 2. Materials and Methods

The fiber-optic sensing device fabricated in this work is based on a single-mode optical fiber SMF-28, purchased from Thorlabs (Newton, NJ, USA). The microsphere is formed on the tip using the optical fiber fusion splicer (FSU 975, Ericsson Network Technologies AB, Stockholm, Sweden). The splicer produces an electronic arc of, in this case, 14.9 mA and a three-step pull, each of a different duration. To obtain the sphere with a diameter of about 240  $\mu\text{m}$  optical fiber was pulled for 3 s, collectively.

All ALD depositions have been carried out in a custom-built ALD reactor described elsewhere [37,38]. Diethyl zinc (DEZ) precursor was purchased from Sigma Aldrich and used as received. The co-reactant was millipore water. The substrates used were p-type (100) silicon wafers (MEMC Korea Company, Cheonan, Korea) and SMF-28 optical fibers (Thorlabs, Newton, NJ, USA). To remove the organic contaminants, the substrates were pre-cleaned in acetone, ethanol and de-ionized water for 5 min in an ultrasonic bath before the depositions. ALD of ZnO was performed using sequential exposures of DEZ and H<sub>2</sub>O at 100 °C separated by purge steps of argon with a flow rate of 100 sccm. The process consisted of 0.4 s pulse DEZ, 30 s exposure, and 40 s purge with dry argon and a 2 s pulse (H<sub>2</sub>O), 30 s exposure and 40 s purge. One thousand ALD cycles were carried out in order to achieve the deposition of ZnO of  $\approx 200$  nm with a growth per cycle of 0.2 nm [39].

Next, the sample has been characterized using scanning electron microscope (SEM, FEI S50, Hillsboro, OR, USA) to determine both geometrical properties and surface topography of the deposited ZnO layer on the microsphere. Raman spectroscopy was performed to analyze the structure of the layer on the surface of the sphere. The Raman spectra were measured by N-TEGRA Spectra (NT-MDT Company, Moscow, Russia) setup. During the experiment, the ZnO film was illuminated by a light beam generated by a laser with central wavelength  $\lambda_c = 532$  nm. The analysis of literature shows the ZnO in wurtzite structure (bulk form) belongs to the space group  $C_{6v}^4$  (Schoenflies notation) with two formula units per primitive cell, for which atoms occupy  $C_{3v}$  sites [40,41]. The group theory describes the Raman active zone-center optical phonon as follows:  $\Gamma_{\text{opt}} = A_1 + 2B_1 + 2E_2 + E_1$  [40–45]. The literature also presents the phonons  $A_1$  as well as  $E_1$  as polar and presenting different frequencies for longitudinal-optical (LO) and transverse-optical (TO) phonons, the  $B_1$  mode is non-active (silent mode) [40–45].

The microsphere was also examined using a measurement setup similar to the Fabry–Pérot interferometer operating in a reflective mode, in order to obtain information about the sensing abilities of the developed device. Operating principle of the utilized setup is shown in Figure 2 below.

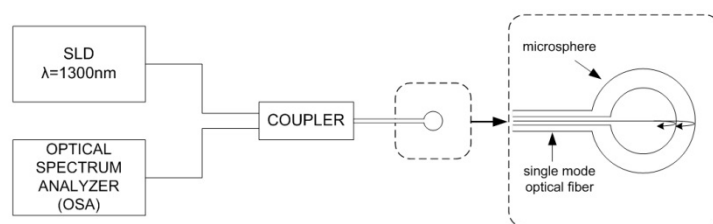


**Figure 2.** Operating principle of Fabry–Pérot interferometer used for measurements.

The signal from a broadband superluminescent diode (SLD) light source with the central wavelength of 1290 nm and the full width at half maximum of 50 nm (S1300-G-I-20, SUPERLUM, Ireland) was applied directly to the input of a fiber-optic coupler. After reflecting on the core–cladding interface of the microsphere and the ZnO layer, the signal was detected by the Optical Spectrum Analyzer (OSA, Ando AQ6319, Kanagawa, Japan). During the experiment the sensor head was immersed in Cargille Refractive Index Liquids (Series A, AA, AAA, Cargille Laboratories, Cedar Grove, NJ, USA), each characterized by a different refractive index as follows: 1.4, 1.5, 1.6, to assess the sensing performance. Refractive indices of those liquids are provided for a wavelength of 589.3 nm. However,

because of dispersion, refractive indices are accordingly lower for a longer wavelength, therefore the actual values of those liquids for a wavelength of 1300 nm are following: 1.390, 1.487, 1.576.

### 3. Theory and Calculation

Firstly, the theoretical modeling of the spectral response was performed to consider the rationale of the device. In formation of the microsphere by use of optical fiber fusion splicer, the localized melting of the fiber by arc discharge results in the creation of a spherical tip due to surface tension. The structure achieved in this process is not uniform, but exhibits the boundary of the core and cladding materials with different refractive indices. When the reflectivity of the mirrors is low, as in the investigated case, the influence of the higher order reflections in a Fabry–Pérot interferometer becomes insignificant. In addition, due to the very low thickness of the ALD film in comparison to the device structure and operating wavelength, the investigated structure can be simplified from a dual cavity interferometer (cladding layer and ZnO film) to a single cladding-material cavity interferometer with a reflection coefficient of the outermost mirror surface modeled by ZnO spectral reflection response. Therefore, the output signal of the sensor can be approximated by two-beam interferometer response—one reflected from the core/cladding interface and the second from the external surface of the microsphere and coupled back to the fiber core (Figure 1). The method for calculation of the ZnO thin film spectral reflection function was described in detail by Majchrowicz et al. [35]. The thickness of the film 200 nm was chosen for the application, as it provides highest reflection value for wavelengths in the 1300–1500 nm range [35].

The field distribution of the light propagated in the fiber core, and thus the first reflected beam, can be approximated by Gaussian distribution [46]. The transformation of the second beam, propagated in the cladding sphere, can be modeled by ray-matrix approach for the Gaussian beam. The ABCD matrix for the microsphere can be written as:

$$M = \begin{bmatrix} 1 & 0 \\ \frac{n_2 - n_1}{n_2 R_{in}} & \frac{n_1}{n_2} \end{bmatrix} \begin{bmatrix} 1 & L \\ 0 & 1 \end{bmatrix} \begin{bmatrix} 1 & 0 \\ \frac{-2}{R_{ex}} & 1 \end{bmatrix} \begin{bmatrix} 1 & L \\ 0 & 1 \end{bmatrix} \begin{bmatrix} 1 & 0 \\ \frac{n_1 - n_2}{n_1 R_{in}} & \frac{n_2}{n_1} \end{bmatrix} \quad (1)$$

where  $n_{1,2}$  are the refractive indices of the core and cladding,  $L$  is the length of the cavity,  $R_{in,ex}$  is the radius of the core and cladded spheres.

In the case of the second interfering beam, it is also important to take into account the coupling coefficient of the reflected wave propagated in the cavity back to the optical fiber core. It can be estimated using the complex beam parameters calculated using M matrix elements and initial beam properties [47]. A detailed description of the theoretical background used for the simulation has been described [48].

## 4. Results

### 4.1. Characterization of the ZnO ALD Coating

First, the morphology of the device has been examined by scanning electron microscopy (SEM). The presented microsphere shows a regular spherical shape and the diameter of the microsphere head was calculated by circle fitting and it is equal to  $\Phi_{rZnO} = 240.7 \mu\text{m}$  for the microsphere with the ZnO layer. The SEM micrograph of the fiber-optic microsphere with deposited ZnO layer measured with 1000x magnification is presented in Figure 3a. Figure 3c shows the same surface topography on the front side of the microsphere head, measured with 5000x magnification. The ZnO layer is clearly visible. In addition, the diameter of optical fiber which was used for fabricating the microsphere was also measured and it is equal to  $\Phi_r = 127.8 \mu\text{m}$  (core with cladding). In the case of the microsphere without ZnO coating, the surface topography is presented in Figure 3b,d.



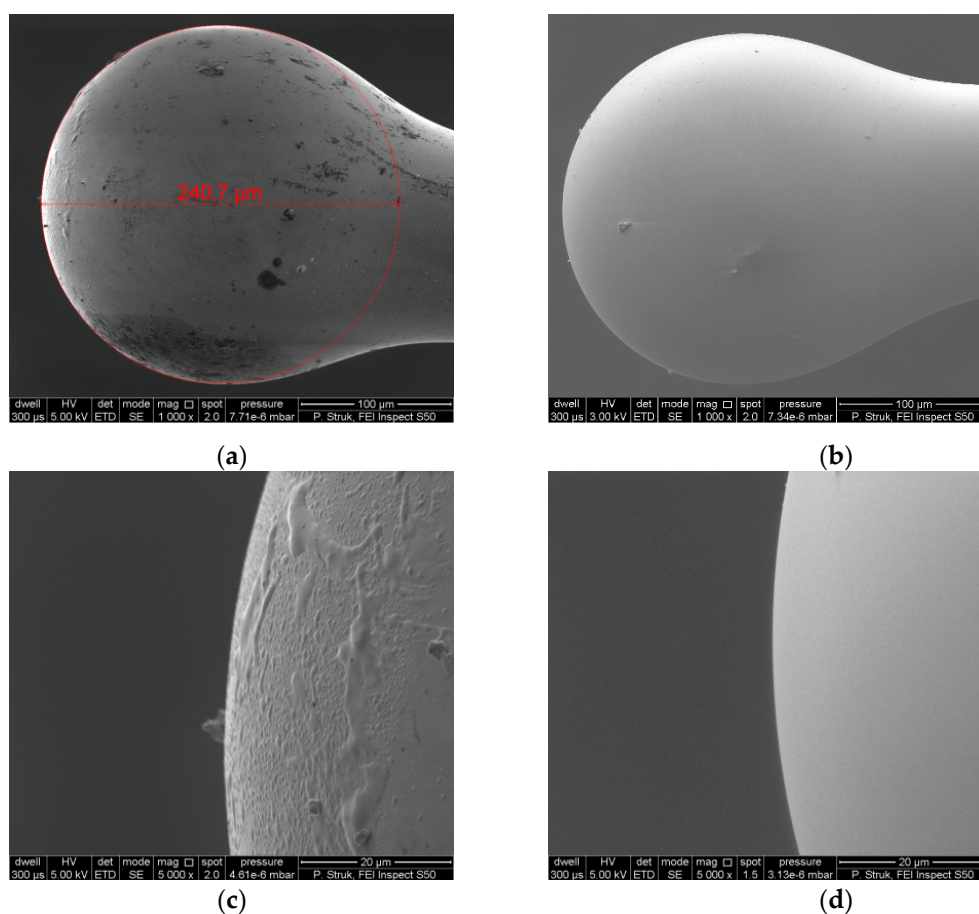


**Figure 3.** SEM images of optical fiber microsphere: (a) the microsphere with 200 nm ZnO coating, (b) the microsphere without ZnO coating, (c) surface topography on the front side of the microsphere with 200 nm ZnO coating, (d) surface topography on the front side of the microsphere without ZnO coating.

The investigation of the ZnO thin film deposited on the microsphere was carried out by Raman spectroscopy method. The Raman spectra of the ZnO film deposited on the microsphere is presented in Figure 4. The analysis of Raman peaks is:  $379\text{ cm}^{-1}$  corresponds to acoustic mode A1 transverse-optical (TO) phonon,  $412\text{ cm}^{-1}$  corresponds to E1 transverse-optical (TO) phonon,  $440\text{ cm}^{-1}$  corresponds to E2,  $537\text{ cm}^{-1}$  corresponds to A1 longitudinal-optical (LO) phonon and  $586\text{ cm}^{-1}$  corresponds to E1 longitudinal-optical (LO) phonon. The Raman peaks for  $494\text{ cm}^{-1}$  and  $611\text{ cm}^{-1}$  correspond to substrate (fiber cladding–fused silica). It should be mentioned that the presented Raman peaks of ZnO are hardly visible, which can be caused by surface curvature ( $\Phi_{\text{rZnO}} = 240.7\text{ }\mu\text{m}$ ) of the microsphere. In this case, the generated Raman signal is highly diffused sideways (in comparison to a flat surface), which means that only a small part of the Raman signal can reach the detector. The presented Raman spectra confirm the ZnO layer has been deposited properly and exists on the microsphere.



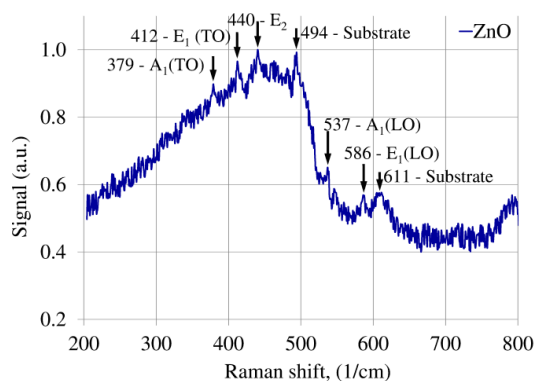


**Figure 4.** Raman spectra of the ZnO layer deposited on microsphere.

#### 4.2. Modeling

In Figure 5a,b normalized reflected spectra of a sphere with and without ZnO film for different values of surrounding refractive index are presented. Sensor response was simulated assuming illumination with a broadband source of Gaussian characteristic; source parameters were set to  $\lambda = 1290$  nm and a full width at half maximum (FWHM)  $\approx 40$  nm, which gives good approximation of a superluminescent diode (SLD) spectra, peak intensity was assumed as 1. The sphere geometry was as follows:  $R_{ex} = 120$   $\mu\text{m}$ ,  $L = 110$   $\mu\text{m}$ ,  $R_{in} = 10$   $\mu\text{m}$ . The refractive index of the fiber core was assumed as 1.46 and for the cladding 1.454 in the investigated wavelength range. Figure 5c,d show dependence of peak intensity of the output signal in function of external refractive index. As can be observed, modulation of source spectra by interference fringes is present, however the visibility of the interference signal is not high. The expected intensity of the signal obtained with the ZnO coated sphere is four times that for the clean sphere. As the external refractive index increases, the peak intensity of the reflected signal diminishes, reaching the minimum in the range between 1.4 and 1.5 for the uncoated sphere. Application of a ZnO thin film allows this extremum to shift to higher refractive index values, thus extending available sensing range to over 1.6.

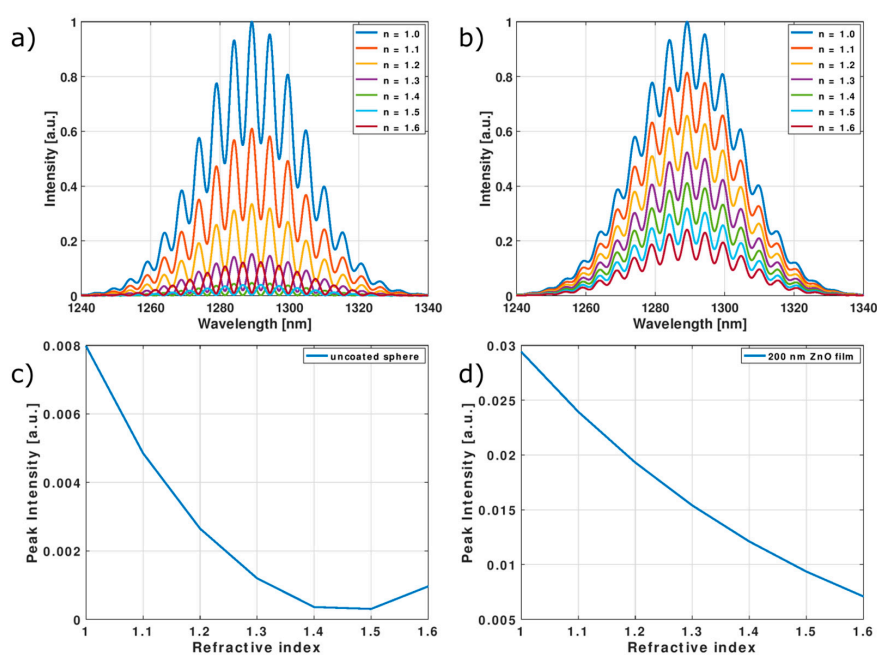


**Figure 5.** Simulation results upon illumination of superluminescent diode (SLD)-like light source: Normalized reflected spectra (a) for uncoated microsphere and (b) with 200 nm ZnO coating and signal peak intensity in function of external refractive index (c) for uncoated sphere and (d) with ZnO film.

### 4.3. Measurement Results

In order to determine the spectral response of the device and to evaluate the potential performance in refractive index sensing applications, a series of measurements were performed. During the experiment, the measurement head was immersed in media characterized by different refractive indices (1, 1.390, 1.487, and 1.576).

In Figure 6, the measured response of the fiber-optic sensor with microsphere coated with ZnO thin film can be seen. The dependence of the signal intensity on the refractive index of the surrounding medium is shown in Figure 7. For each refractive index, the values of peak intensity were normalized to the reference value (highest value for  $n = 1$ ). Theoretical modeling was included to facilitate comparison of the simulation and experimental results. Coefficient of determination, R-squared, indicates the accuracy of the measurements is close to 1 (0.9999).

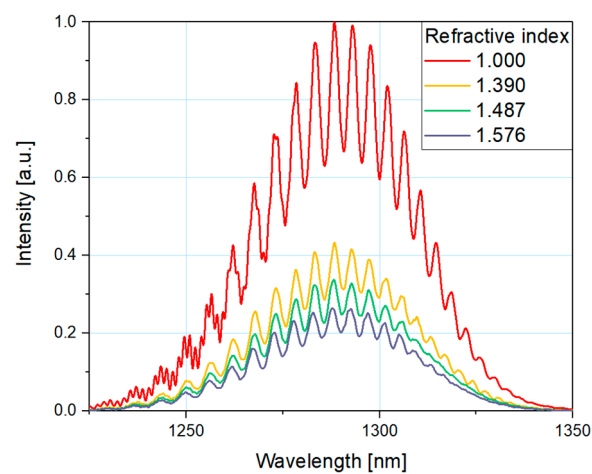


**Figure 6.** Measured response of the fiber-optic interferometer for a microsphere with ZnO layer.

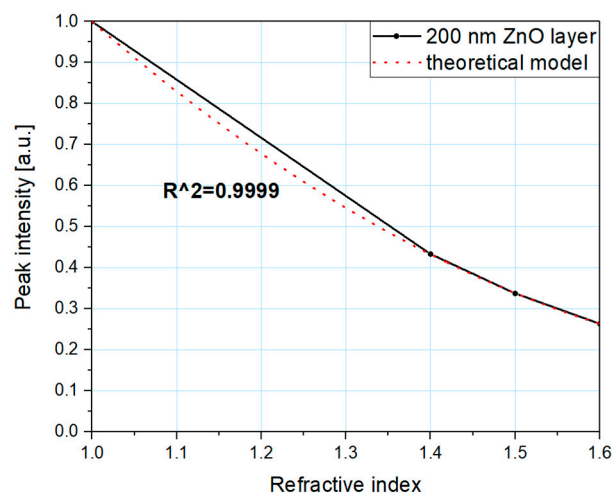


**Figure 7.** Measured response of the fiber-optic interferometer for a microsphere with ZnO layer.

It can be observed that this plot similarly traces the modeled characteristics presented in Figure 5b. The intensity of a measured signal from the sensor with ZnO coated microsphere decreases with the increase of the refractive index. The results of the experiments are in close agreement with the theoretical modeling. The signal is easily detectable in the full investigated range (up to 1.6), showing that the sensing range of a fiber-optic refractive index sensor can be successfully extended by application of a ZnO thin film coating. The modulation of reflected signal due to the interference in the microsphere structure is also clearly visible in the whole range. The density of interference fringes

is not dependent on the external medium, therefore it can be used for remote checking of the integrity of sensor structure.

## 5. Conclusions

In this paper, the interferometric fiber-optic sensor with the incorporation of a microsphere coated with a thin film of ZnO by ALD at the tip of the optical fiber is reported for the first time. The sensor was first characterized using scanning electron microscope and Raman spectroscopy, confirming the presence of a conformal 200 nm ALD ZnO film around the microsphere. Theoretical simulations as well as experimental measurements have been performed to assess the performance of the device as a refractive index sensor. The measurements carried out confirmed its successful use as an optical sensor, and the enhanced sensing abilities when the microsphere was coated with the ZnO layer. Compared to other refractive index sensors reported in literature, this design allowed the measurement range to be extended. The application of a ZnO layer at the surface of a microsphere allowed us to perform measurements for refractive indices close to those of an optical fiber (1.4). Furthermore, the application of the sensor with the ALD modified microsphere allowed us to observe the interference fringes coming from the microsphere, which worked as a two-beam interferometer operating in a reflective mode. The innovative results presented in this paper open new perspectives for the sensing community and will promote the use of fiber-optic sensing devices.

**Author Contributions:** The manuscript was written through contributions of all authors. M.W. and M.B. performed the ALD experiments. P.L. and M.J.-S. conceived and designed the experiments. M.H. performed theoretical modeling. P.L. performed the experiments. P.S. performed characterization of the developed device (SEM, Raman spectroscopy).

**Funding:** The authors M.W. and M.B. want to thank the French national research agency (ANR, program MeNiNA—ANR-17-CE09-0049) for funding. The authors P.L., M.H. and M.J.-S. acknowledge the financial support by the Polish National Centre for Research and Development (NCBiR) under the project Techmatstrateg Diamsec 347324 and DS Programs of the Faculty of Electronics, Telecommunications and Informatics of the Gdańsk University of Technology. P.S. The research was partially financed by habilitation grant 05/040/RGH18/0025—Silesian University of Technology Gliwice.

**Acknowledgments:** The authors M.W. and M.B. want to thank the French national research agency (ANR, program MeNiNA—ANR-17-CE09-0049) for funding. The authors P.L., M.H. and M.J.-S. acknowledge the financial support by the Polish National Centre for Research and Development (NCBiR) under the project Techmatstrateg Diamsec 347324 and DS Programs of the Faculty of Electronics, Telecommunications and Informatics of the Gdańsk University of Technology and P.S. thanks Silesian University of Technology Gliwice for funding.

**Conflicts of Interest:** The authors declare no conflict of interest.

## Abbreviations

ZnO	zinc oxide
ALD	atomic layer deposition
SEM	scanning electron microscopy

## References

1. Zhang, S.; Zhao, Y.; Zhang, C.; Jiang, S.; Yang, C.; Xiu, X.; Li, C.; Li, Z.; Zhao, X.; Man, B. In-situ growth of AuNPs on WS<sub>2</sub>@U-bent optical fiber for evanescent wave absorption sensor. *Appl. Surf. Sci.* **2018**, *441*, 1072–1078. [[CrossRef](#)]
2. Deng, D.; Feng, W.; Wei, J.; Qin, X.; Chen, R. Trace hydrogen sulfide gas sensor based on tungsten sulfide membrane-coated thin-core fiber modal interferometer. *Appl. Surf. Sci.* **2017**, *423*, 492–497. [[CrossRef](#)]
3. Jędrzejewska-Szczerska, M.; Majchrowicz, D.; Hirsch, M.; Struk, P.; Bogdanowicz, R.; Bechelany, M.; Tuchin, V.V. Nanolayers in Fiber-Optic Biosensing. In *Nanotechnology and Biosensors*; Elsevier: Amsterdam, The Netherlands, 2018; pp. 395–426, ISBN 978-0-12-813855-7.
4. Chiavaioli, F.; Baldini, F.; Tombelli, S.; Trono, C.; Giannetti, A. Biosensing with optical fiber gratings. *Nanophotonics* **2017**, *6*, 663–679. [[CrossRef](#)]

5. El-Sherif, M.; Bansal, L.; Yuan, J. Fiber Optic Sensors for Detection of Toxic and Biological Threats. *Sensors* **2007**, *7*, 3100–3118. [[CrossRef](#)] [[PubMed](#)]
6. Munkholm, C.; Walt, D.R.; Milanovich, F.P.; Klainer, S.M. Polymer Modification of Fiber Optic Chemical Sensors as a Method of Enhancing Fluorescence Signal for pH Measurement. *Anal. Chem.* **1986**, *58*, 1427–1430. [[CrossRef](#)]
7. Pérez, M.A.; González, O.; Arias, J.R. Optical Fiber Sensors for Chemical and Biological Measurements. In *Current Developments in Optical Fiber Technology*; Harun, S.W., Ed.; InTech: London, UK, 2013; ISBN 978-953-51-1148-1.
8. Coelho, L.; de Almeida, J.M.; Santos, J.L.; da Silva Jorge, P.A.; Martins, M.C.L.; Viegas, D.; Queirós, R.B. Aptamer-based fiber sensor for thrombin detection. *J. Biomed. Opt.* **2016**, *21*, 087005. [[CrossRef](#)] [[PubMed](#)]
9. Rozycki-Bakon, R.; Koba, M.; Firek, P.; Rozniecka, E.; Niedziolka-Jonsson, J.; Smietana, M. Stack of Nano-Films on Optical Fiber End Face for Label-Free Bio-Recognition. *J. Lightwave Technol.* **2016**, *34*, 5357–5362. [[CrossRef](#)]
10. Chiavaioli, F.; Zubiate, P.; Del Villar, I.; Zamarreño, C.R.; Giannetti, A.; Tombelli, S.; Trono, C.; Arregui, F.J.; Matias, I.R.; Baldini, F. Femtomolar Detection by Nanocoated Fiber Label-Free Biosensors. *ACS Sens.* **2018**, *3*, 936–943. [[CrossRef](#)] [[PubMed](#)]
11. Xu, X.; Chen, W.; Zhao, G.; Li, Y.; Lu, C.; Yang, L. Wireless whispering-gallery-mode sensor for thermal sensing and aerial mapping. *Light Sci. Appl.* **2018**, *7*, 62. [[CrossRef](#)] [[PubMed](#)]
12. Ramakrishnan, M.; Rajan, G.; Semenova, Y.; Farrell, G. Overview of Fiber Optic Sensor Technologies for Strain/Temperature Sensing Applications in Composite Materials. *Sensors* **2016**, *16*, 99. [[CrossRef](#)] [[PubMed](#)]
13. Yang, M.; Xie, W.; Dai, Y.; Lee, D.; Dai, J.; Zhang, Y.; Zhuang, Z. Dielectric multilayer-based fiber optic sensor enabling simultaneous measurement of humidity and temperature. *Opt. Express* **2014**, *22*, 11892. [[CrossRef](#)] [[PubMed](#)]
14. Konidakis, I.; Androulidaki, M.; Zito, G.; Pissadakis, S. Growth of ZnO nanolayers inside the capillaries of photonic crystal fibres. *Thin Solid Films* **2014**, *555*, 76–80. [[CrossRef](#)]
15. Islam, M.; Ali, M.; Lai, M.-H.; Lim, K.-S.; Ahmad, H. Chronology of Fabry-Perot Interferometer Fiber-Optic Sensors and Their Applications: A Review. *Sensors* **2014**, *14*, 7451–7488. [[CrossRef](#)] [[PubMed](#)]
16. Chiavaioli, F.; Gouveia, C.; Jorge, P.; Baldini, F. Towards a Uniform Metrological Assessment of Grating-Based Optical Fiber Sensors: From Refractometers to Biosensors. *Biosensors* **2017**, *7*, 23. [[CrossRef](#)] [[PubMed](#)]
17. Jagadish, C.; Pearton, S.J. *Zinc Oxide Bulk, Thin Films and Nanostructures: Processing, Properties and Applications*; Elsevier: Amsterdam, The Netherlands; London, UK, 2006; ISBN 978-0-08-044722-3.
18. Jang, J.-T.; Ryu, H.; Lee, W.-J. Effect of ALD surface treatment on structural and optical properties of ZnO nanorods. *Appl. Surf. Sci.* **2013**, *276*, 558–562. [[CrossRef](#)]
19. Struk, P.; Pustelny, T.; Gołaszewska, K.; Borysiewicz, M.A.; Piotrowska, A. Optical investigations of ZnO layers affected by some selected gases in the aspect of their application in optical gas sensors. *Bull. Pol. Acad. Sci. Tech. Sci.* **2015**, *63*, 829–836. [[CrossRef](#)]
20. Struk, P.; Pustelny, T.; Gołaszewska, K.; Kamińska, E.; Borysiewicz, M.A.; Ekielski, M.; Piotrowska, A. Hybrid photonics structures with grating and prism couplers based on ZnO waveguides. *Opto-Electron. Rev.* **2013**, *21*, 376–381. [[CrossRef](#)]
21. Morkoç, H.; Özgür, Ü. *Zinc Oxide: Fundamentals, Materials and Device Technology*; Wiley-VCH Verlag GmbH & Co. KGaA: Weinheim, Germany, 2009; ISBN 978-3-527-62394-5.
22. Özgür, Ü.; Alivov, Y.I.; Liu, C.; Teke, A.; Reshchikov, M.A.; Doğan, S.; Avrutin, V.; Cho, S.-J.; Morkoç, H. A comprehensive review of ZnO materials and devices. *J. Appl. Phys.* **2005**, *98*, 041301. [[CrossRef](#)]
23. Boyadjiev, S.I.; Georgieva, V.; Yordanov, R.; Raicheva, Z.; Szilágyi, I.M. Preparation and characterization of ALD deposited ZnO thin films studied for gas sensors. *Appl. Surf. Sci.* **2016**, *387*, 1230–1235. [[CrossRef](#)]
24. Pawar, D.; Kitture, R.; Kale, S.N. ZnO coated Fabry-Perot interferometric optical fiber for detection of gasoline blend vapors: Refractive index and fringe visibility manipulation studies. *Opt. Laser Technol.* **2017**, *89*, 46–53. [[CrossRef](#)]
25. Weber, M.; Julbe, A.; Ayral, A.; Miele, P.; Bechelany, M. Atomic Layer Deposition for Membranes: Basics, Challenges, and Opportunities. *Chem. Mater.* **2018**, *30*, 7368–7390. [[CrossRef](#)]
26. Viter, R.; Chaaya, A.A.; Iatsunskyi, I.; Nowaczyk, G.; Kovalevskis, K.; Erts, D.; Miele, P.; Smyntyna, V.; Bechelany, M. Tuning of ZnO 1D nanostructures by atomic layer deposition and electrospinning for optical gas sensor applications. *Nanotechnology* **2015**, *26*, 105501. [[CrossRef](#)] [[PubMed](#)]

27. Tereshchenko, A.; Fedorenko, V.; Smyntyna, V.; Konup, I.; Konup, A.; Eriksson, M.; Yakimova, R.; Ramanavicius, A.; Balme, S.; Bechelany, M. ZnO films formed by atomic layer deposition as an optical biosensor platform for the detection of Grapevine virus A-type proteins. *Biosens. Bioelectron.* **2017**, *92*, 763–769. [[CrossRef](#)] [[PubMed](#)]
28. Graniel, O.; Weber, M.; Balme, S.; Miele, P.; Bechelany, M. Atomic layer deposition for biosensing applications. *Biosens. Bioelectron.* **2018**, *122*, 147–159. [[CrossRef](#)] [[PubMed](#)]
29. George, S.M. Atomic Layer Deposition: An Overview. *Chem. Rev.* **2010**, *110*, 111–131. [[CrossRef](#)] [[PubMed](#)]
30. Weber, M.; Koonkaew, B.; Balme, S.; Utke, I.; Picaud, F.; Iatsunskyi, I.; Coy, E.; Miele, P.; Bechelany, M. Boron Nitride Nanoporous Membranes with High Surface Charge by Atomic Layer Deposition. *ACS Appl. Mater. Interfaces* **2017**, *9*, 16669–16678. [[CrossRef](#)] [[PubMed](#)]
31. Weber, M.J.; Mackus, A.J.M.; Verheijen, M.A.; van der Marel, C.; Kessels, W.M.M. Supported Core/Shell Bimetallic Nanoparticles Synthesis by Atomic Layer Deposition. *Chem. Mater.* **2012**, *24*, 2973–2977. [[CrossRef](#)]
32. Cabello-Aguilar, S.; Balme, S.; Chaaya, A.A.; Bechelany, M.; Balanzat, E.; Janot, J.-M.; Pochat-Bohatier, C.; Miele, P.; Dejardin, P. Slow translocation of polynucleotides and their discrimination by  $\alpha$ -hemolysin inside a single track-etched nanopore designed by atomic layer deposition. *Nanoscale* **2013**, *5*, 9582–9586. [[CrossRef](#)] [[PubMed](#)]
33. Viter, R.; Balevicius, Z.; Abou Chaaya, A.; Baleviciute, I.; Tumenas, S.; Mikoliunaite, L.; Ramanavicius, A.; Gertner, Z.; Zaleska, A.; Vataman, V.; et al. The influence of localized plasmons on the optical properties of Au/ZnO nanostructures. *J. Mater. Chem. C* **2015**, *3*, 6815–6821. [[CrossRef](#)]
34. Liang, L.; Li, M.; Liu, N.; Sun, H.; Rong, Q.; Hu, M. A high-sensitivity optical fiber relative humidity sensor based on microsphere WGM resonator. *Opt. Fiber Technol.* **2018**. [[CrossRef](#)]
35. Majchrowicz, D.; Hirsch, M.; Wierzba, P.; Bechelany, M.; Viter, R.; Jędrzejewska-Szczerska, M. Application of Thin ZnO ALD Layers in Fiber-Optic Fabry-Pérot Sensing Interferometers. *Sensors* **2016**, *16*, 416. [[CrossRef](#)] [[PubMed](#)]
36. Hirsch, M.; Majchrowicz, D.; Wierzba, P.; Weber, M.; Bechelany, M.; Jędrzejewska-Szczerska, M. Low-Coherence Interferometric Fiber-Optic Sensors with Potential Applications as Biosensors. *Sensors* **2017**, *17*, 261. [[CrossRef](#)] [[PubMed](#)]
37. Makhoulouf, H.; Weber, M.; Messaoudi, O.; Tingry, S.; Moret, M.; Briot, O.; Chtoutou, R.; Bechelany, M. Study of Cu<sub>2</sub>O/ZnO nanowires heterojunction designed by combining electrodeposition and atomic layer deposition. *Appl. Surf. Sci.* **2017**, *426*, 301–306. [[CrossRef](#)]
38. Bechelany, M.; Drobek, M.; Vallicari, C.; Abou Chaaya, A.; Julbe, A.; Miele, P. Highly crystalline MOF-based materials grown on electrospun nanofibers. *Nanoscale* **2015**, *7*, 5794–5802. [[CrossRef](#)] [[PubMed](#)]
39. Baitimirova, M.; Viter, R.; Andzane, J.; van der Lee, A.; Voiry, D.; Iatsunskyi, I.; Coy, E.; Mikoliunaite, L.; Tumenas, S.; Załęski, K.; et al. Tuning of Structural and Optical Properties of Graphene/ZnO Nanolaminates. *J. Phys. Chem. C* **2016**, *120*, 23716–23725. [[CrossRef](#)]
40. Ojha, A.K.; Srivastava, M.; Kumar, S.; Hassanein, R.; Singh, J.; Singh, M.K.; Materny, A. Influence of crystal size on the electron–phonon coupling in ZnO nanocrystals investigated by Raman spectroscopy. *Vib. Spectrosc.* **2014**, *72*, 90–96. [[CrossRef](#)]
41. Hadžić, B.; Romčević, N.; Trajić, J.; Kostić, R.; Stanišić, G.; Timotijević, D. Vibrational Spectroscopy of SOP Modes in ZnO Doped with CoO, MnO and Fe<sub>2</sub>O<sub>3</sub>. In *Proceedings of the III Advanced Ceramics and Applications Conference*; Lee, W.E., Gadow, R., Mitic, V., Obradovic, N., Eds.; Atlantis Press: Paris, France, 2016; pp. 159–172, ISBN 978-94-6239-156-7.
42. Procek, M.; Pustelny, T.; Stolarczyk, A. Influence of External Gaseous Environments on the Electrical Properties of ZnO Nanostructures Obtained by a Hydrothermal Method. *Nanomaterials* **2016**, *6*, 227. [[CrossRef](#)] [[PubMed](#)]
43. Guo, S.; Du, Z.; Dai, S. Analysis of Raman modes in Mn-doped ZnO nanocrystals. *Phys. Status Solidi* **2009**, *246*, 2329–2332. [[CrossRef](#)]
44. Cuscó, R.; Alarcón-Lladó, E.; Ibáñez, J.; Artús, L.; Jiménez, J.; Wang, B.; Callahan, M.J. Temperature dependence of Raman scattering in ZnO. *Phys. Rev. B* **2007**, *75*, 165202. [[CrossRef](#)]
45. Klingshirn, C.F.; Waag, A.; Hoffmann, A.; Geurts, J. *Zinc Oxide: From Fundamental Properties towards Novel Applications*; Klingshirn, C.F., Ed.; Springer Series in Materials Science; Springer: Heidelberg, Germany; London, UK, 2010; ISBN 978-3-642-10576-0.

46. Pluciński, J.; Karpieńko, K. Fiber optic Fabry-Pérot sensors: Modeling versus measurements results. In Proceedings of the 1st Integrated Optics—Sensors, Sensing Structures and Methods, Szczyrk, Poland, 29 February–4 March 2016; p. 100340H.
47. Goldsmith, P.F. *Quasioptical Systems: Gaussian Beam Quasioptical Propagation and Applications*; IEEE Press/Chapman & Hall Publishers Series on Microwave Technology and RF; IEEE Press: Piscataway, NJ, USA, 1998; ISBN 978-0-7803-3439-7.
48. Hirsch, M. Fiber optic microsphere with ZnO thin film for potential application in refractive index sensor—Theoretical study. *Photonics Lett. Pol.* **2018**, *10*, 85–87. [[CrossRef](#)]



© 2019 by the authors. Licensee MDPI, Basel, Switzerland. This article is an open access article distributed under the terms and conditions of the Creative Commons Attribution (CC BY) license (<http://creativecommons.org/licenses/by/4.0/>).



[PL2]

Hirsch, M.; **Listewnik, P.**; Struk, P.; Weber, M.; Bechelany, M.; Szczerska, M. ZnO coated fiber optic microsphere sensor for the enhanced refractive index sensing. *Sensors Actuators, A Phys.* 2019, 298, doi:10.1016/j.sna.2019.111594

*Description of the fabrication and characterization of the microsphere-based fiber-optic sensor and with ZnO ALD coatings thickness of 50 nm and 100 nm. Analysis of the results obtained from an experimental investigation of the refractive index.*





# ZnO coated fiber optic microsphere sensor for the enhanced refractive index sensing



Marzena Hirsch<sup>a</sup>, Paulina Listewnik<sup>a,\*</sup>, Przemysław Struk<sup>b</sup>, Matthieu Weber<sup>c</sup>,  
Mikhael Bechelany<sup>c,\*</sup>, Małgorzata Szczerska<sup>a,\*</sup>

<sup>a</sup> Department of Metrology and Optoelectronics, Faculty of Electronics, Telecommunications and Informatics, Gdańsk University of Technology, 11/12 Narutowicza Street, 80-233, Gdańsk, Poland

<sup>b</sup> Department of Optoelectronics, Faculty of Electrical Engineering, Silesian University of Technology, 2 Krzywoustego Street, 44-100, Gliwice, Poland

<sup>c</sup> Institut Européen des Membranes, IEM – UMR 5635, ENSCM, CNRS, Univ Montpellier, Montpellier, France

## ARTICLE INFO

### Article history:

Received 26 May 2019

Received in revised form 4 August 2019

Accepted 4 September 2019

Available online 10 September 2019

### Keywords:

ZnO

Atomic layer deposition

Coating

Microsphere

Fiber-optic

Sensors

Refractive index

## ABSTRACT

Optical fiber-based sensors are expected to become key components in the control of industrial processes, and the tuning and the enhancement of their sensing properties are crucial for the further development of this technology. Atomic Layer Deposition (ALD), a vapor phase technique allowing for the deposition of conformal thin films, is particularly suited for the deposition of controllable thin films on challenging substrates. In this work, we report the tuning of fiber-optic microsphere sensors using an ALD process of zinc oxide (ZnO) based on diethylzinc (DEZ) and H<sub>2</sub>O at 90 °C. Nanolayers of 50 and 100 nm were deposited on the fiber-optic microspheres sensors, using 250 and 500 ALD cycles respectively. The fabricated samples were characterized using Scanning Electron Microscopy (SEM), and the spectral responses of the devices were investigated theoretically and experimentally, by measuring the refractive index of different oils. It has been found that the biocompatible ZnO functional nanocoatings of the fiber-optic microsphere sensors allowed for a wider measurement range of refractive indexes, opening up new prospects for fiber-based sensing devices.

© 2019 Published by Elsevier B.V.

## 1. Introduction

The advantages of fiber optic sensors make them popular for various applications, from industrial and quality control processes to medical diagnostics. Therefore, optical fibers technologies have been involved in the field of sensing applications for decades, and fiber-optic sensors have been the focus of interest for their effective, easy and low cost fabrication process [1–5]. Refractive index is one of the key optical parameters measured in medical diagnostics, chemical and food industries [6,7]. The refractive index value is directly connected the concentration of the chemical solutions, therefore the measurements are used for investigation of sample composition in various fields, e.g. determination of sucrose or fat content in beverages [8,9], water salinity measurements [10],

quality control in chemical production [11–13]. Many features of fiber-optic sensors – like small size, possibility of remote and real time measurements, biocompatibility, immunity to electromagnetic noise and corrosive environment – are the reason they are used for refractive index sensing in demanding biomedical and industrial applications [14–19].

Recently, thanks to advance in nanotechnology, the nanolayer deposition techniques are made accessible more broadly to scientists and engineers in many fields, among them the fiber optic sensors. It was shown that the application of titanium dioxide thin films in SPR and Bragg grating sensors allowed to increase the sensitivity and tune the resonance wavelength [20–23] and to expand the sensing range of a fiber optic interferometer [24]. Also, in recent years, fiber optic gas sensors based on metal-oxides materials as sensing media have been reported to enhance both the gas sensitivity and selectivity [25,26]. Zinc oxide (ZnO) is an attractive material for optics and optoelectronic devices. For example, it has been applied as a coating layer on fiber-based sensors, semiconductor mirrors, waveguide layer in integrated photonic structures and as an active part in optoelectronic sensors structures [27–33]. ZnO is an n-type semiconductor with excellent optoelectronic properties, a wide band gap (3.36 eV), a high dielectric constant and

*Abbreviations:* ZnO, Zinc Oxide; ALD, Atomic Layer Deposition; SEM, Scanning Electron Microscopy.

\* Corresponding authors.

*E-mail addresses:* [paulist@o2.pl](mailto:paulist@o2.pl) (P. Listewnik), [mikhael.bechelany@umontpellier.fr](mailto:mikhael.bechelany@umontpellier.fr) (M. Bechelany), [malszcze@pg.edu.pl](mailto:malszcze@pg.edu.pl) (M. Szczerska).

<https://doi.org/10.1016/j.sna.2019.111594>

0924-4247/© 2019 Published by Elsevier B.V.





refractive index at  $n \sim 1.9\text{--}2$  depending on the deposition technology and wavelength [29,31,32,34,35]. In addition, ZnO is nontoxic and biocompatible, making it very suitable for medical diagnostic applications [36,37]. The physical properties of ZnO can be tailored to meet the requirements for a given application, as this material can be prepared with different physical properties using numerous methods, such as magnetron sputtering, Molecular Beam Epitaxy (MBE), Chemical Vapor Deposition (CVD), and Atomic Layer Deposition (ALD), among others [28,28,29,30,31,32,33,38].

ALD is a gas phase deposition technique allowing for the preparation of thin films on challenging 3D substrates with excellent thickness control. It is based on sequential pulses of precursors and coreactants in the gas phase, enabling for self-limiting chemical reactions to take place at the substrate surface [39–42]. The nanomaterials typically synthesized by ALD are metal oxides such as  $\text{Al}_2\text{O}_3$  and ZnO [43,44], but metals [40,45,46] and nitrides [47–49] have been prepared as well. The subnanometer thickness control and the excellent conformality allowed by ALD enabled this technique to become a key technology for the deposition of thin films for numerous applications, from microelectronics [50] to photovoltaics [51], and from biosensing [52] to membranes [53]. The key benefits of thin films prepared by ALD allow them to be used for optical sensing applications as well [24,27,54].

In this work, we demonstrate the possibility to tune the parameters of fiber-optic microsphere sensors, using ZnO nanolayers prepared by ALD. We first developed a ZnO ALD process and used it to prepare thin film coatings on fiber-optic microsphere sensor heads. We then show that the prepared coatings of 50 nm and 100 nm enable to modify the metrological parameters of the sensors. The measurement range of investigated refractive index and the intensity of the measured optical signal have been investigated, both theoretically and experimentally.

## 2. Materials and methods

### 2.1. Theoretical investigation

For the theoretical analysis of the reflected spectra for an interferometer presented in this paper, a few assumptions have been made. First, for a low-finesse Fabry-Pérot interferometer the influence of the high order reflections can be neglected, and two-beam interferometer approximation can be used. Thanks to the fact that ALD allows for the deposition of ultra-thin films, the thickness of the ZnO layer can be assumed to be very thin compared to the dimensions of the device structure as well as wavelength of the light source. Hence, reflected spectra calculation for the investigated in-line interferometer can be simplified to two-beam Fabry-Pérot interferometer approximation, where upon illumination of the structure via optical fiber, the light is first reflected from the internal core-cladding boundary and then from the external surface of the sphere. The intensity of field distribution for light propagated in the fiber core is approximated by Gaussian distribution, with the reflection coefficient of the first boundary determined by Fresnel equations, while the ray transfer matrix analysis is used to determine the transformation of the beam travelling through the cladding-material cavity and reflected from the outer interface of the structure. The reflection coefficient of ZnO coated microsphere surface is highly dependent to the refractive index of the surrounding medium as well as the thickness of the film [27]. To determine ZnO film reflection function we used method proposed for description of reflectance spectra of ALD films deposited on the end-face of the fiber [27] – the highest value of reflectance in 1300–1600 nm range, which is in particular interest because of compatibility with optical fibers typically used in telecommunication, can be achieved for films with thickness close to 200 nm. However, due to the time-

consuming nature of ALD deposition process, it is worthwhile to investigate how the lowered thickness of the layer is affecting the response of the device.

Detailed description of the theoretical model assumed for the microsphere structure and formulas used in calculations were presented in [55].

### 2.2. Microsphere development and ALD process

Fig. 1 presents a schematic representation of the investigated fiber-optic microsphere structure. In this microsphere sensor structure (1), the original interface between the cladding (2) and the core (3) material is preserved and forms a reflective surface for the light (4) propagating in the core of the optical fiber. The core-cladding interface (M1) together with the external surface (M2) of the sphere creates a low-finesse in-line Fabry-Pérot interferometer with the cavity length dependent on the radius of the sphere. The free spectral range of such interferometer is directly dependent on the sphere geometry and cladding refractive index and can be assumed to be constant in normal operating conditions. However, the intensity of the reflected signal (5) is highly sensitive to changes of the refractive index of the surrounding medium.

The microspheres were developed at the end of single mode optical fibers (SMF-28, Thorlabs, USA), using a single fiber fusion splicer (FSU 975, Ericsson, Sweden). During the initial fabrication of the microsphere sensor, the tip of the fiber is melted under the influence of the heat created by an electric arc and forms a new shape due to the surface tension by simultaneous pulling at the fiber. Inconsistencies in the diameter between the spheres could result from the variability of the technological process, however, the observed deviations were limited to 1.3% ( $245.7 \mu\text{m} \pm 3 \mu\text{m}$ ). The prepared microspheres were then coated using ALD of ZnO.

The ALD process allowing for the synthesis of ZnO thin films around the microsphere sensor has been carried out in a low-pressure hot-wall (home-built) ALD reactor. The base pressure was around 10–2 mbar. The process was based on the successive pulses and exposures of diethylzinc (DEZ) precursor and water ( $\text{H}_2\text{O}$ ) as coreactant, separated by purge steps. Precisely, the ALD cycle consisted of 0.1 s pulse of DEZ, 20 s exposures, and 45 s purge, followed by a 1 s pulse  $\text{H}_2\text{O}$ , 20 s exposure and 60 s purge to complete the cycle. To obtain the 50 and 100 nm ZnO conformal thin films around the fiber optic microspheres, we applied 250 and 500 ALD cycles, respectively. The time for pulse, exposure, and purge cycles were chosen to ensure saturation. The thickness of the films has been controlled on Si wafers placed in parallel in the reactor, using spectroscopic ellipsometry (Semilab GES5E, Budapest, Hungary). Further details about both this deposition process and the associated ALD reactor can be found elsewhere [24,44,56].

The morphological properties of presented the fiber-optic microsphere structures were determined by Scanning Electron Microscopy method (SEM, FEI S50, Hillsboro, USA).

### 2.3. Sensor experimental setup

The device sensing functionality was validated using a measurement setup, similar to that of Fabry-Pérot interferometer operated in a reflective mode [27]. The signal from the light source, in this experiment a superluminescent diode (SLD) with a central wavelength of 1300 nm (S1300-G-I-20, SUPERLUM, Ireland), is applied through the optical coupler to the input of a single-mode optical fiber (SMF-28, Thorlabs, USA). The light is reflected at the interface between core and cladding and again on the external surface of the microsphere. At the exit, an Optical Spectrum Analyzer (OSA, Ando AQ6319, Japan) is used to detect and process the measured signal. Schematic representation of described setup is shown in Fig. 2 below.

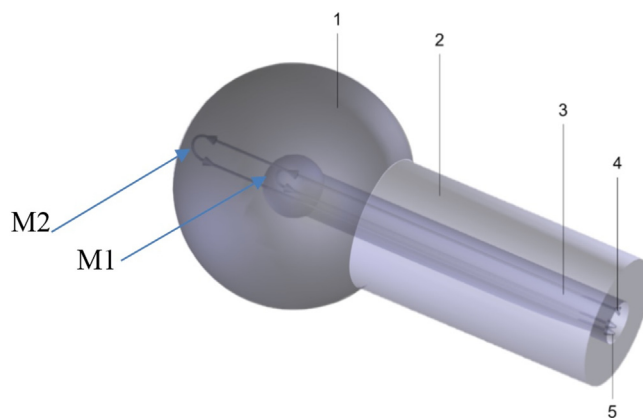


**Fig. 1.** Schematic representation of a microsphere fiber optic sensor with ZnO coating, where: 1 – ZnO coated microsphere, 2 – fiber-optic cladding, 3 – fiber-optic core, 4 – input signal, 5 – signals reflected from the mirrors made by the border between the fiber-optic core and cladding (M1) and microsphere and surrounding medium (M2).

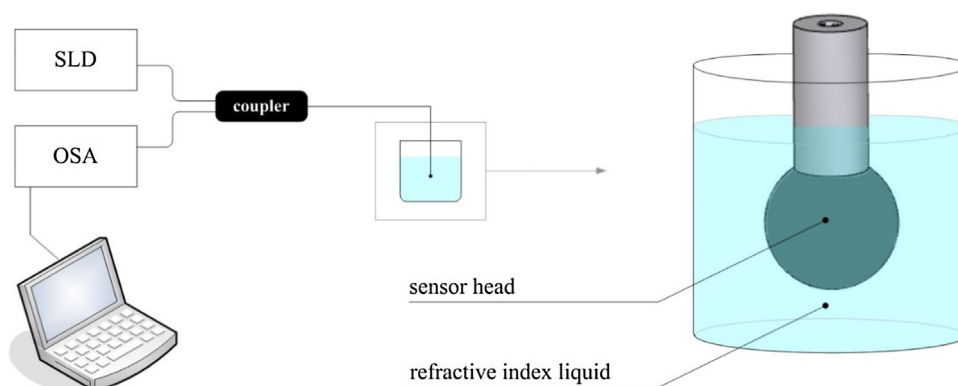


**Fig. 2.** Schematic representation of a microsphere fiber optic sensor experimental setup, during immersion of the sensor head in the refractive index liquids, where: SLD – superluminescent diode light source, OSA – Optical Spectrum Analyzer.

During the measurements, each microsphere was immersed in four refractive oils (Cargille Refractive Index Liquids, USA), whose refractive indexes varied from 1.3 to 1.6, with 0.1 step. The value of refractive indexes is at 589.3 nm. Additionally, the microspheres sensing properties were measured without immersing in refractive oils to establish a reference spectrum.

### 3. Results and discussion

#### 3.1. Results of simulations

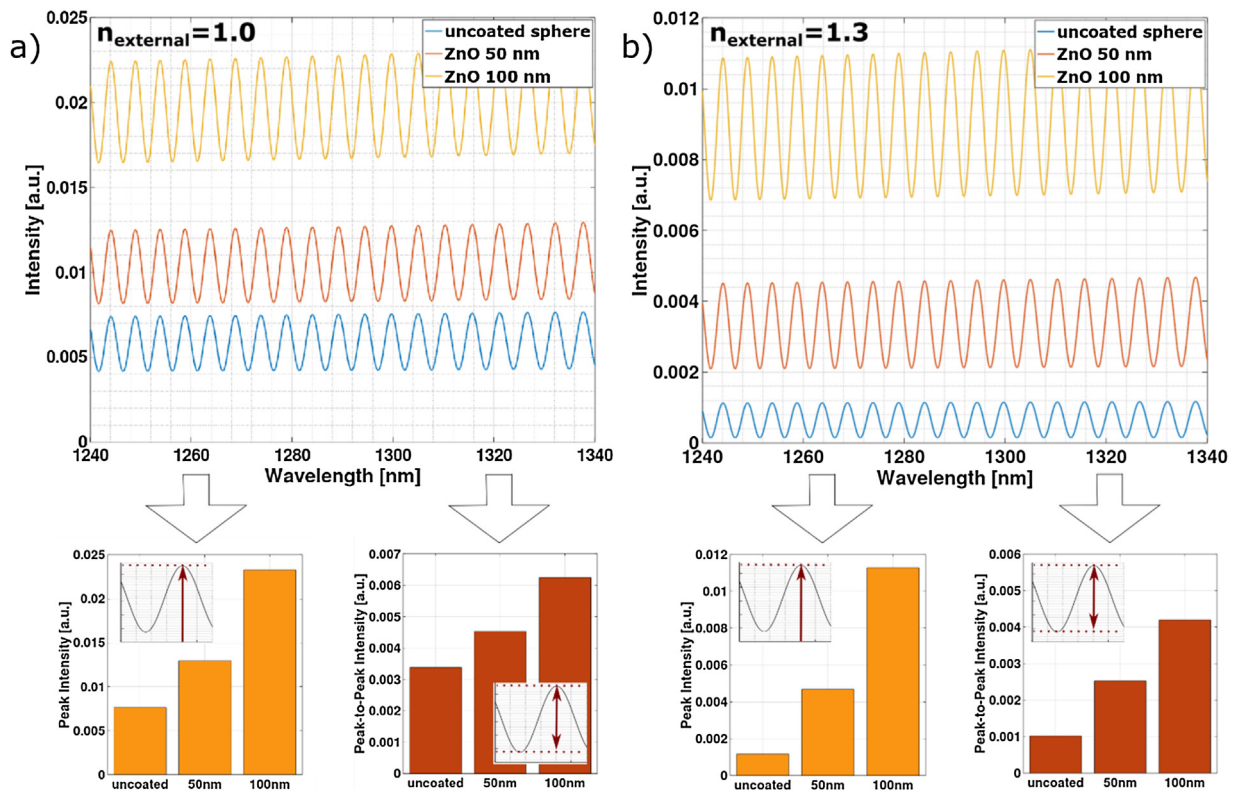
The reflected spectra were simulated for three setups of microsphere: an uncoated one, one coated with a ZnO film presenting a thickness of 50 nm, and one coated with a 100 nm ZnO film. The assumed parameters of the microspheres were as follows:  $R_{ex} = 120 \mu\text{m}$ ,  $R_{in} = 10 \mu\text{m}$ ,  $L = 110 \mu\text{m}$ ,  $n_{core} = 1.46$ ,  $n_{cladding} = 1.454$ . The value of ZnO refractive index was close to 1.83 for investigated wavelength range (1240–1340 nm), the dispersion curve was calculated in accordance with the references [27,55,57]. The calculations were performed using GNU Octave.

In Fig. 4a) are presented simulation data obtained for refractive index of external medium set as 1.0 – which correspond to microsphere placed in air. The results show that the deposition of ALD thin films on the microspheres allows for a higher reflected signal intensity. The increase of the intensity observed for the microsphere with 50 nm ZnO film is 1.7 higher than for the uncoated sphere and is multiplied by 3 for the microsphere with the 100 nm

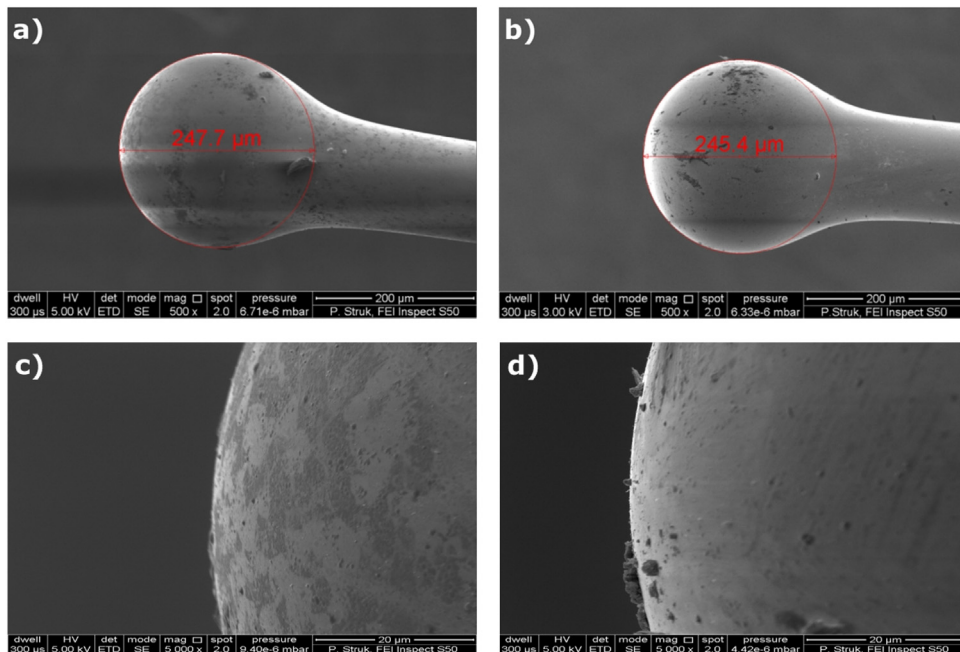
nanolayer. The depth of the interference pattern also grows with the thickness of the ZnO layer. This behavior can be attributed to the influence of the reflectance of the ZnO film. In the investigated wavelength range and for the selected thicknesses of the films, the reflection function shows that the increase of the reflection is well correlated with the presented results [27].

Fig. 4b) shows the results obtained for refractive index of surrounding medium equal to 1.3 – which is in the lower range of values typically encountered in applications involving liquid solutions (1.3–1.5). As can be noted, the intensity of reflected signal is significantly lower – in case of 100 nm ZnO coated device it is half of the original signal, for 50 nm the intensity is 3 times lower. In case of an uncoated sphere the reflected signal is 7 times lower with peak intensity of about 0.001, which would probably be hard to detect in real-life application. The difference is caused by diminished reflection from the outer surface of the microsphere, due to lower difference between the refractive index value of optical fiber and surrounding media.

Application of ZnO film of different thickness allows to affect the intensity response of the device in function of external refractive index. The tuning of the sensor response by differentiation of thickness coating can be used to optimize the device and its fabrication process to the target application – for example 100 nm coating might be necessary to achieve required signal strength and sensitivity in the refractive index range 1.4–1.5, whereas for the measurements of value close to 1.3 device coated with 50 nm film would work well enough and offer faster production time.



**Fig. 3.** SEM images of fiber-optic microsphere sensor head with ALD nanolayers, magnification of 500x: (a) 50 nm and (b) 100 nm and magnification of 5000x: (c) 50 nm and (d) 100 nm. The diameter of the spheres ( $246 \mu\text{m} \pm 3 \mu\text{m}$ ) is indicated.



**Fig. 4.** Comparison of the simulated reflected spectra for uncoated microsphere and with ZnO coating of 50 and 100 nm thickness, obtained for refractive index of external medium equal (a) 1.0 and (b) 1.3.

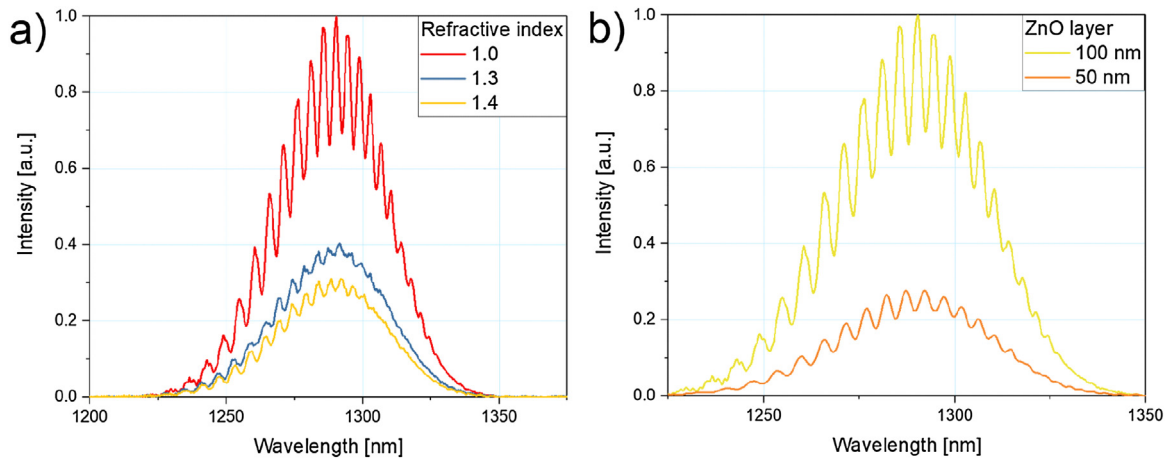


**Fig. 5.** Normalized measured reflected spectra of: (a) microsphere fiber-optic interferometer with 100 nm ZnO coating immersed in refractive indexes of 1, 1.3, 1.4 and (b) microsphere ZnO coated fiber-optic interferometers in medium with  $n = 1$ .

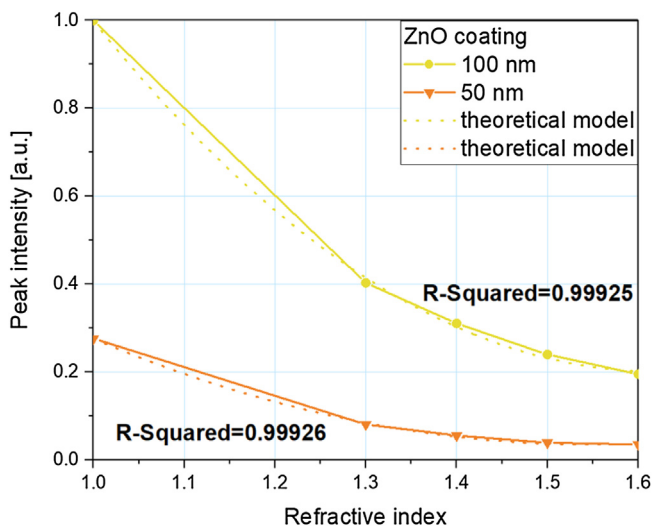


**Fig. 6.** Normalized values of peak intensities of the signal measured as a function of the media refractive index for the microsphere-based sensor with 100 nm and 50 nm ALD ZnO coating.

### 3.2. Device characterization

In this work, ALD of ZnO has been used to prepare thin film coatings on fiber-optic microsphere sensors. First, the fiber-optic microspheres were coated using ALD of ZnO. The ALD of ZnO process was based on DEZ and H<sub>2</sub>O pulses separated by Argon purge steps (see Materials and Methods section for details). By applying 250 and 500 ALD cycles, ZnO nanolayers of 50 and 100 nm have been deposited on the fiber-optic microspheres. Spectroscopic ellipsometry has been used to confirm the thicknesses of the films deposited on Si wafers placed in parallel in the reactor [45,58]. The morphological properties of the resulting two fiber-optic microspheres with the different thicknesses (50 and 100 nm) have been investigated using Scanning Electron Microscopy (SEM). The SEM images of the ZnO coated fiber-optic microspheres are presented in Fig. 3 (magnification x500). The microspheres are characterized by a very regular and spherical shape. The microsphere with the 50 nm ZnO layer presented a diameter of  $\Phi_{ZnO50} = 248 \mu\text{m}$ , whereas microsphere with 100 nm layer has a diameter equal to  $\Phi_{ZnO100} = 246 \mu\text{m}$ . Each sample was measured by circumscribing the head of a sensor. The difference in diameter of the spheres is not due to the

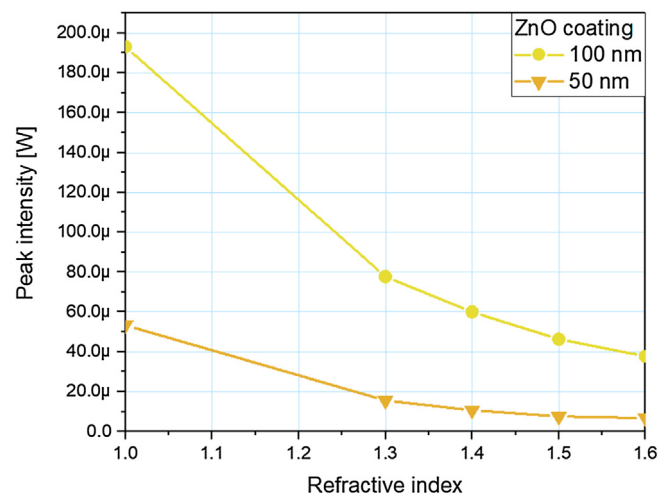


**Fig. 7.** Absolute values of peak intensities of the signal measured as a function of the media refractive index for the microsphere-based sensor with 100 nm and 50 nm ALD ZnO coating.

ALD coating but can be attributed to the variability of the melting process. However, please note that the observed deviations were limited to 1.3% ( $246 \mu\text{m} \pm 3 \mu\text{m}$ ). The analysis carried out with the use of SEM has also confirmed the high repeatability of fabrication technology of fiber-optic microsphere.

### 3.3. Experimental results

Fig. 5(a) presents the measured reflected spectra for ZnO coating of 100 nm, while the sensor head was immersed in media with the different refractive indexes  $n = 1.0, 1.3,$  and  $1.4$ . Fig. 5(b) shows the reflected signals measured on the microspheres coated with 50 and 100 nm ZnO layers. All values were normalized to the highest intensity, which in a medium with  $n = 1$  equals  $193 \mu\text{W}$  for a sensor with 100 nm ALD ZnO coating and  $53.4 \mu\text{W}$  for a sensor with 50 nm ALD ZnO coating. It can be clearly seen that the modulation of the signal, in both cases, remains the same, but the intensity increases with the increase of the layer thickness. The visibility of interference fringes is also increased for the thicker ZnO coating, as was predicted by the prior theoretical analysis.

Additionally, Fig. 6 presents the signal peak intensity measured during immersion of the microspheres with 50 nm and 100 nm ZnO



coatings in solutions of refractive indexes from 1.0 to 1.6. The second order polynomial regression has also been calculated for the 50 nm ZnO coating by equation:  $y_{50} = 2.6x^2 - 8.1x + 6.5$  and for the 100 nm ZnO coating  $y_{100} = 1.4x^2 - 5x + 4.6$ .

The R-squared parameter demonstrates over 99.99% closeness between collected data and the theoretical model. The first observation is that the reflected intensity of a microsphere with a 50 nm ZnO layer is substantially lower (155  $\mu\text{W}$ ) – about 70% – than the intensity of the 100 nm coated microsphere. An interesting observation is that the sensitivity to the refractive index variation is significantly improved for the 100 nm ZnO coating especially for values in the range of 1.4–1.6.

To get a better understanding of the sensor parameters, peak intensities absolute values of the signal, for a sensor with 100 nm ZnO and 50 nm ALD coating, are presented in Fig. 7.

Sensitivity of this setup gets up to 259  $\mu\text{W}/\text{RIU}$ , while sensitivity of the sensor with a coating of 50 nm reaches 78  $\mu\text{W}/\text{RIU}$ . Depending on the target application, the parameters of the fiber optic sensors have to be fitted by properly tuning the thickness of the ZnO layer. Commonly used setups of fiber optic sensors for refractive index measurements are based on the mechanism of reflection on the interface between a bare fiber and tested substance. However, the typical measurement range is strongly limited by the fact that when the refractive index of the tested sample is close to the fiber one (1.4–1.5), the reflection value is drastically lowered. The application of ALD ZnO films allows expanding the measurement range above that value, making the measurements of many substances possible with refractive index close to 1.5 like benzene, toluene, glycerol and various oils.

#### 4. Conclusion

We reported the preparation of fiber-optic microspheres sensing devices, using ALD of ZnO to coat the microsphere sensor tip. The proof-of-concept results presented in this work were obtained with different thicknesses of ZnO ALD thin film coatings on a microsphere fiber-optic sensor head, which allowed the tailoring of the sensor parameters. A broader measurement range of the investigated refractive index has been obtained. Application of ZnO films of different thickness allowed controlling the intensity of reflected signal and amplitude of the interference fringes. The measured increase of the intensity observed for the microsphere with 100 nm ZnO film is over 3 times higher than for the microsphere with the 50 nm nanolayer. In the proposed refractive index sensing application, the interference fringe spacing is not affected by external medium, yet the effect can be used for remote validation of presence and integrity of the sensor head. As typical measurement ranges of fiber optic sensors are limited by low reflection values when the refractive index of the tested samples is close to the fiber one, the application of ALD ZnO films allows for the considerable expansion of the measurement range. These proof-of-concept results open prospects for the development of fiber-optic sensing devices and the application of ALD to this growing field.

#### Funding sources

The authors M.W. and M.B. want to thank the French national research agency (ANR, program MeNiNA - ANR-17-CE09-0049) for funding. The authors P.L., M.H. and M.S. acknowledge the financial support of the Polish National Centre for Research and Development (NCBiR) under the project Techmatstrateg Diamsec 347324

and DS Programs of the Faculty of Electronics, Telecommunications and Informatics of the Gdańsk University of Technology. P.S. The research was partially financed by habilitation grant 05/040/RGH18/0025 - Silesian University of Technology Gliwice.

#### Acknowledgements

P.L. would like to thank Katarzyna Gajdecka for valuable help in visualization of measurement setup. M.W. and M.B. want to thank Bruno Navarra for its technical assistance.

#### References

- [1] Md. Islam, M. Ali, M.-H. Lai, K.-S. Lim, H. Ahmad, Chronology of Fabry-Perot Interferometer Fiber-Optic Sensors and Their Applications: a Review, *Sensors* 14 (2014) 7451–7488.
- [2] S.M. Tripathi, W.J. Bock, P. Mikulic, A wide-range temperature immune refractive-index sensor using concatenated long-period-fiber-gratings, *Sens. Actuators B Chem.* 243 (2017) 1109–1114.
- [3] Y. Du, S. Jothibasu, Y. Zhuang, C. Zhu, J. Huang, Rayleigh backscattering based macrobending single mode fiber for distributed refractive index sensing, *Sens. Actuators B Chem.* 248 (2017) 346–350.
- [4] M. Hernaiz, B. Acevedo, A.G. Mayes, S. Melendi-Espina, High-performance optical fiber humidity sensor based on lossy mode resonance using a nanostructured polyethylenimine and graphene oxide coating, *Sens. Actuators B Chem.* 286 (2019) 408–414.
- [5] J. Hromadka, N.N. Mohd Hazlan, F.U. Hernandez, R. Correia, A. Norris, S.P. Morgan, S. Korposh, Simultaneous in situ temperature and relative humidity monitoring in mechanical ventilators using an array of functionalised optical fibre long period grating sensors, *Sens. Actuators B Chem.* 286 (2019) 306–314.
- [6] Y. Zhao, R. Tong, M.-Q. Chen, F. Xia, Relative humidity sensor based on hollow core fiber filled with QDs-PVA, *Sens. Actuators B Chem.* 284 (2019) 96–102.
- [7] Y. Peng, Y. Zhao, M.-Q. Chen, F. Xia, Research advances in microfiber humidity sensors, *Small* 14 (2018), 1800524.
- [8] P. Zaca-Morán, J.P. Padilla-Martínez, J.M. Pérez-Corte, J.A. Dávila-Pintle, J.G. Ortega-Mendoza, N. Morales, Etched optical fiber for measuring concentration and refractive index of sucrose solutions by evanescent waves, *Laser Phys.* 28 (2018), 116002.
- [9] A. Gowri, A.S. Rajamani, B. Ramakrishna, V.V.R. Sai, U-bent plastic optical fiber probes as refractive index based fat sensor for milk quality monitoring, *Opt. Fiber Technol.* 47 (2019) 15–20.
- [10] Y. Qian, Y. Zhao, Q. Wu, Y. Yang, Review of salinity measurement technology based on optical fiber sensor, *Sens. Actuators B Chem.* 260 (2018) 86–105.
- [11] J.J. Espada, R. Rodríguez, Prediction of density and refractive index in furfural+lubricating oil systems, *Fluid Phase Equilib.* 438 (2017) 29–36.
- [12] M.R. Siddiqui, Z.A. AlOthman, N. Rahman, Analytical techniques in pharmaceutical analysis: a review, *Arab. J. Chem.* 10 (2017), S1409–S1421.
- [13] Y. Zhao, M. Lei, S.-X. Liu, Q. Zhao, Smart hydrogel-based optical fiber SPR sensor for pH measurements, *Sens. Actuators B Chem.* 261 (2018) 226–232.
- [14] M. Fisser, R.A. Badcock, P.D. Teal, A. Hunze, High-sensitivity fiber-optic sensor for hydrogen detection in gas and transformer oil, *IEEE Sens. J.* 19 (2019) 3348–3357.
- [15] P. Zubiate, J.M. Corres, C.R. Zamarreno, I.R. Matias, F.J. Arregui, Fabrication of optical Fiber sensors for measuring ageing transformer oil in Wavelength, *IEEE Sens. J.* 16 (2016) 4798–4802.
- [16] D. Li, X. Zhang, R. Zhu, P. Wu, H. Yu, K. Xu, A method to detect the mixed petrol interface by refractive index measurement with a fiber-optic SPR sensor, *IEEE Sens. J.* 14 (2014) 3701–3707.
- [17] C. Viphavakit, S.O. Keefe, M. Yang, S. Andersson-Engels, E. Lewis, Gold enhanced hemoglobin interaction in a fabry-Pérot based optical Fiber sensor for measurement of blood refractive index, *J. Light. Technol.* 36 (2018) 1118–1124.
- [18] M. Jędrzejewska-Szczerska, Response of a new low-coherence fabry-perot sensor to hematocrit levels in human blood, *Sensors* 14 (2014) 6965–6976.
- [19] T.K. Yadav, R. Narayanaswamy, M.H. Abu Bakar, Y.M. Kamil, M.A. Mahdi, Single mode tapered fiber-optic interferometer based refractive index sensor and its application to protein sensing, *Opt. Express* 22 (2014) 22802.
- [20] A.A. Rifat, G.A. Mahdiraji, Y.M. Sua, R. Ahmed, Y.G. Shee, F.R.M. Adikan, Highly sensitive multi-core flat fiber surface plasmon resonance refractive index sensor, *Opt. Express* 24 (2016) 2485.
- [21] M. Smietana, M. Koba, E. Brzozowska, K. Krogulski, J. Nakonieczny, L. Wachnicki, P. Mikulic, M. Godlewski, W.J. Bock, Label-free sensitivity of long-period gratings enhanced by atomic layer deposited TiO<sub>2</sub> nano-overlays, *Opt. Express* 23 (2015) 8441.
- [22] L. Coelho, D. Viegas, J.L. Santos, J.M.M. Almeida, Enhanced refractive index sensing characteristics of optical fibre long period grating coated with titanium dioxide thin films, *Sens. Actuators B Chem.* 202 (2014) 929–934.



- [23] Z. Li, Q. Luo, B. Yan, X. Ruan, Y. Zhang, Y. Dai, Z. Cai, T. Chen, Titanium dioxide film coated excessively tilted Fiber Grating for ultra-sensitive refractive index sensor, *J. Light. Technol.* 36 (2018) 5285–5297.
- [24] M. Hirsch, D. Majchrowicz, P. Wierzba, M. Weber, M. Bechelany, M. Jędrzejewska-Szczerska, low-coherence interferometric fiber-optic sensors with potential applications as biosensors, *Sensors* 17 (2017) 261.
- [25] A.Og. Dikovska, P.A. Atanasov, T.R. Stoyanov, A.T. Andreev, E.I. Karakoleva, B.S. Zafirova, Pulsed laser deposited ZnO film on side-polished fiber as a gas sensing element, *Appl. Opt.* 46 (2007) 2481.
- [26] J. Xu, J. Han, Y. Zhang, Y. Sun, B. Xie, Studies on alcohol sensing mechanism of ZnO based gas sensors, *Sens. Actuators B Chem.* 132 (2008) 334–339.
- [27] D. Majchrowicz, M. Hirsch, P. Wierzba, M. Bechelany, R. Viter, M. Jędrzejewska-Szczerska, Application of thin ZnO ALD layers in fiber-optic fabry-pérot sensing interferometers, *Sensors* 16 (2016) 416.
- [28] S.I. Boyadjiev, V. Georgieva, R. Yordanov, Z. Raicheva, I.M. Szilágyi, Preparation and characterization of ALD deposited ZnO thin films studied for gas sensors, *Appl. Surf. Sci.* 387 (2016) 1230–1235.
- [29] P. Struk, T. Pustelny, K. Gołaszewska, M.A. Borysiewicz, A. Piotrowska, Optical investigations of ZnO layers affected by some selected gases in the aspect of their application in optical gas sensors, *Bull. Polish Acad. Sci. Tech. Sci.* 63 (2015) 829–836.
- [30] J.-W. Kim, Y. Porte, K.Y. Ko, H. Kim, J.-M. Myoung, Micropatternable double-faced ZnO nanoflowers for flexible gas sensor, *ACS Appl. Mater. Interfaces* 9 (2017) 32876–32886.
- [31] P. Struk, T. Pustelny, K. Gołaszewska, E. Kamińska, M. Borysiewicz, M. Ekielski, A. Piotrowska, Hybrid photonics structures with grating and prism couplers based on ZnO waveguides, *Opto-electronics Rev.* 21 (2013).
- [32] P. Struk, T. Pustelny, K. Gołaszewska, A.M. Borysiewicz, E. Kamińska, T. Wojciechowski, A. Piotrowska, ZnO - wide bandgap semiconductor and possibilities of its application in optical waveguide structures, *Metro. Meas. Syst.* 21 (2014) 401–412.
- [33] G. Eranna, *Metal Oxide Nanostructures as Gas Sensing Devices*, Series in sensors; CRC Press, Boca Raton, FL, 2012, ISBN 978-1-4398-6340-4.
- [34] H. Morko, *Zgr. Mit Zinc Oxide: Fundamentals, Materials and Device Technology*, Wiley-VCH Verlag GmbH & Co. KGaA, Weinheim, Germany, 2009, ISBN 978-3-527-62394-5.
- [35] C.F. Klingshirn (Ed.), *Zinc Oxide: from Fundamental Properties Towards Novel Applications*, Springer series in materials science; Springer, Heidelberg; London, 2010, ISBN 978-3-642-10576-0.
- [36] H. Sharma, A. Singh, N. Kaur, N. Singh, ZnO-based imine-linked coupled biocompatible chemosensor for nanomolar detection of Co<sup>2+</sup>, *ACS Sustain. Chem. Eng.* 1 (2013) 1600–1608.
- [37] A. Tereshchenko, M. Bechelany, R. Viter, V. Khranovskyy, V. Smyntyna, N. Starodub, R. Yakimova, Optical biosensors based on ZnO nanostructures: advantages and perspectives. A review, *Sens. Actuators B Chem.* 229 (2016) 664–677.
- [38] D.C. Look, Recent advances in ZnO materials and devices, *Mater. Sci. Eng. B* 80 (2001) 383–387.
- [39] S.M. George, Atomic layer deposition: an overview, *Chem. Rev.* 110 (2010) 111–131.
- [40] M.J. Weber, M.A. Verheijen, A.A. Bol, W.M.M. Kessels, Sub-nanometer dimensions control of core/shell nanoparticles prepared by atomic layer deposition, *Nanotechnology* 26 (2015), 094002.
- [41] M. Baitimirova, R. Viter, J. Andzane, A. van der Lee, D. Voiry, I. Iatsunskiy, E. Coy, L. Mikoliunaite, S. Tumenas, K. Załęski, et al., Tuning of structural and optical properties of Graphene/ZnO nanolaminates, *J. Phys. Chem. C* 120 (2016) 23716–23725.
- [42] H. Makhlof, M. Weber, O. Messaoudi, S. Tingry, M. Moret, O. Briot, R. Chtoutou, M. Bechelany, Study of Cu<sub>2</sub>O/ZnO nanowires heterojunction designed by combining electrodeposition and atomic layer deposition, *Appl. Surf. Sci.* 426 (2017) 301–306.
- [43] R.L. Puurunen, Surface chemistry of atomic layer deposition: a case study for the trimethylaluminum/water process, *J. Appl. Phys.* 97 (2005) 121301.
- [44] M. Moret, A. Abou Chaaya, M. Bechelany, P. Miele, Y. Robin, O. Briot, Atomic Layer Deposition of zinc oxide for solar cell applications, *Superlattices Microstruct.* 75 (2014) 477–484.
- [45] N. Leick, J.W. Weber, A.J.M. Mackus, M.J. Weber, M.C.M. van de Sanden, W.M.M. Kessels, *In situ* spectroscopic ellipsometry during atomic layer deposition of Pt, Ru and Pd, *J. Phys. D Appl. Phys.* 49 (2016), 115504.
- [46] M.J. Weber, A.J.M. Mackus, M.A. Verheijen, V. Longo, A.A. Bol, W.M.M. Kessels, Atomic layer deposition of high-purity palladium films from Pd(hfac)<sub>2</sub> and H<sub>2</sub> and O<sub>2</sub> plasmas, *J. Phys. Chem. C* 118 (2014) 8702–8711.
- [47] H. Kim, Atomic layer deposition of metal and nitride thin films: current research efforts and applications for semiconductor device processing, *J. Vac. Sci. Technol. B Microelectron. Nanometer Struct.* 21 (2003) 2231.
- [48] M. Weber, C. Lamboux, B. Navarra, P. Miele, S. Zanna, M. Dufond, L. Santinacci, M. Bechelany, Boron nitride as a novel support for highly stable palladium nanocatalysts by atomic layer deposition, *Nanomaterials* 8 (2018) 849.
- [49] M. Weber, E. Coy, I. Iatsunskiy, L. Yate, P. Miele, M. Bechelany, Mechanical properties of boron nitride thin films prepared by atomic layer deposition, *CrystEngComm* 19 (2017) 6089–6094.
- [50] F. Zaera, The surface chemistry of thin film atomic layer deposition (ALD) processes for electronic device manufacturing, *J. Mater. Chem.* 18 (2008) 3521.
- [51] J.A. van Delft, D. Garcia-Alonso, W.M.M. Kessels, Atomic layer deposition for photovoltaics: applications and prospects for solar cell manufacturing, *Semicond. Sci. Technol.* 27 (2012), 074002.
- [52] O. Graniel, M. Weber, S. Balme, P. Miele, M. Bechelany, Atomic layer deposition for biosensing applications, *Biosens. Bioelectron.* 122 (2018) 147–159.
- [53] M. Weber, A. Julbe, A. Ayrál, P. Miele, M. Bechelany, Atomic layer deposition for membranes: basics, challenges, and opportunities, *Chem. Mater.* 30 (2018) 7368–7390.
- [54] M. Jędrzejewska-Szczerska, D. Majchrowicz, M. Hirsch, P. Struk, R. Bogdanowicz, M. Bechelany, V.V. Tuchin, Nanolayers in fiber-optic biosensing, in: *Nanotechnology and Biosensors*, Elsevier, 2018, pp. 395–426, ISBN 978-0-12-813855-7.
- [55] M. Hirsch, Fiber optic microsphere with ZnO thin film for potential application in refractive index sensor – theoretical study, *Photonics Lett. Pol.* 10 (2018) 85.
- [56] R. Raghavan, M. Bechelany, M. Parlinska, D. Frey, W.M. Mook, A. Beyer, J. Michler, I. Utke, Nanocrystalline-to-amorphous transition in nanolaminates grown by low temperature atomic layer deposition and related mechanical properties, *Appl. Phys. Lett.* 100 (2012) 191912.
- [57] Refractive index database: <http://refractiveindex.info/?shelf=main&book=ZnO&page=Bond-o> (Accessed on September 23, 2018).
- [58] P.L. Washington, H.C. Ong, J.Y. Dai, R.P.H. Chang, Determination of the optical constants of zinc oxide thin films by spectroscopic ellipsometry, *Appl. Phys. Lett.* 72 (1998) 3261–3263.

## Biographies

**Marzena Hirsch** received her M.Sc. in Electronics and Telecommunication specialty: Optoelectronics, from Gdansk University of Technology in 2014. She is currently a Ph.D. student. Her research focuses on use of low-coherence interferometry, fiber-optic technology and application of optical measurements in chemical and biosensing.

**Paulina Listewnik** is a Ph.D. student at Gdansk University of Technology. She received her MSc in Electronics and Telecommunication in 2016. Her research is focused on fiber-optic technology and application of microstructures into optoelectronic sensors.

**Przemysław Struk** is an adjunct in Department of Optoelectronics, Faculty of Electrical Engineering, Silesian University of Technology in Gliwice, Poland. He received the Eng. degree (2005) in electronics and telecommunications from Faculty of Mathematics and Physics, Silesian University of Technology in Poland. He received the M.Sc. degree (2007) in electronics and telecommunications engineering and Ph.D. degree (2013) in domain: technical sciences, in discipline: electronics from Faculty of Electrical Engineering, Silesian University of Technology in Poland. His current scientific interest is focused on the design and development of integrated optics structures, micro-interferometric circuits and micro-optics circuits produced in MOEMS technology for biosensors applications. His scientific interest also include research of physical properties of semiconductors materials for sensors and biosensors applications.



**Dr. Matthieu Weber** obtained a double M.Sc. in Material science Engineering and Nanotechnologies in 2009 from the University of Technology of Troyes (UTT), a leading French engineering school. He completed his Master's thesis at the Helmholtz-Zentrum Berlin (Germany), where he worked on the development of ZnO thin films for solar photovoltaics. He then carried out his doctoral research work in the frame of a collaborative European project (Marie Curie Actions), focusing on ALD of noble metal nanoparticles in the Kessels group, and obtained his Ph.D. in 2014 from the Eindhoven University of Technology (The Netherlands). He is currently working as a postdoctoral researcher at the European Institute of Membranes of Montpellier (France), where he focuses his work on the ALD synthesis of nitrides and metals nanomaterials for water filtration and gas separation membranes. His research interests include as well the synthesis of nanostructured membranes and MOFs. He is a member of the Marie Curie Fellows Association (MCFA) and he is also the co-organiser of the yearly French ALD conferences (RAFALD 2017 and 2018).

**Mikhael Bechelany** (born in March 1979) obtained his Ph.D. in Materials Chemistry from the University of Lyon (France) in 2006. His Ph.D. work was devoted to the synthesis and characterization of silicon and boron based 1D nanostructures (nanotubes, nanowires and nanocables). Then, he worked as a post-doc at EMPA (Switzerland). His research included the fabrication of nanomaterials (nanoparticles and nanowires), their organization and their nanomanipulation for applications in different field such as photovoltaic, robotic, chemical and bio-sensing. In 2010, he became a Scientist at CNRS. His current research interest in the European Institute of Membranes in Montpellier (France) focuses on novel synthesis methods for metals and ceramics nanomaterials like Atomic Layer Deposition (ALD), electrodeposition, electrospinning, 3D printing and/or on the nanostructuring using natural lithography (nanospheres and/or membranes). His research efforts include the design of nanostructured membranes for health, environment and renewable energy. Beginning of 2019, he is the author and co-author of more than 180 publications, 13 book chapters and 6 patents (h-index = 34). He is also the co-founder of 3 Startups.



**Małgorzata Szczerska** is an Associate Professor in the Department of Metrology and Optoelectronics of Gdansk University of Technology, where she leads the research group in the area of biophotonics and fiber-optic sensors. She received a Ph.D. in 2008 and a D.Sc. in 2016 from Gdansk University of Technology. Her main area of research is biophotonics and she focuses on the use of low-coherence interferometry, fiber-optic technology, and the application of optical measurements in biomedicine. Apart from her main research subject, she also deals with research in the areas of: using low-coherence interferometry in metrology, constructing an electronic system supporting behavioural therapy for children with autism,

and investigating the biocompatibility of new optoelectronic materials. She has supervised seven doctoral theses and has published more than 60 research articles and review papers. She has served as a leader of many scientific projects and has been awarded by the first edition of the INTER competition, organized by the Foundation for Polish Science for the implementation of interdisciplinary research (2013–2014). She was the winner of the first edition of the eNgage competition of the Foundation for Polish Science for the implementation of the work of disseminating research results (2014–2015). She is the author and co-author of 3 patents.

[PL3]

**Listewnik, P.;** Bechelany, M.; Jasinski, J.B.; Szczerska, M. ZnO ALD-coated Microsphere-Based Sensors for Temperature Measurements. *Sensors (Switzerland)* 2020, 20, 1–8, doi:10.3390/s20174689

*Analysis of the results from an experimental investigation of the temperature obtained with a microsphere-based fiber-optic sensor with a 200 nm ZnO ALD coating.*



Communication

# ZnO ALD-Coated Microsphere-Based Sensors for Temperature Measurements

Paulina Listewnik <sup>1,\*</sup>, Mikhael Bechelany <sup>2</sup> , Jacek B. Jasinski <sup>3</sup>  and Małgorzata Szczerska <sup>1</sup>

<sup>1</sup> Department of Metrology and Optoelectronics, Faculty of Electronics, Telecommunications and Informatics, Gdańsk University of Technology, 11/12 Narutowicza Street, 80-233 Gdańsk, Poland; malszcze@pg.edu.pl

<sup>2</sup> Institut Européen des Membranes, IEM—UMR 5635, University of Montpellier, ENSCM, CNRS, 34095 Montpellier, France; mikhael.bechelany@umontpellier.fr

<sup>3</sup> Conn Center for Renewable Energy Research, University of Louisville, Louisville, KY 40292, USA; jacek.jasinski@louisville.edu

\* Correspondence: pauliste@student.pg.edu.pl

Received: 7 July 2020; Accepted: 18 August 2020; Published: 20 August 2020



**Abstract:** In this paper, the application of a microsphere-based fiber-optic sensor with a 200 nm zinc oxide (ZnO) coating, deposited by the Atomic Layer Deposition (ALD) method, for temperature measurements between 100 and 300 °C, is presented. The main advantage of integrating a fiber-optic microsphere with a sensing device is the possibility of monitoring the integrity of the sensor head in real-time, which allows for higher accuracy during measurements. The study has demonstrated that ZnO ALD-coated microsphere-based sensors can be successfully used for temperature measurements. The sensitivity of the tested device was found to be 103.5 nW/°C when the sensor was coupled with a light source of 1300 nm central wavelength. The measured coefficient  $R^2$  of the sensor head was over 0.99, indicating a good fit of the theoretical linear model to the measured experimental data.

**Keywords:** atomic layer deposition; fiber-optic; microsphere; temperature; ZnO

## 1. Introduction

Temperature is one of the most important parameters, measured in many different fields, such as science, medicine or industry [1–5]. It is used to monitor quality of the products, procedures and energy consumption. Accurate temperature measurements are highly dependent on carefully chosen instruments, which should be selected based on conditions in which the device will be used, external influences and the parameters suitable for each task, especially temperature range, pollution, sensitivity and period of time, over which the measurements will be performed [6,7].

One of the fields, where the temperature is strictly controlled is the food industry. This is to ensure that the proper standards are preserved and to minimize the risks, such as bacteria growth and formation of toxins, while processing and storing the food [8,9]. Maintaining the right temperature helps to avoid food poisoning or its spoiling [10,11]. Another area, where those measurements are also highly utilized are electrochemical batteries and energy storage cells, where temperature control is used to monitor device performance and stability during charging cycles, therefore preserving its properties for as long as possible and estimating its lifetime [12,13]. Monitoring temperature is also useful during plastic or metal production to ensure the quality of the products and workplace security [14–16].

There is an abundance of instruments for temperature measurements, from contact sensors, such as thermocouples and thermistors to contactless devices, i.e., infrared thermal detectors [17–19]. Among them, all fiber-optic sensors stand out and, as a consequence, their development has been steadily progressing throughout the years thanks to the ease of use of these devices, their high durability, low fabrication cost, and chemical inertness [20–22]. Over the last decade, researchers gained new measurement

techniques using fiber-optic sensors, such as: hybrid fiber-optic sensing, GOD-complex-based (glucose oxidase complex) sensors, multi-parameter sensors, deformable micro-mirror sensors or core-offset splicing [23–28]. The requirement for the long-term monitoring of temperature in severe, remote conditions caused fiber-optic sensors application in many fields, including industry, e.g., building applications, oil leakage railway infrastructure [29–33], but also they are used in biochemistry [34]. Moreover, fiber-optic sensors can be adapted to best suit the needs of specific applications, by modifying geometrical parameters or by adding additional passive components, such as coatings [35–37].

In traditional fiber-optic sensors, many desired properties have been hampered by low sensitivity, limited measurement range and the lack of protection against mechanical damage. In order to address these shortcomings, the sensors with various coatings (metal, metal oxides, diamond, etc.), deposited on the surface of the sensor head by different methods (atomic layer deposition, magnetron sputtering, electron beam evaporation e-beam) [38–40], have started to be developed in recent years.

Geometrical modifications have also been introduced to increase resolution, employ phenomena such as resonance or Whispering Mode Gallery, and control the optical path of the light within the utilized medium [41]. The most used optical-fiber structures include tapers and microspheres [42,43].

One of the most challenging aspects in remote sensing, especially under volatile conditions, is determining whether the integrity of the sensor head remains preserved. Ensuring that the sensor head keeps its integrity, it helps to eliminate inaccuracies from the obtained data and prevent major disruptions of the measurement process. Incorporating a microsphere to the fiber-optic sensor allows one to monitor the state of the sensor head during real-time measurements.

This work presents the advantages of combining a fiber-optic microsphere and ZnO (zinc oxide) ALD (Atomic Layer Deposition) 200 nm coating into one sensor, designed for temperature measurements at the central wavelength of 1300 nm.

## 2. Materials and Methods

### 2.1. Microsphere Development

The fiber-optic microsphere was manufactured at the end of a standard single-mode optical fiber (SMF-28, Thorlabs Inc., Newton, NJ, USA) by using an electric arc from the splicer (FSU975, Ericsson, Sweden), which provided sufficient energy to affect the original structure of the fiber and allowed for the microsphere to be formed by a three-step pull. During the fabrication process, the splicing parameters were carefully controlled, ensuring the high reproducibility of the microsphere structure. The diameter of the microsphere used for this study was 245  $\mu\text{m}$ .

The microsphere was coated with a 200-nm-thick ZnO layer using Atomic Layer Deposition (ALD), as described elsewhere [38,44].

The described device worked as an interferometric fiber-optic sensor with an intrinsic fixed cavity. The principle of the operation of the sensor is shown in Figure 1.

During operation, part of the optical signal propagating through the fiber is reflected at the boundary between the core and the cladding of the microsphere, whereas the rest passes through and reflects off the microsphere surface. Cross-section of the sensor head presented in Figure 1b provides visualization how the signal propagates through the sensor.

These two beams interfere with each other. While the reflection on the boundary between the core and the cladding is constant, the reflection from the microsphere surface depends on the optical properties of the deposited ZnO coating. By adjusting the thermal radiation around the device, the ZnO coating is influenced, which affects the intensity of the output signal.

The sensor head has been subjected to Scanning Electron Microscopy (SEM) imaging to provide the characterization of the ZnO coating after its deposition on the surface of the microsphere. The image presented in Figure 2 is of 5000 $\times$  magnification and it shows the uniformity of the ALD ZnO coating.

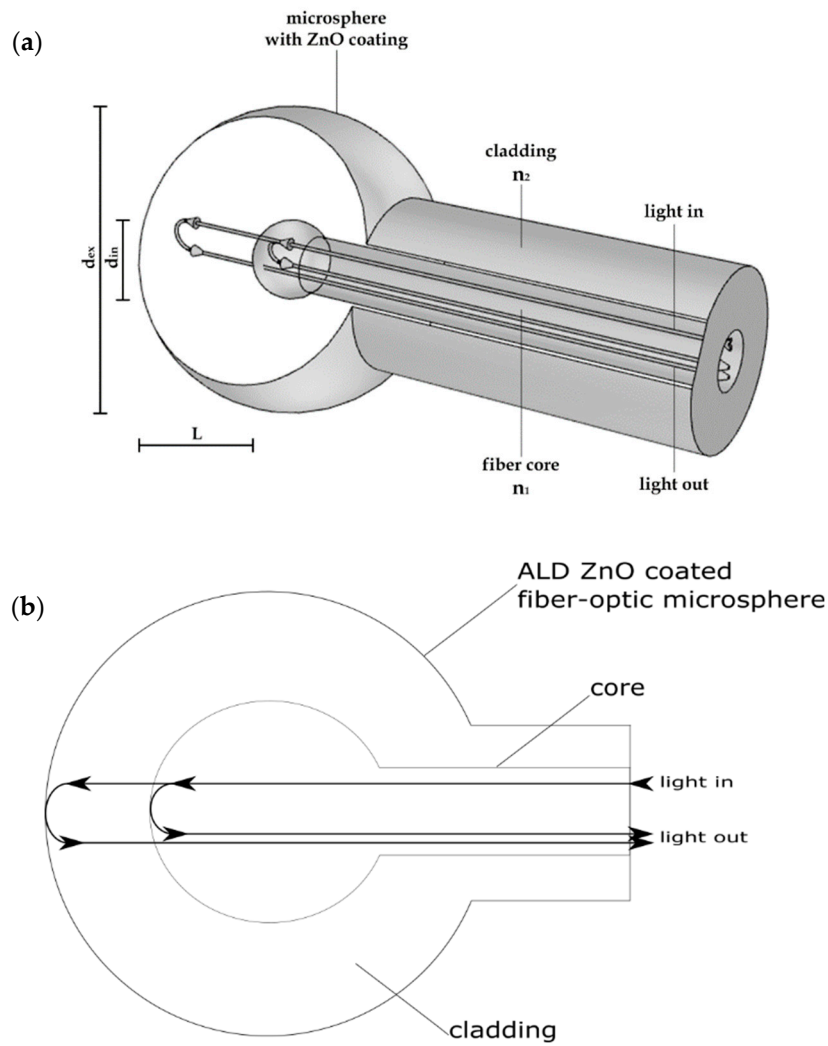


**Figure 1.** Principle of operation of the microsphere-based sensor with ZnO Atomic Layer Deposition (ALD) coating for temperature measurement: (a) schematic representation of a sensor, (b) cross-section of the sensor head.

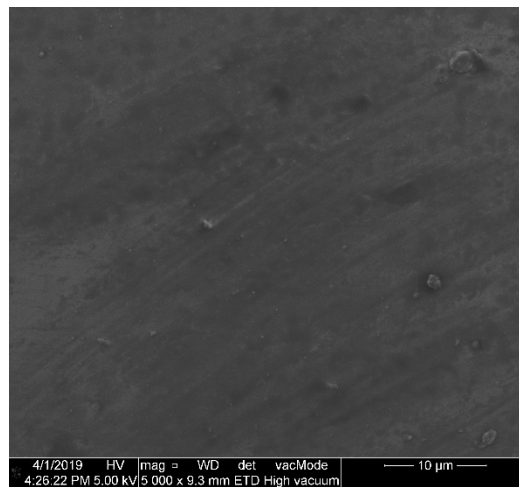


**Figure 2.** Scanning Electron Microscopy (SEM) image of the ALD ZnO coating deposited on the surface of the microsphere with 5000 $\times$  magnification.

## 2.2. Experimental Setup

To validate the sensing capabilities of the device, experimental measurements were performed. Test measurements were performed in order to obtain a spectral response of the signal during temperature changes. The temperature was measured using a low-coherence light source, temperature calibrator and an optical signal analyzer in a configuration presented in Figure 3.

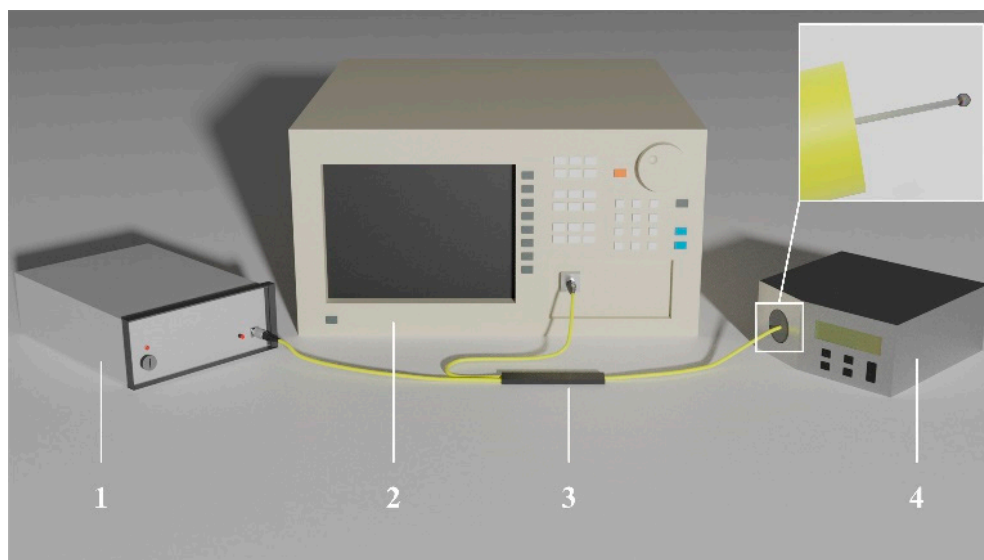


**Figure 3.** Schematic of the experimental setup used for temperature measurement, where: 1—superluminescent diode, 2—Optical Signal Analyzer, 3—optical coupler, 4—temperature calibrator.

During measurements, an optical signal, that was generated and provided by the low-coherent light source—superluminescent diode with a center wavelength of 1310 nm (SLD-1310-18-W, FiberLabs Inc., Fujimino, Japan), propagated through a typical 2:1 50/50% optical coupler (G657A, CELLCO, Kobylanka, Poland) to the microsphere-based fiber-optic sensor, placed in the temperature calibrator (ETC-400A, Ametek, Berwyn, PA, USA).

The reflected signal intensity was measured in a temperature range from 100 to 300 °C with a 10 °C step. The temperature was adjusted every 5 min in order to allow the sensor to adapt to the change. After the signal was reflected by the microsphere, it was received and analyzed by the Optical Signal Analyzer (OSA, Ando AQ6319, Yokohama, Japan).

## 3. Results and Discussion

The results presented in this section were obtained according to the procedures described in Section 2.

Several series of measurements were carried out in order to test the device temperature sensing abilities. During measurements, the sensor head was placed inside the temperature calibrator, while the range was increased with 10 °C steps, between 100 and 300 °C.

Figure 4 shows an example of the measured response of the microsphere-based fiber-optic sensor at a wavelength of 1300 nm. As shown, the intensity of the reflected signal increased with the increase in the temperature. Not all of the measured responses were plotted to maintain clarity of the graph. A slight shift in wavelength ( $\pm 2$  nm) is a result of an optical coupler loss.



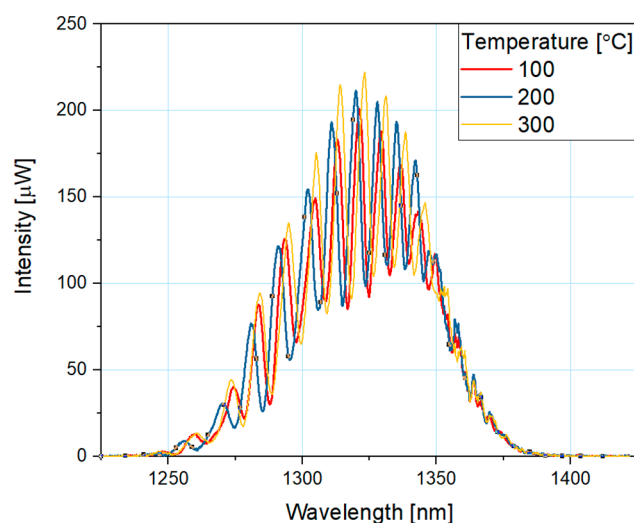


**Figure 4.** Measured response of the reflected signal intensity for the microsphere-based sensor with 200 nm ZnO ALD coating at 100, 200 and 300 °C.

The temperature dependence of the reflected signal peak intensity measured in the entire temperature range is presented in Figure 5. Additionally, Figure 5 shows a theoretical linear fit indicating the accuracy of the device. As shown, the intensity of the reflected signal increased linearly with the temperature. The obtained coefficient  $R^2$ , which represents the quality of the fit, is 0.995, i.e., close to 1, suggesting good agreement of the experimental data and theoretical linear fit.

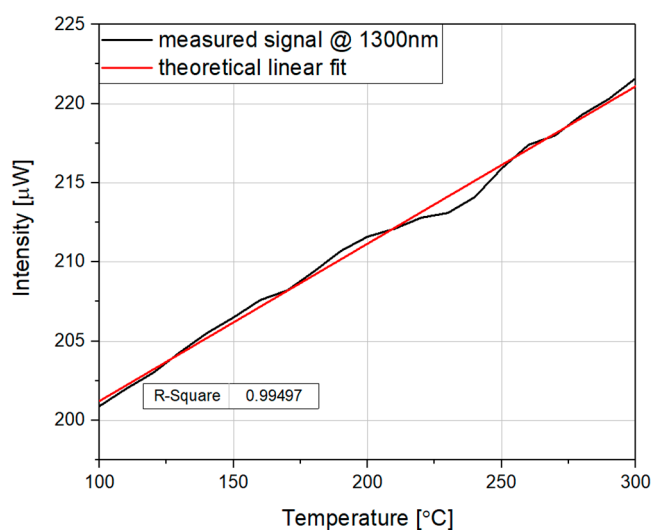


**Figure 5.** Dependence of the reflected signal peak intensity vs. temperature for a microsphere-based sensor with 200 nm ZnO ALD coating, measured at a wavelength of 1300 nm. A theoretical linear fit is also included.

The sensitivity of the sensor was calculated according to Formula (1):

$$S = \frac{\Delta I}{\Delta T} \quad (1)$$

where:  $S$ —sensitivity,  $\Delta I$ —intensity,  $\Delta T$ —temperature.

The sensitivity of the sensor calculated from the data in Figure 5 equals 103.5 nW/°C.

The presented results indicate that the microsphere-based sensor with 200 nm ZnO ALD coating is a promising device for temperature measurements. The described device maintains stable conditions

to perform such measurements. In addition, its design provides an opportunity for constant, real-time monitoring of the integrity of the sensor head structure.

#### 4. Conclusions

This paper introduces a ZnO ALD coated microsphere-based sensor for temperature measurements. The presented ZnO ALD coated microsphere-based sensor is demonstrated to be a precise device ideal for long-term monitoring temperature, which is crucial for industrial applications, such as manufacturing, processing, storing and controlling products in various sectors. Investigated sensor is a reliable device during harsh conditions and remote or hard-to-get places, where the cost of measurement system is balanced by safety considerations or service and operation costs. The presented sensor can, for example, be utilized for the investigation of processes occurring inside of electrochemical battery cells during their charging-discharging cycles. The sensor is fabricated at the end-face of an optical fiber and the coating of 200 nm in thickness is deposited on its surface by the ALD method. By using a microsphere sensor head, not only can the measured parameters be controlled, but also the structural integrity of the sensor. To optimize the metrological parameters of the device, such as sensitivity or resolution, the thickness of the coating can be modified as needed [44].

**Author Contributions:** Conceptualization, P.L. and M.S.; methodology, P.L. and M.S.; validation, P.L. and M.S.; formal analysis, P.L. and M.S.; investigation, P.L.; writing—original draft preparation, P.L. and M.S.; writing—review and editing, M.B. and J.B.J.; visualization, P.L.; supervision, M.S.; funding acquisition, M.S. and M.B. All authors have read and agreed to the published version of the manuscript.

**Funding:** The authors acknowledge the financial support of the Polish National Agency for Academic Exchange—NAWA under bilateral exchange of scientists between France and Poland PHC Polonium (PPN/BFR/2019/1/00005). The authors P.L. and M.S. acknowledge the financial support of the DS Programs of the Faculty of Electronics, Telecommunications and Informatics of the Gdańsk University of Technology.

**Acknowledgments:** P.L. would like to thank Katarzyna Gajdecka for valuable help in the visualization of the sensor head.

**Conflicts of Interest:** The authors declare no conflict of interest.

#### References

1. Sergejev, D.; Solovjov, A.; Shunkeyev, K.; Zhanturina, N. Temperature dependences of the excess current and pseudogap in high-temperature superconductor Bi<sub>2</sub>Sr<sub>2</sub>CaCu<sub>2</sub>O<sub>9</sub>. In Proceedings of the 2017 International Siberian Conference on Control and Communications (SIBCON), Astana, Kazakhstan, 29–30 June 2017; pp. 1–6.
2. Teunissen, L.P.J.; Klewer, J.; de Haan, A.; de Koning, J.J.; Daanen, H.A.M. Non-invasive continuous core temperature measurement by zero heat flux. *Physiol. Meas.* **2011**, *32*, 559–570. [[CrossRef](#)] [[PubMed](#)]
3. D'Acquisto, L.; Scardulla, F.; Pasta, S. Steam sterilization processes affect the stability of clinical thermometers: Thermistor and prototypal FBG probe comparison. *Opt. Fiber Technol.* **2020**, *55*, 102156. [[CrossRef](#)]
4. Kocjan, B.; Krawczyk, K.; Snopek, L.; Jasinski, R.; Dudek, E. Temperature chamber with precise temperature stability. In Proceedings of the 2018 Conference on Precision Electromagnetic Measurements (CPEM 2018), Paris, France, 8–13 July 2018; pp. 1–2.
5. Jia, R.; Xiong, Q.; Liang, S.; Shi, W.; Wang, L. The study of temperature distribution reconstruction based on the singular value decomposition and the griddata interpolation algorithm in industry microwave heating. In Proceedings of the 27th Chinese Control and Decision Conference (2015 CCDC), Qingdao, China, 16–18 July 2015; pp. 4015–4020.
6. Chen, P.-K.; Chen, C.-H.; Lin, S.-C.; Kuan, Y.-T.; Lin, H.-L.; Chen, J.-W. Study of the Water Temperature and Quality Change with Hot and Cold Springs. In Proceedings of the 2017 International Conference on Information, Communication and Engineering (ICICE), Xiamen, China, 17–20 November 2017; pp. 193–196.
7. Wang, W.; Ma, Z.; Wang, X.; Li, C.; Ma, J.; Long, K.; Hao, Z.; Liu, S.; Wu, Y. Distribution of moisture in oil immersed pressboard under transient temperature condition. In Proceedings of the 2012 IEEE International Conference on Condition Monitoring and Diagnosis, Bali, Indonesia, 23–27 September 2012; pp. 897–900.



8. Vadivambal, R.; Jayas, D.S. Applications of thermal imaging in agriculture and food industry—A review. *Food Bioprocess Technol.* **2011**, *4*, 186–199. [[CrossRef](#)]
9. Raghunathan, N.; Xiaofan, J.; Peroulis, D.; Ganguly, A. Wireless low-power temperature probes for food/pharmaceutical process monitoring. In Proceedings of the 2015 IEEE SENSORS, Busan, Korea, 1–4 November 2015; pp. 1–4.
10. Patel, H.; Sheth, S.; Farhad, S.M. Cloud based temperature and humidity alert system to prevent food poisoning. In Proceedings of the 2019 Cybersecurity and Cyberforensics Conference (CCC), Melbourne, Australia, 8–9 May 2019; pp. 1–5.
11. Bansal, B.; Chen, X.D. Effect of temperature and power frequency on milk fouling in an ohmic heater. *Food Bioprod. Process.* **2006**, *84*, 286–291. [[CrossRef](#)]
12. Mutyala, M.S.K.; Zhao, J.; Li, J.; Pan, H.; Yuan, C.; Li, X. In-situ temperature measurement in lithium ion battery by transferable flexible thin film thermocouples. *J. Power Sources* **2014**, *260*, 43–49. [[CrossRef](#)]
13. Novais, S.; Nascimento, M.; Grande, L.; Domingues, M.F.; Antunes, P.; Alberto, N.; Leitão, C.; Oliveira, R.; Koch, S.; Kim, G.T.; et al. Internal and external temperature monitoring of a Li-Ion battery with fiber bragg grating sensors. *Sensors* **2016**, *16*, 1394. [[CrossRef](#)]
14. Utada, S.; Rame, J.; Hamadi, S.; Delautre, J.; Villechaise, P.; Cormier, J. Kinetics of creep damage accumulation induced by a room-temperature plastic deformation introduced during processing of AM1 Ni-based single crystal superalloy. *Mater. Sci. Eng. A* **2020**, *789*, 139571. [[CrossRef](#)]
15. Jung, J.G.; Lee, K.; Lee, B.; Lee, H.S. Effect of rapid thermal annealing on bulk micro-defects and plastic deformation in silicon during high temperature processing. *Mater. Sci. Semicond. Process.* **2018**, *85*, 83–89. [[CrossRef](#)]
16. Dubois, A.; Dubar, M.; Dubar, L. Warm and hot upsetting sliding test: Tribology of metal processes at high temperature. *Procedia Eng.* **2014**, *81*, 1964–1969. [[CrossRef](#)]
17. Debey, D.; Bluhm, R.; Habets, N.; Kurz, H. Fabrication of planar thermocouples for real-time measurements of temperature profiles in polymer melts. *Sens. Actuators A Phys.* **1997**, *58*, 179–184. [[CrossRef](#)]
18. Souza, E.L.d.J.; Santos, T.L.M. Transient compensation for thermistor-based sensors in constant temperature configuration. *Sens. Actuators A Phys.* **2020**, *305*, 111920. [[CrossRef](#)]
19. Zhao, B.; Feng, F.; Tian, B.; Yu, Z.; Li, X. Micro thermal conductivity detector based on SOI substrate with low detection limit. *Sens. Actuators B Chem.* **2020**, *308*, 127682. [[CrossRef](#)]
20. Bhadra, S.; Tan, D.S.Y.; Thomson, D.J.; Freund, M.S.; Bridges, G.E. A wireless passive sensor for temperature compensated remote pH monitoring. *IEEE Sens. J.* **2013**, *13*, 2428–2436. [[CrossRef](#)]
21. Guo, Y.; Xiong, L.; Liu, H. Research on the durability of metal-packaged fiber bragg grating sensors. *IEEE Photon. Technol. Lett.* **2019**, *31*, 525–528. [[CrossRef](#)]
22. Wen, J.; Liu, W.; Huang, Y.; Liu, Y.; Luo, Y.; Peng, G.-D.; Pang, F.; Chen, Z.; Wang, T. Spun-related effects on optical properties of spun silica optical fibers. *J. Lightwave Technol.* **2015**, *33*, 2674–2678. [[CrossRef](#)]
23. Chen, K.; Zhou, X.; Yang, B.; Peng, W.; Yu, Q. A hybrid fiber-optic sensing system for down-hole pressure and distributed temperature measurements. *Optics Laser Technol.* **2015**, *73*, 82–87. [[CrossRef](#)]
24. Huang, J.; Zhang, P.; Li, M.; Zhang, P.; Ding, L. Complex of hydrogel with magnetic immobilized GOD for temperature controlling fiber optic glucose sensor. *Biochem. Eng. J.* **2016**, *114*, 262–267. [[CrossRef](#)]
25. Bremer, K.; Reinsch, T.; Leen, G.; Roth, B.; Lochmann, S.; Lewis, E. Pressure, temperature and refractive index determination of fluids using a single fibre optic point sensor. *Sens. Actuators A Phys.* **2017**, *256*, 84–88. [[CrossRef](#)]
26. Velázquez-González, J.S.; Monzón-Hernández, D.; Moreno-Hernández, D.; Martínez-Piñón, F.; Hernández-Romano, I. Simultaneous measurement of refractive index and temperature using a SPR-based fiber optic sensor. *Sens. Actuators B Chem.* **2017**, *242*, 912–920. [[CrossRef](#)]
27. Guermat, A.; Guessoum, A.; Demagh, N.-E.; Zaboub, M.; Bouhafs, Z. Fibre-optic temperature and pressure sensor based on a deformable concave micro-mirror. *Sens. Actuators A Phys.* **2018**, *270*, 205–213. [[CrossRef](#)]
28. Gao, S.; Ji, C.; Ning, Q.; Chen, W.; Li, J. High-sensitive Mach-Zehnder interferometric temperature fiber-optic sensor based on core-offset splicing technique. *Opt. Fiber Technol.* **2020**, *56*, 102202. [[CrossRef](#)]
29. Tregubov, A.V.; Svetukhin, V.V.; Novikov, S.G.; Berintsev, A.V.; Prikhodko, V.V. A novel fiber optic distributed temperature and strain sensor for building applications. *Results Phys.* **2016**, *6*, 131–132. [[CrossRef](#)]
30. Kesavan, K.; Ravisankar, K.; Parivallal, S.; Sreeshylam, P.; Sridhar, S. Experimental studies on fiber optic sensors embedded in concrete. *Measurement* **2010**, *43*, 157–163. [[CrossRef](#)]

31. Mirzaei, A.; Bahrampour, A.R.; Taraz, M.; Bahrampour, A.; Bahrampour, M.J.; Ahmadi Foroushani, S.M. Transient response of buried oil pipelines fiber optic leak detector based on the distributed temperature measurement. *Int. J. Heat Mass Transf.* **2013**, *65*, 110–122. [[CrossRef](#)]
32. Fuhr, P.L.; Huston, D.R. Corrosion detection in reinforced concrete roadways and bridges via embedded fiber optic sensors. *Smart Mater. Struct.* **1998**, *7*, 217–228. [[CrossRef](#)]
33. Du, C.; Dutta, S.; Kurup, P.; Yu, T.; Wang, X. A review of railway infrastructure monitoring using fiber optic sensors. *Sens. Actuators A Phys.* **2020**, *303*, 111728. [[CrossRef](#)]
34. Huang, J.; Liu, Y.; Zhang, P.; Li, Y.; Ding, L. A temperature-triggered fiber optic biosensor based on hydrogel-magnetic immobilized enzyme complex for sequential determination of cholesterol and glucose. *Biochem. Eng. J.* **2017**, *125*, 123–128. [[CrossRef](#)]
35. Gomes, A.D.; Monteiro, C.S.; Silveira, B.; Frazão, O. A brief review of new fiber microsphere geometries. *Fibers* **2018**, *6*, 48. [[CrossRef](#)]
36. Renganathan, B.; Sastikumar, D.; Gobi, G.; Rajeswari Yogamalar, N.; Chandra Bose, A. Nanocrystalline ZnO coated fiber optic sensor for ammonia gas detection. *Optics Laser Technol.* **2011**, *43*, 1398–1404. [[CrossRef](#)]
37. Wang, Y.; Yang, M.; Zhang, G.; Dai, J.; Zhang, Y.; Zhuang, Z.; Hu, W. Fiber optic hydrogen sensor based on fabry–perot interferometer coated with Sol-Gel Pt/WO<sub>3</sub> coating. *J. Lightwave Technol.* **2015**, *33*, 2530–2534. [[CrossRef](#)]
38. Listewnik, P.; Hirsch, M.; Struk, P.; Weber, M.; Bechelany, M.; Jędrzejewska-Szczerska, M. Preparation and characterization of microsphere ZnO ALD coating dedicated for the fiber-optic refractive index sensor. *Nanomaterials* **2019**, *9*, 306. [[CrossRef](#)] [[PubMed](#)]
39. Niedziałkowski, P.; Biało-brzeska, W.; Burnat, D.; Sezemsky, P.; Stranak, V.; Wulff, H.; Ossowski, T.; Bogdanowicz, R.; Koba, M.; Śmietana, M. Electrochemical performance of indium-tin-oxide-coated lossy-mode resonance optical fiber sensor. *Sens. Actuators B Chem.* **2019**, *301*, 127043. [[CrossRef](#)]
40. Wei, H.; Yunhui, D.; Lianqing, Z.; Mingli, D. Angular sensing system based on Y-type twin-core fiber and reflective varied-line spacing grating fabricated by electron beam lithography. *Results Phys.* **2020**, *18*, 103193. [[CrossRef](#)]
41. Ma, Q.; Rossmann, T.; Guo, Z. Whispering-gallery mode silica microsensors for cryogenic to room temperature measurement. *Meas. Sci. Technol.* **2010**, *21*, 025310. [[CrossRef](#)]
42. Vikas; Verma, R.K. Design considerations of a surface plasmon resonance (SPR) based tapered fiber optic bio-sensing probe with graphene-MoS<sub>2</sub> over layers. *Optik* **2019**, *180*, 330–343. [[CrossRef](#)]
43. Cai, L.; Wang, J.; Pan, J.; Liu, Q.; Chen, Y. A tunable fiber-optic Fabry–Perot cavity formed between a silica microsphere and a target. *Opt. Commun.* **2020**, *459*, 124996. [[CrossRef](#)]
44. Hirsch, M.; Listewnik, P.; Struk, P.; Weber, M.; Bechelany, M.; Szczerska, M. ZnO coated fiber optic microsphere sensor for the enhanced refractive index sensing. *Sens. Actuators A Phys.* **2019**, *298*, 111594. [[CrossRef](#)]



© 2020 by the authors. Licensee MDPI, Basel, Switzerland. This article is an open access article distributed under the terms and conditions of the Creative Commons Attribution (CC BY) license (<http://creativecommons.org/licenses/by/4.0/>).



[PL4]

**Listewnik, P.** Temperature Fiber-Optic Sensor with ZnO ALD Coating. Eng. Proc. 2021, 2, 99, doi:10.3390/engproc2020002099.

*Analysis of the results from an experimental investigation of the temperature obtained with a microsphere-based fiber-optic sensor with a 100 nm ZnO ALD coating.*

Proceedings

# Temperature Fiber-Optic Sensor with ZnO ALD Coating <sup>†</sup>

**Paulina Listewnik**

Department of Metrology and Optoelectronics, Faculty of Electronics, Telecommunications and Informatics, Gdańsk University of Technology, 11/12 Narutowicza Street, 80-233 Gdańsk, Poland; pauliste@student.pg.edu.pl

<sup>†</sup> Presented at the 7th Electronic Conference on Sensors and Applications, 15–30 November 2020;

Available online: <https://ecsa-7.sciforum.net/>.

Published: 4 March 2021

**Abstract:** This study presents a microsphere-based fiber-optic sensor with a ZnO Atomic Layer Deposition (ALD) coating thickness of 100 nm for temperature measurements. Metrological properties of the sensor were investigated over the temperature range of 100 °C to 300 °C, with a 10 °C step. An interferometric signal is used to control whether the microstructure is whole. Spectrum shift of a reflected signal is used to ascertain changes in the measured parameter. With changing temperature, the peak position of a reflected signal also changes. The  $R^2$  coefficient of the presented sensor indicates a good linear fit of over 0.99 to the obtained data. The sensitivity of the sensor investigated in this study equals 0.019 nm/°C.

**Keywords:** atomic layer deposition; fiber-optic; microsphere; temperature; ZnO

## 1. Introduction

Fiber-optic sensors have been developed and improved upon for over a decade. Due to their versatility, they are used in numerous fields, such as industry, science or medicine [1–4]. Optimization of measurement parameters plays a significant role in development of the fiber-optic sensors. While planning measurements, selection of the sensor is a crucial element, depending on their purpose and conditions in which they will perform. Based on the type of sensor, diversity of designs and parameters can be optimized: adjustable cavity length, structure modification [5–8], as well as metrological properties, such as: resolution, precision, sensitivity, accuracy [9,10]. Many researchers contribute to the determination of the properties and parameters of various materials and structures [11,12].

This study investigates sensing abilities of the microsphere-based fiber-optic sensor with a 100-nm ZnO Atomic Layer Deposition (ALD) coating during temperature measurements.

## 2. Materials and Methods

Measurements were performed using a sensor made of a standard single-mode telecommunication optical fiber (SMF-28, Thorlabs Inc., Newton, NJ, USA) with a microsphere structure produced at the end of the fiber, using a fiber-optic splicer (FSU975, Ericsson, Sweden). The obtained microsphere has a diameter of 245  $\mu\text{m}$ . After the manufacturing of the microsphere, the ZnO coating of 100 nm thickness was deposited on its surface by Atomic Layer Deposition (ALD) method. Detailed description of the deposition process is presented elsewhere [13,14].

To assess quality of the structure and the deposited ZnO ALD coating of 100 nm thickness, it was then investigated under a Scanning Electron Microscope (SEM, Phenom XL G2, Thermo Fisher Scientific, Waltham, MA, USA), the results of which are shown in Figure 1.



**Figure 1.** SEM image of the microsphere-sensor with a 100-nm ZnO Atomic Layer Deposition (ALD) coating. Magnification of 1000 $\times$ .

The image shows the device with a magnification of 1000 $\times$  and it can be seen that the structure exhibits excellent roundness. Furthermore, the presence of ZnO coating is apparent.

Moreover, metrological properties of the sensor were validated by performing experimental measurements. During investigation, the sensor is placed in a temperature calibrator (ETC-400A, Ametek, Berwyn, PA, USA), which was increased from 100  $^{\circ}$ C to 300  $^{\circ}$ C, with a 10  $^{\circ}$ C step. The temperature was stabilized for 3 min, at each step, allowing the sensor to adjust to altered conditions. The measurements were executed using a light source with a center wavelength of 1310 nm  $\pm$  20 nm (SLD-1310-18-W, FiberLabs Inc., Fujimino, Japan). The signal was propagated through a 2:1 50/50% optical coupler (G657A, CELLCO, Kobylanka, Poland) to the sensor head coated with a 100-nm ZnO ALD coating, which is highly reflective, allowing the wave to superpose, therefore inciting interference as shown in Figure 2.

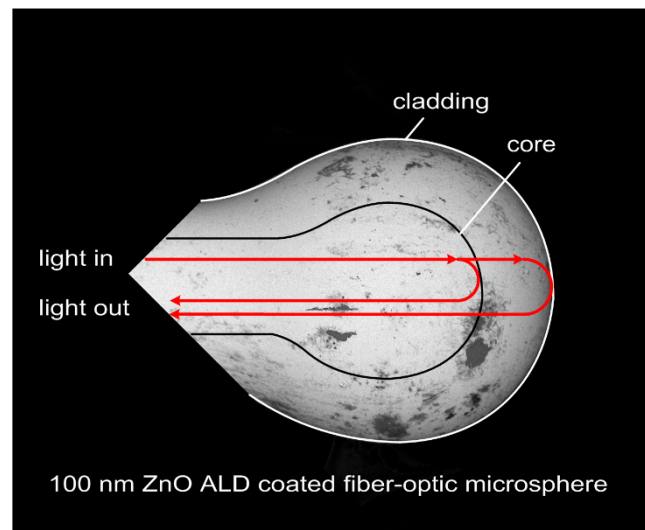


**Figure 2.** Principle of operation of a microsphere-based fiber-optic sensor.

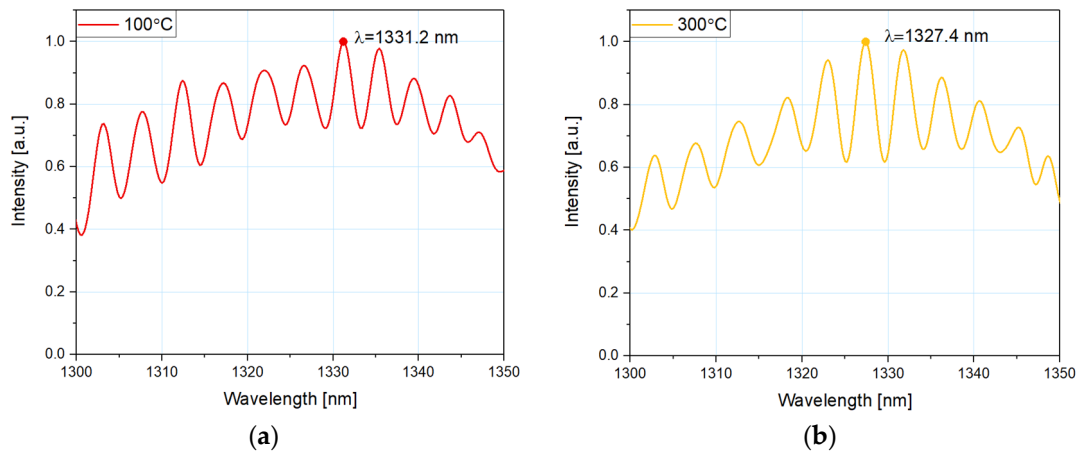
By obtaining interference, the integrity of the structure can be monitored, ensuring the sensor is not damaged. The reflected signal is then collected by Optical Spectrum Analyzer (OSA, Ando AQ6319, Yokohama, Japan). Depending on the position of the spectral peak of the signal, temperature can be determined.



### 3. Results and Discussion

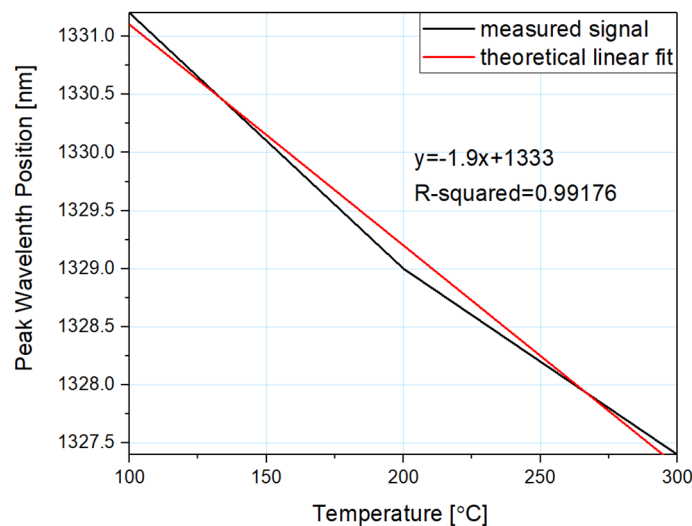
This section presents results, which were acquired from the measurements performed with the setup shown above.

Figure 3 shows normalized values of the measured signal response for the microsphere-based sensor with a 100-nm ZnO ALD coating, at 100 °C and 300 °C to preserve readability of the plot. In rising the temperature, spectral peak of the reflected signal shifts toward lower values of the wavelength. The envelope, however, remains similar for each temperature. In addition, interference fringes visible in the Figure inform about the integrity of the sensor head structure, which allows the monitoring of its condition in real-time.



**Figure 3.** The normalized measured response of the reflected signal for the microsphere-based sensor with 100-nm ZnO ALD coating at: (a) 100 °C and (b) 300 °C.

Dependence of the peak wavelength position on the temperature can be observed in Figure 4. Moreover, theoretical linear fit is also presented, as well as coefficient  $R^2$ , which equals 0.99176, being determined to confirm fitness of the obtained data to the theoretical model. Furthermore, the results presented in Figure 4 allowed to calculate the sensitivity of the microsphere-based sensor with a 100-nm ZnO ALD coating  $-0.019 \text{ nm}/^\circ\text{C}$ .



**Figure 4.** Dependence of the spectral shift of a reflected signal on the temperature.

The spectrum changes its peak wavelength position when the temperature is altered. The higher the temperature, the spectrum shift is constant throughout whole range of roughly 2 nm per 100 °C. By following linear regression, it is possible to determine the position of the reflected signal peak for each measured temperature.

#### 4. Conclusions

Microsphere-based sensors are ideal for long-term and remote measurements of parameters such as temperature or refractive index due to their ability to constantly monitor the integrity of the sensor head. The study presents a 100-nm ZnO ALD coating on the surface of a microsphere-based fiber-optic sensor for temperature measurements. Selection of an optimal coating is crucial for long-term and remote measurements. While devising the measurements, it is important to select proper parameters of the fiber-optic sensor coating for optimal efficiency. The sensor with a 100-nm ZnO ALD coating exhibits a close match between measurement data and theoretical linear fit, which is confirmed by an  $R^2$  coefficient of over 0.99. The sensitivity of the sensor with a 100-nm coating equals 0.019 nm/°C. Additionally, for the microsphere-based sensor with a 100-nm ZnO ALD coating, changes of temperature can be observed based on the spectral shift, which coincides with rise of the temperature. The sensor also indicates its proper operation by inciting interference.

**Funding:** This research was funded by the Polish National Agency for Academic Exchange—NAWA under bilateral exchange of scientists between France and Poland PHC Polonium (PPN/BFR/2019/1/00005). The author acknowledges the financial support of the DS Programs of the Faculty of Electronics, Telecommunications and Informatics of the Gdańsk University of Technology.

**Conflicts of Interest:** The authors declare no conflict of interest.

#### References

1. Xiong, F.B.; Sisler, D. Determination of low-level water content in ethanol by fiber-optic evanescent absorption sensor. *Opt. Commun.* **2010**, *283*, 1326–1330, doi:10.1016/j.optcom.2009.11.075.
2. Ramakrishnan, M.; Rajan, G.; Semenova, Y.; Farrell, G. Overview of Fiber Optic Sensor Technologies for Strain/Temperature Sensing Applications in Composite Materials. *Sensors* **2016**, *16*, 99, doi:10.3390/s16010099.
3. Karpienko, K.; Wróbel, M.S.; Jędrzejewska-Szczerska, M. Determination of refractive index dispersion using fiber-optic low-coherence Fabry–Perot interferometer: Implementation and validation. *Opt. Eng.* **2014**, *53*, 077103, doi:10.1117/1.OE.53.7.077103.
4. Witt, J.; Narbonneau, F.; Schukar, M.; Krebber, K.; De Jonckheere, J.; Jeanne, M.; Kinet, D.; Paquet, B.; Depre, A.; D’Angelo, L.T.; et al. Medical Textiles with Embedded Fiber Optic Sensors for Monitoring of Respiratory Movement. *IEEE Sens. J.* **2012**, *12*, 246–254, doi:10.1109/JSEN.2011.2158416.
5. Arif, M.F.H.; Ahmed, K.; Asaduzzaman, S.; Azad, Md.A.K. Design and optimization of photonic crystal fiber for liquid sensing applications. *Photonic Sens.* **2016**, *6*, 279–288, doi:10.1007/s13320-016-0323-y.
6. Van Newkirk, A.; Antonio-Lopez, E.; Salceda-Delgado, G.; Amezcua-Correa, R.; Schülzgen, A. Optimization of multicore fiber for high-temperature sensing. *Opt. Lett.* **2014**, *39*, 4812, doi:10.1364/OL.39.004812.
7. Wierzba, P.; Jędrzejewska-Szczerska, M. Optimization of a Fabry-Perot Sensing Interferometer Design for an Optical Fiber Sensor of Hematocrit Level. *Acta Phys. Pol. A* **2013**, *124*, 586–588, doi:10.12693/APhysPolA.124.586.
8. Wang, Q.; Wei, W.; Guo, M.; Zhao, Y. Optimization of cascaded fiber tapered Mach–Zehnder interferometer and refractive index sensing technology. *Sens. Actuators B Chem.* **2016**, *222*, 159–165, doi:10.1016/j.snb.2015.07.098.
9. Azad, S.; Sadeghi, E.; Parvizi, R.; Mazaheri, A.; Yousefi, M. Sensitivity optimization of ZnO clad-modified optical fiber humidity sensor by means of tuning the optical fiber waist diameter. *Opt. Laser Technol.* **2017**, *90*, 96–101, doi:10.1016/j.optlastec.2016.11.005.
10. Mishra, A.K.; Mishra, S.K.; Gupta, B.D. SPR based fiber optic sensor for refractive index sensing with enhanced detection accuracy and figure of merit in visible region. *Opt. Commun.* **2015**, *344*, 86–91, doi:10.1016/j.optcom.2015.01.043.
11. Song, N.; Cai, W.; Song, J.; Jin, J.; Wu, C. Structure optimization of small-diameter polarization-maintaining photonic crystal fiber for mini coil of spaceborne miniature fiber-optic gyroscope. *Appl. Opt.* **2015**, *54*, 9831, doi:10.1364/AO.54.009831.
12. Tu, M.H.; Sun, T.; Grattan, K.T.V. Optimization of gold-nanoparticle-based optical fibre surface plasmon resonance (SPR)-based sensors. *Sens. Actuators B Chem.* **2012**, *164*, 43–53, doi:10.1016/j.snb.2012.01.060.

13. Listewnik, P.; Hirsch, M.; Struk, P.; Weber, M.; Bechelany, M.; Jędrzejewska-Szczerska, M. Preparation and Characterization of Microsphere ZnO ALD Coating Dedicated for the Fiber-Optic Refractive Index Sensor. *Nanomaterials* **2019**, *9*, 306, doi:10.3390/nano9020306.
14. Hirsch, M.; Listewnik, P.; Struk, P.; Weber, M.; Bechelany, M.; Szczerska, M. ZnO coated fiber optic microsphere sensor for the enhanced refractive index sensing. *Sens. Actuators A Phys.* **2019**, *298*, 111594, doi:10.1016/j.sna.2019.111594.

**Publisher's Note:** MDPI stays neutral with regard to jurisdictional claims in published maps and institutional affiliations.



© 2021 by the authors. Licensee MDPI, Basel, Switzerland. This article is an open access article distributed under the terms and conditions of the Creative Commons Attribution (CC BY) license (<http://creativecommons.org/licenses/by/4.0/>).

[PL5]

Kosowska, M.; **Listewnik, P.**; Majchrowicz, D.; Rycewicz, M.; Bechelany, M.; Fleger, Y.; Chen, M.; Fixler, D.; Dholakia, K.; Szczerska, M. Microscale diamond protection for a ZnO coated fiber optic sensor. Sci. Rep. 2020, 10, doi:10.1038/s41598-020-76253-5.

*Analysis of the preliminary results of the influence of nanocrystalline diamond sheet on the measured response of the Fabry-Pérot fiber-optic sensor.*



OPEN

## Microscale diamond protection for a ZnO coated fiber optic sensor

Monika Kosowska<sup>1✉</sup>, Paulina Listewnik<sup>1</sup>, Daria Majchrowicz<sup>1,2✉</sup>, Michał Ryciewicz<sup>1</sup>, Mikhael Bechelany<sup>3</sup>, Yafit Fleger<sup>4</sup>, Mingzhou Chen<sup>2</sup>, Dror Fixler<sup>4,5</sup>, Kishan Dholakia<sup>2</sup> & Małgorzata Szczerska<sup>1✉</sup>

Fiber optic sensors are widely used in environmental, biological and chemical sensing. Due to the demanding environmental conditions in which they can be used, there is a risk of damaging the sensor measurement head placed in the measuring field. Sensors using nanolayers deposited upon the fiber structure are particularly vulnerable to damage. A thin film placed on the surface of the fiber end-face can be prone to mechanical damage or deteriorate due to unwanted chemical reactions with the surrounding agent. In this paper, we investigated a sensor structure formed with a Zinc Oxide (ZnO) coating, deposited by Atomic Layer Deposition (ALD) on the tip of a single-mode fiber. A nanocrystalline diamond sheet (NDS) attached over the ZnO is described. The diamond structure was synthesized in a Microwave Plasma Assisted Chemical Vapor Deposition System. The deposition processes of the nanomaterials, the procedure of attaching NDS to the fiber end-face covered with ZnO, and the results of optical measurements are presented.

Fiber-optic sensors are widely used in environmental, biological and chemical sensing<sup>1–6</sup>. That is due to their well-known advantages that allow for their use in demanding applications – they have the ability to perform real-time and remote measurements, have immunity to electromagnetic interferences and are of compact size, amongst other attributes<sup>7–9</sup>. As new technologies become available, the structures of fiber-optic sensors are growing more elaborate, with integrated thin films, nanoparticles, microstructured fibers, which aim to offer increased sensing abilities. One such group are thin film-based sensors that use nanolayers deposited on the fiber surface<sup>10–12</sup>. These are used to design and create structures that can be applied on the measuring heads of fiber-optic sensors, for example thin (tens of nanometers) dielectric layers made of materials characterized by high refractive index, e.g. ZnO ( $n = 2.1$  at 500 nm)<sup>13,14</sup>.

Using ZnO as a coating for the fiber-optic sensor has many advantages. It allows to broaden the measuring range, improves sensitivity of measured parameter, in comparison to the sensor without a coating. It also enables to perform measurements in a medium, which refractive index is close to this of optical fiber core ( $n = 1.4$ ). Furthermore, deposition techniques of ZnO are highly developed, especially Atomic Layer Deposition (ALD) method, which ensures uniformity of the coating. However, there are several instances, in which ZnO can adversely affect the surrounding medium, therefore CVD nanocrystalline diamond sheet attached over the ZnO, is required to protect both the sensor head and the measured medium from damage in case of an unwanted reaction.

In addition, fiber-optic sensors are often used in remote places, where other devices cannot be utilized due to their physical dimensions or mechanical properties. By using CVD layer, the sensor can withstand more severe conditions and it can be utilized for longer periods of time, which in turn minimizes involvement of an operator and the cost of maintenance.

Among many extraordinary properties of synthesized diamond, several of those are of particular interest from an optical point of view. It has a very high refractive index ( $n = 2.4$  at a wavelength of 500 nm), and it is transparent in the broad wavelength range. It can also work as a reflective layer when doped with other materials, e.g. boron, nitrogen<sup>15–17</sup>. Diamond is also characterized by its excellent mechanical and chemical properties, as well as biocompatibility. The properties of the diamond can be also tuned by changing the parameters of the

<sup>1</sup>Department of Metrology and Optoelectronics, Faculty of Electronics, Telecommunications and Informatics, Gdańsk University of Technology, 11/12 Narutowicza Street, 80-233 Gdańsk, Poland. <sup>2</sup>SUPA, School of Physics and Astronomy, University of St Andrews, North Haugh, St Andrews KY16 9SS, UK. <sup>3</sup>Institut Européen Des Membranes, IEM UMR 5635, University of Montpellier, ENSCM, CNRS, Place Eugène Bataillon, 34095 Montpellier, France. <sup>4</sup>Institute for Nanotechnology and Advanced Materials, Bar-Ilan University, 52900 Ramat-Gan, Israel. <sup>5</sup>Faculty of Engineering, Bar-Ilan University, 52900 Ramat-Gan, Israel. ✉email: monkosow@student.pg.edu.pl; darmajch@pg.edu.pl; malszcze@pg.edu.pl



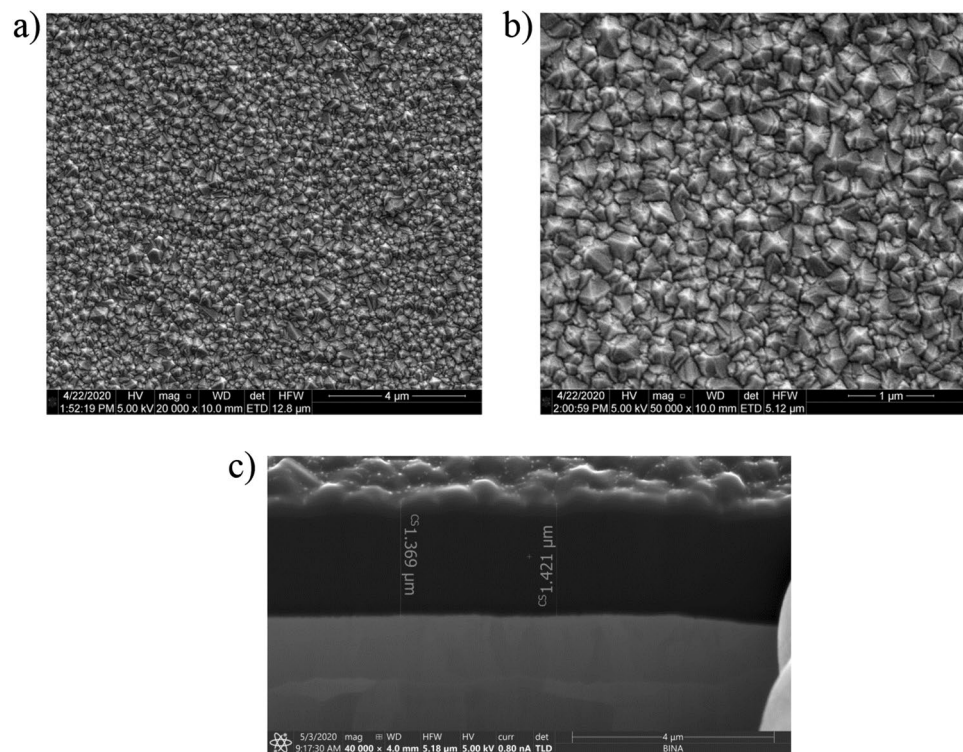


**Figure 1.** SEM images of nanocrystalline diamond sheet (a) magnification 20,000× (b) magnification 50,000× (c) cross-section magnification 40,000×.

deposition process e.g. temperature, time, working gas mixture composition. A set of such outstanding properties resulted in lots of applications of diamond in numerous fields of science, biomedicine and technology<sup>18–21</sup>.

In this work, we investigate an undoped nanocrystalline diamond sheet attached to the ZnO-coated fiber-optic sensor head. The diamond structure was synthesized in the Microwave Plasma Assisted Chemical Vapor Deposition (MW PA CVD) system. The construction of the measurement setup with the focus on the measurement head and the results of the optical measurements are presented. The sensing abilities of the fiber-optic sensor with a ZnO coating deposited by the Atomic Layer Deposition (ALD) method, investigated for temperature change as well as refractive index, are presented elsewhere<sup>10,22</sup>.

**Material characterization—nanocrystalline diamond sheet.** The obtained nanocrystalline diamond sheet surface morphology was investigated with the use of an Environmental Scanning Electron Microscope (E-SEM, Quanta FEG 250, FEI, Hillsboro, Oregon, USA). Figure 1 shows SEM images of the NDS attached to the tantalum substrate for two system magnifications, 20,000× and 50,000×, and for a cross-section magnification of 40,000×.

Figure 1a shows that the diamond had covered the substrate evenly, and over sufficient areas that are large enough for use in the construction of fiber-optic measurement head (with the fiber core dimensions of 8 μm). The obtained structure is uniform and continuous. No damage or other visible abnormalities of the surface were noted during the investigation. Figure 1b proves the crystalline character of the sample, with a grain size smaller than 500 nm. The nanocrystalline diamond sheet was investigated in terms of its thickness, and therefore, cross-section measurements were also taken.

Microscope photographs of the sample were taken with a (C-5060, Olympus, Japan) camera and a (LAB 40 POL, OPTA-TECH, Poland) microscope.

Camera and microscope pictures of a diamond sheet (1 cm × 1 cm in size) are presented in Fig. 2. The rough nanodiamond surface is caused by the delamination process, which facilitates the fabrication of freestanding diamond sheets.

The Raman spectra of the diamond films were measured by using a home-made wavelength modulated Raman system. The details of this system may be found in our previous works<sup>23,24</sup>.

The strong fluorescence background makes it impossible to locate the Raman peaks from a standard Raman spectrum as seen in Fig. 3a. However, our approach of using wavelength modulated Raman system enabled by a tunable narrow linewidth laser can remove the strong fluorescent background efficiently and reveal the underlying Raman features. To achieve this, the wavelength of the laser is tuned in five steps over a range of 1.5 nm from 785 nm. At each step, a Raman spectrum with an integration time of 1 s is recorded. As the fluorescence background does not change over this small wavelength interval, it can be removed with a post-processing algorithm, namely principal component analysis (PCA). This way, the characteristic Raman peak for nanocrystalline diamond sheet at room temperature can be recovered<sup>25,26</sup>, visualized as a zero-crossing, at 1331 cm<sup>-1</sup>, as shown

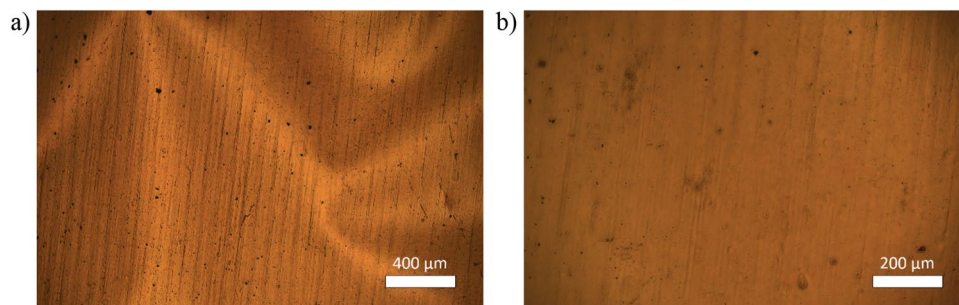


**Figure 2.** Optical microscope photographs of the diamond sheet (a) magnification 50×, (b) magnification 100×.

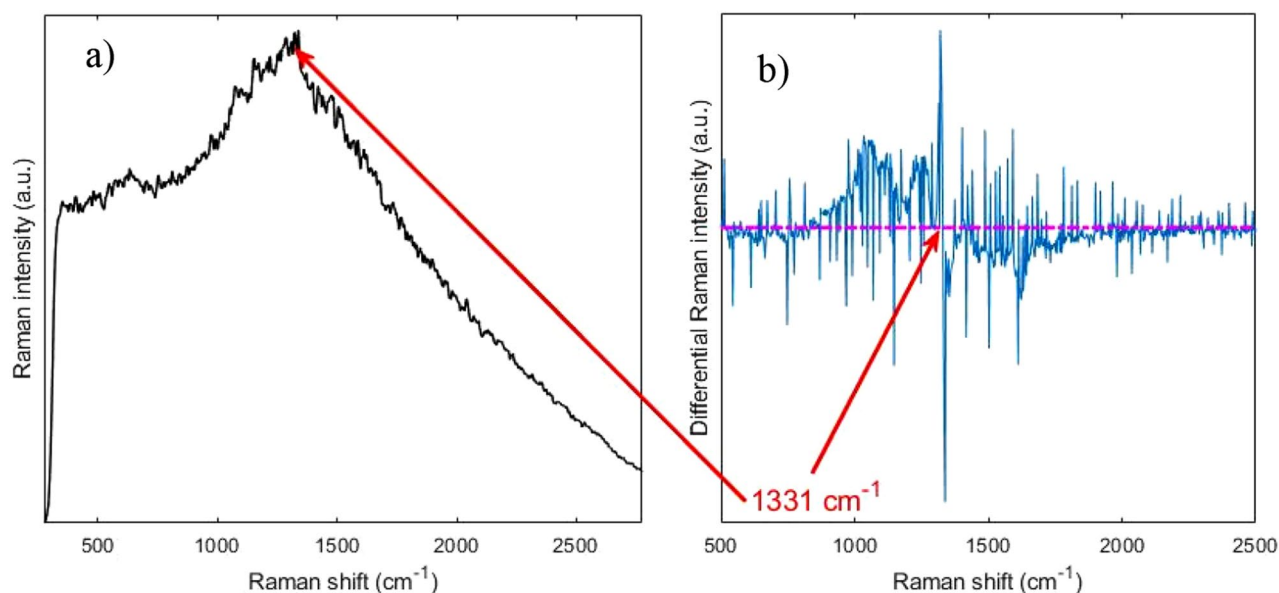


**Figure 3.** Raman spectra acquired from the nanocrystalline diamond sheet. (a) Shows a standard Raman spectrum with a very strong fluorescence background. (b) Shows the wavelength modulated Raman spectrum with the  $1331\text{ cm}^{-1}$  peak. Arrows point at the zero crossings where the peak is and its possible location in the standard Raman spectrum.

in Fig. 3b. As this dominant band is assigned to the diamond at room temperature, the investigation proved the successful deposition process resulting in the diamond structure.

## Results

This section contains the experimental measurements, which were performed to evaluate the influence of nanocrystalline diamond sheet attached over ALD ZnO coating. The series of measurements were executed by increasing the distance between the sensor head and the silver mirror by a fixed increment over  $500\text{ }\mu\text{m}$ . The measurements were performed using the sensor in two configurations: firstly, with only ZnO coating deposited on the end-face of the fiber, followed by attachment of the NDS and repeating the measurements. The results for both configurations are presented including comparison between them. Figure 4 shows the representative spectra, where the intensity of the obtained signal was normalized. The Fabry–Perot cavity length was set to  $50\text{ }\mu\text{m}$ ,  $100\text{ }\mu\text{m}$ ,  $150\text{ }\mu\text{m}$  and  $200\text{ }\mu\text{m}$ , respectively.

It can be noted from representative spectra that there is a visible signal modulation while changing the cavity length—the longer the cavity, the greater number of maxima in the investigated wavelength range. This behavior agrees with our previous findings<sup>27</sup>. Figure 5 shows the representative spectra, where the obtained signals for the measurement head with ZnO coating, as well as ZnO coating and nanocrystalline diamond sheet were compared. It can be noted that the intensity of the signal is decreasing while applying the nanocrystalline diamond sheet, which can be observed in Fig. 5. The decrease in the signal intensity does not impact the number of maxima in the spectrum. This demonstrates that NDS provides protection for the fiber end-face covered with a ZnO coating.

The application of the nanodiamond sheets decreases the signal intensity, but the signal visibility is not significantly changed.

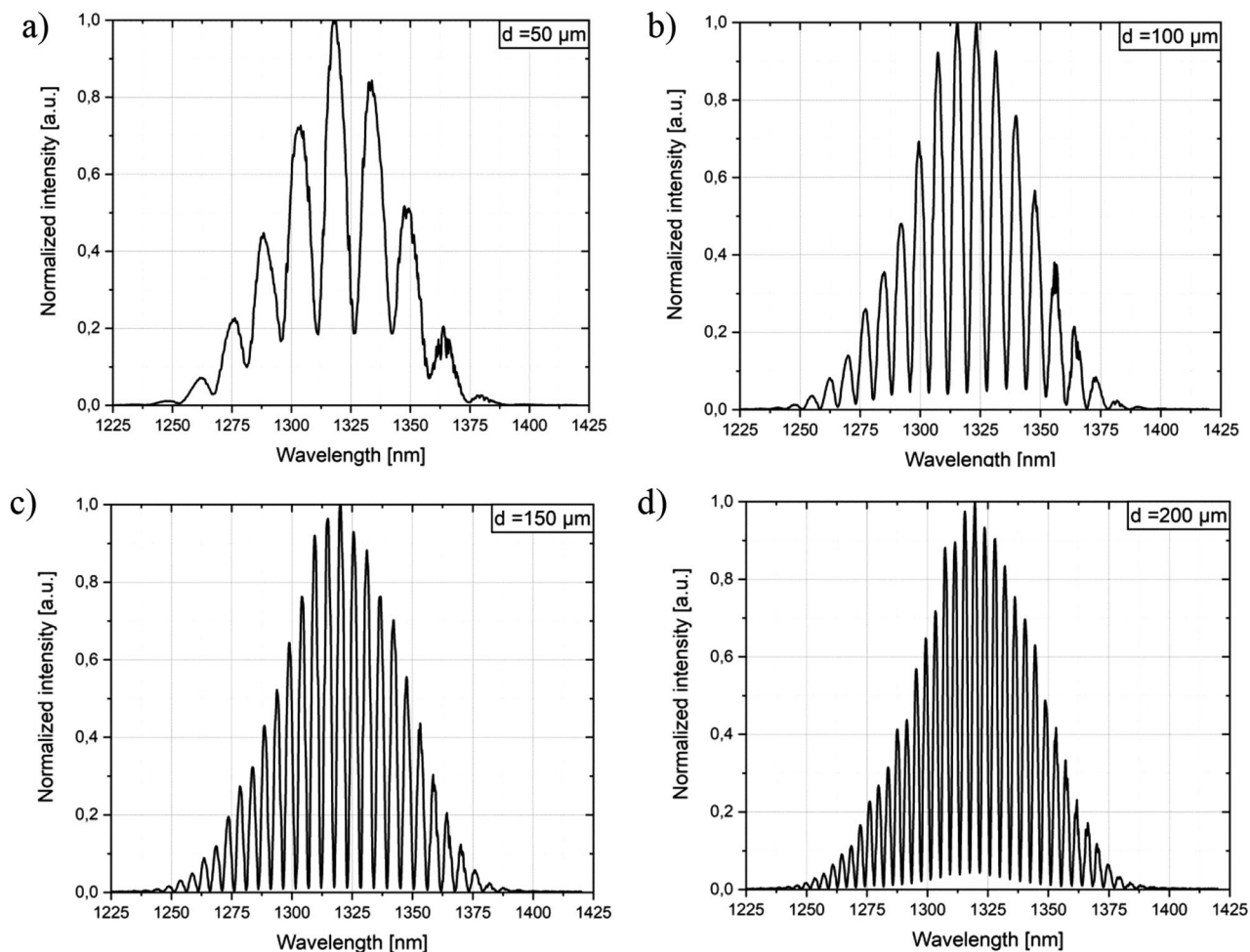


**Figure 4.** Signal obtained for the measurement head with ZnO layer and nanocrystalline diamond sheet. The Fabry-Perot cavity length was set to: (a) 50  $\mu\text{m}$ , (b) 100  $\mu\text{m}$ , (c) 150  $\mu\text{m}$ , (d) 200  $\mu\text{m}$ .

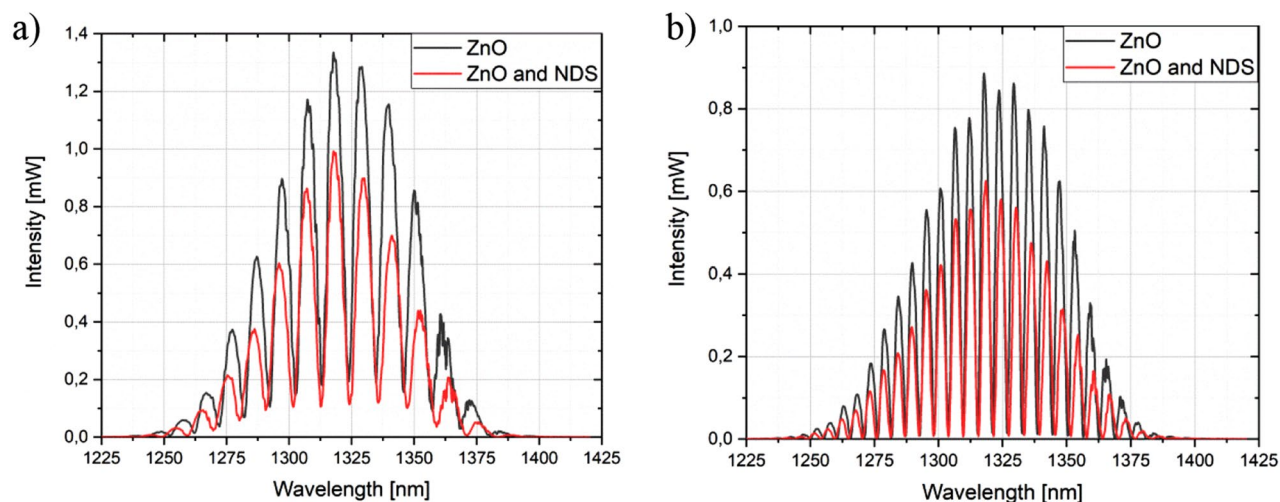


**Figure 5.** Measurement signals obtained for the measurement head with ZnO coating, and ZnO coating and nanocrystalline diamond sheet. The Fabry-Perot cavity length was set to: (a) 70  $\mu\text{m}$ , (b) 140  $\mu\text{m}$ .

Cavity length ( $\mu\text{m}$ )	Visibility for measurement head with ZnO layer and NDS
50	0.690
80	0.844
110	0.947
140	0.979
200	0.921
300	0.767

**Table 1.** Representative values of visibility for different Fabry–Perot cavity lengths.

The important parameter indicating the contrast of the measurement signal is the visibility value. It can be described with the following formula (1)<sup>28,29</sup>:

$$V = \frac{I_{\text{max}} - I_{\text{min}}}{I_{\text{max}} + I_{\text{min}}} \quad (1)$$

where  $I_{\text{max}}$ —maximum value of the signal intensity and  $I_{\text{min}}$ —minimum value of the signal intensity.

Table 1 presents values of visibility for measurement head with ZnO layer and nanodiamond sheets for different Fabry–Perot cavity lengths.

## Discussion

To date, only several research groups work on the nanocrystalline diamond sheets, focusing on deposition process, characterization of such structure and methods to transfer the resulting material onto the target surface<sup>30–32</sup>. However, example applications are scarce so far. Bogdanowicz et al. presented the deposition process of a large area NDS, characterization of its properties and demonstration of potential application. This leads to the development of a prototypical, low-temperature diamond-on-graphene transistor<sup>27</sup>. Seshan et al. showed the fabrication process and development of a transfer technique of the obtained diamond sheets with the use of a visco-elastic stamp. The NDS sheets were then used in the fabrication of mechanical resonators<sup>33</sup>.

To the best of author's knowledge, only our research group reports the application of the NDS in the fiber-optic sensors. The main goal of this study was to investigate the possibility of elaborating a fiber-optic measurement head applying a ZnO coating and the nanocrystalline diamond sheet attached over it as a protection. We showed that such integration can be performed in a simple way, assuring the correct operation of the interferometric sensor. Addition of the NDS provides a protective cover while maintaining the sensing abilities and metrological parameters. Such configuration can extend the lifespan of the sensor and prevent the coating underneath from degradation in challenging environments.

Further investigation regarding the usage of NDS for fiber-optic measurement heads in chemically aggressive media is planned. The comparison of measurement head (with and without NDS) metrological parameters after such experiments, as well as specifying the lifespan difference between them, would be the next step to directly show the benefits of NDS protection.

## Conclusions

In this paper, the fiber-optic measurement head comprising of a single-mode optical fiber, ZnO coating deposited on its end-face, and with an attached nanocrystalline diamond sheet was performed. The results of the optical measurements were described. The study proves that a NDS can be applied as a protection of the fiber-optic end-face. The attachment of the NDS did not influence the sensing abilities of the fiber sensor. This provided protection for the measurement head, which can be exposed to demanding environmental conditions. Furthermore, such protection does not influence meteorological parameters of the fiber-optic sensors because even with the NDS it was able to obtain the visibility of measured signal at the value of 0.979.

On the other hand, maximum visibility can be achieved with a small cavity length at 140  $\mu\text{m}$ , which guarantees the possibility of using very small samples, which is extremely important for example during biological measurement and with the use of biological samples.

## Methods

**Chemical vapor deposition.** Nanocrystalline diamond sheets were synthesized in a Microwave Plasma Enhanced Chemical Vapor Deposition (MW PECVD) reactor with a frequency of 2.45 GHz (SEKI Techntron AX5400S, Japan) on mirror-polished tantalum substrates (Sigma-Aldrich Chemie, thickness 0.025 mm, 99.9% metal base) and attached to the sensor head by employing the Van der Waals force. Prior to growth, the substrates were ultrasonically abraded for 30 min in a water suspension consisting of nanodiamond particles of 4–7 nm in diameter, followed by ultrasonic cleaning in acetone and 2-propanol. The temperature of the graphite stage, on which the substrates rested, was kept at 500 °C with a deposition time of 3 h. The microwave power, gas flow rate, and  $\text{CH}_4:\text{H}_2$  molar ratio were 1.1 kW, 300 sccm, and 1%, respectively. The chemical vapor deposition process pressure was maintained at 50 Torr. The detailed description of the deposition process may be found elsewhere<sup>26,27</sup>.



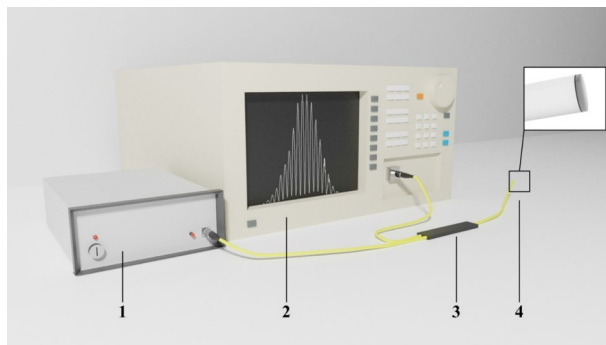


**Figure 6.** Schematic of the experimental setup, where: 1—light source, 2—Optical Spectrum Analyzer, 3—optical coupler, 4—measurement head.



**Figure 7.** The nanodiamonds structure deposition on the tantalum substrate.

**Fiber-optic interferometer.** To verify the sensing parameters of each layer, they were examined in an experimental setup, presented in Fig. 6.

The configuration of the setup was that of Fabry–Perot operated in a reflective mode. A light source with a wavelength of  $1310 \pm 10$  nm—superluminescent diode (SLD-1310-18-W, FiberLabs Inc., Japan) was chosen to perform experimental measurements. The light propagated through the optical coupler and the end-face of the measuring head, and it was reflected of the silver mirror, which was placed directly under the sensor head. The signal reflected from fiber end-face (in configuration ZnO coating and a diamond sheet) and the mirror superpose, resulting in an interference, which can be observed on an Optical Spectrum Analyzer (OSA, AndoAQ6319, Japan). Obtained interferograms can be then analyzed.

**The attachment of the nanocrystalline diamond sheet.** To assess the impact of the nanocrystalline diamond sheet on the obtained signal, NDS was attached over fiber end-face with deposited ZnO. Figure 7 shows the structure of the nanodiamond deposited on the tantalum substrate.

The procedure of the application of the NDS starts with its delamination from the tantalum substrate. The deposition process of the diamond structure was designed in such a way, that the resulting NDS shows low adhesion to the substrate, to ease the process of its release. A scalpel was used to induce stress in the structure in order to achieve a free-standing diamond sheet. Due to this, a part of the sheet detached from the tantalum in the form of an irregular flake which can be transferred onto the desired surface. The NDS was placed on a table of a micromechanical setup, where the fiber-optic measurement head was mounted. The diamond structure was then positioned centrally beneath the fiber. To attach the diamond structure to the measurement head, the van der Waals force was employed by slowly decreasing the distance between the structures, using micrometer screw. The bond was then strengthened by a slight press against the NDS.

Received: 7 August 2020; Accepted: 26 October 2020

Published online: 05 November 2020

## References

- Jiao, L. *et al.* Recent advances in fiber-optic evanescent wave sensors for monitoring organic and inorganic pollutants in water. *TrAC Trends Anal. Chem.* **127**, 115892 (2020).
- Calcerrada, M., García-Ruiz, C. & González-Herráez, M. Chemical and biochemical sensing applications of microstructured optical fiber-based systems. *Laser Photon. Rev.* **9**, 604–627 (2015).

3. Pospíšilová, M., Kuncová, G. & Trögl, J. Fiber-optic chemical sensors and fiber-optic bio. *Sensors* **15**, 25208–25259 (2015).
4. Wang, X. & Wolfbeis, O. S. Fiber-optic chemical sensors and biosensors (2015–2019). *Anal. Chem.* **92**, 397–430 (2020).
5. Wencel, D. *et al.* Optical sensor for real-time pH monitoring in human tissue. *Small* **14**, 1803627 (2018).
6. Wang, J. *et al.* Diaphragm-based optical fiber sensor for pulse wave monitoring and cardiovascular diseases diagnosis. *J. Biophoton.* **12**, e201900084 (2019).
7. Huang, Y. W., Tao, J. & Huang, X. G. Research progress on F-P interference—based fiber-optic sensors. *Sensors* **16**, 1424 (2016).
8. Castellon-Urbe, J. Optical fiber sensors: an overview. *Fiber Opt. Sens.* <https://doi.org/10.5772/28529> (2012).
9. Roriz, P., Frazão, O., Lobo-Ribeiro, A. B., Santos, J. L. & Simoes, J. A. Review of fiber-optic pressure sensors for biomedical and biomechanical applications. *JBO* **18**, 050903 (2013).
10. Hirsch, M. *et al.* ZnO coated fiber optic microsphere sensor for the enhanced refractive index sensing. *Sens. Actuators A* **298**, 111594 (2019).
11. Yin, M. *et al.* Recent development of fiber-optic chemical sensors and biosensors: mechanisms, materials, micro/nano-fabrications and applications. *Coord. Chem. Rev.* **376**, 348–392 (2018).
12. Yang, M. & Dai, J. Review on optical fiber sensors with sensitive thin films. *Photon. Sens.* **2**, 14–28 (2012).
13. Bond, W. L. Refractive index of ZnO (Zinc monoxide): Bond-o. <https://refractiveindex.info/?shelf=main&book=ZnO&page=Bond-o> (2020).
14. Coelho, L., Viegas, D., Santos, J. L. & de Almeida, J. M. M. Characterization of zinc oxide coated optical fiber long period gratings with improved refractive index sensing properties. *Sens. Actuators B* **223**, 45–51 (2016).
15. Coe, S. E. & Sussmann, R. S. Optical, thermal and mechanical properties of CVD diamond. *Diam. Relat. Mater.* **9**, 1726–1729 (2000).
16. Phillip, H. R. & Taft, E. A. Refractive index of C (Carbon, diamond, graphite, graphene). <https://doi.org/10.1103/PhysRev.136.A1445> (2020).
17. Kosowska, M. *et al.* Doped nanocrystalline diamond films as reflective layers for fiber-optic sensors of refractive index of liquids. *Materials* **12**, 1–12 (2019).
18. Yang, N. *et al.* Conductive diamond: synthesis, properties, and electrochemical applications. *Chem. Soc. Rev.* **48**, 157–204 (2019).
19. Rifai, A. *et al.* Polycrystalline diamond coating of additively manufactured titanium for biomedical applications. *ACS Appl. Mater. Interfaces* **10**, 8474–8484 (2018).
20. Koizumi, S., Nebel, C. & Nesladek, M. *Physics and Applications of CVD Diamond* (Wiley, Hoboken, 2008).
21. *CVD Diamond for Electronic Devices and Sensors*. (Wiley, Hoboken, 2009). <https://doi.org/10.1002/9780470740392.fmatter>.
22. Jędrzejewska-Szczerska, M. *et al.* Chapter 14 - Nanolayers in Fiber-Optic Biosensing. in *Nanotechnology and Biosensors* (eds. Nikolelis, D. P. & Nikoleli, G.-P.) 395–426 (Elsevier, Amsterdam, 2018). <https://doi.org/10.1016/B978-0-12-813855-7.00014-3>.
23. Baron, V. O. *et al.* Real-time monitoring of live mycobacteria with a microfluidic acoustic-Raman platform. *Commun. Biol.* **3**, 1–8 (2020).
24. Woolford, L., Chen, M., Dholakia, K. & Herrington, C. S. Towards automated cancer screening: label-free classification of fixed cell samples using wavelength modulated Raman spectroscopy. *J. Biophoton.* **11**, e201700244 (2018).
25. Ficek, M. *et al.* Optical and electrical properties of boron doped diamond thin conductive films deposited on fused silica glass substrates. *Appl. Surf. Sci.* **387**, 846–856 (2016).
26. Bogdanowicz, R. *et al.* Growth and isolation of large area boron-doped nanocrystalline diamond sheets: a route toward diamond-on-graphene heterojunction. *Adv. Func. Mater.* **29**, 1805242 (2019).
27. Kosowska, M. *et al.* Nanocrystalline diamond sheets as protective coatings for fiber-optic measurement head. *Carbon* **156**, 104–109 (2020).
28. Born, M. & Wolf, E. *Principles of Optics* (Pergamon, New York, 1980).
29. Majchrowicz, D. *et al.* Application of thin ZnO ALD layers in fiber-optic Fabry–Pérot sensing interferometers. *Sensors* **16**, 416 (2016).
30. Behroudj, A. & Strehle, S. *Transfer of Nanocrystalline Diamond Films Grown by Chemical Vapor Deposition for Sensors and Other Applications*. (VDE, 2016).
31. Lodes, M. A., Kachold, F. S. & Rosiwal, S. M. Mechanical properties of micro- and nanocrystalline diamond foils. *Philos. Trans. R. Soc. A* **373**, 20140136 (2015).
32. Engenhorst, M. *et al.* Thermoelectric transport properties of boron-doped nanocrystalline diamond foils. *Carbon* **81**, 650–662 (2015).
33. Seshan, V. *et al.* Pick-up and drop transfer of diamond nanosheets. *Nanotechnology* **26**, 125706 (2015).

## Acknowledgements

The authors want to acknowledge the financial support of the Polish National Science Centre under Grant No. 2017/25/N/ST7/01610, the Polish National Agency for Academic Exchange NAWA under Bilateral exchange of scientists between France and Poland PHC Polonium PPN/BFR/2019/1/00005/U/00001, Polish National Agency for Academic Exchange under Iwanowska Programme PPN/IWA/2018/1/00026/U/00001, Polish National Agency for Academic Exchange under Iwanowska Programme PPN/IWA/2018/1/00058/U/00001, and DS Programs of Faculty of Electronics, Telecommunications and Informatics of Gdańsk University of Technology. KD thanks the UK Engineering and Physical Sciences Research Council for funding (Grant EP/P030017/1).

## Author contributions

M.K., P.L. D.M. and M.S. conceived and designed the experiments. M.K., D.M., M.R., Y.F. and M.C. performed the experiments; M.K., P.L., D.M. and M.S. analyzed the data of optical spectrum analyzer; M.K. and Y.F. performed images with SEM; D.M. and M.C. performed and analyzed data from Raman System; M.R. contributed NDS; M.R. prepared the images from optical microscope; M.B. contributed the ZnO coating on the optical fibers. M.K., P.L., D.M., M.R., Y.F. and M.C. wrote the main manuscript text; M.K., P.L., M.R., Y.F., D.M., M.C. prepared figures. M.B., D.F. K.D and M.S. checked, reviewed; M.S. edited the paper.

## Competing interests

The authors declare no competing interests.

## Additional information

**Correspondence** and requests for materials should be addressed to M.K., D.M. or M.S.

**Reprints and permissions information** is available at [www.nature.com/reprints](http://www.nature.com/reprints).

**Publisher's note** Springer Nature remains neutral with regard to jurisdictional claims in published maps and institutional affiliations.



**Open Access** This article is licensed under a Creative Commons Attribution 4.0 International License, which permits use, sharing, adaptation, distribution and reproduction in any medium or format, as long as you give appropriate credit to the original author(s) and the source, provide a link to the Creative Commons licence, and indicate if changes were made. The images or other third party material in this article are included in the article's Creative Commons licence, unless indicated otherwise in a credit line to the material. If material is not included in the article's Creative Commons licence and your intended use is not permitted by statutory regulation or exceeds the permitted use, you will need to obtain permission directly from the copyright holder. To view a copy of this licence, visit <http://creativecommons.org/licenses/by/4.0/>.

© The Author(s) 2020

[PL6]

**Listewnik P.**; Szczerska M.; Jakóbczyk P. Measurements of the optical and thermal properties of the 2D black phosphorus coating. Mater. Res. Express 2021, 8, doi: 10.1088/2053-1591/ac07e2

*Analysis of the results of the optical and thermal properties of the few-layer black phosphorus coating measured with a microsphere-based fiber-optic sensor.*

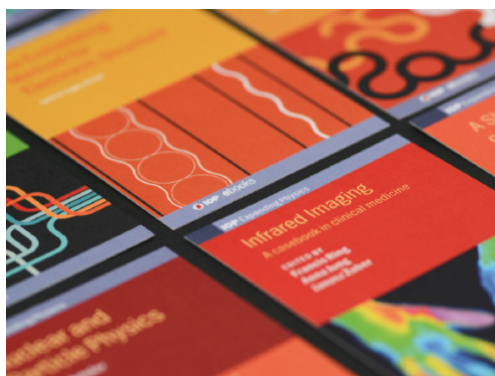


PAPER • OPEN ACCESS

## Measurements of the optical and thermal properties of the 2D black phosphorus coating

To cite this article: Paulina Listewnik *et al* 2021 *Mater. Res. Express* **8** 065004

View the [article online](#) for updates and enhancements.



**IOP | ebooks™**

Bringing together innovative digital publishing with leading authors from the global scientific community.

Start exploring the collection—download the first chapter of every title for free.

# Materials Research Express



## PAPER

# Measurements of the optical and thermal properties of the 2D black phosphorus coating

### OPEN ACCESS

#### RECEIVED

21 April 2021

#### REVISED

18 May 2021

#### ACCEPTED FOR PUBLICATION

3 June 2021

#### PUBLISHED

11 June 2021

Paulina Listewnik\* , Małgorzata Szczerska\* and Paweł Jakóbczyk

Department of Metrology and Optoelectronics, Faculty of Electronics, Telecommunications and Informatics, Gdańsk University of Technology, Narutowicza Street 11/12, 80-233 Gdańsk, Poland

\* Authors to whom any correspondence should be addressed.

E-mail: [pauliste@student.pg.edu.pl](mailto:pauliste@student.pg.edu.pl) and [malszcze@pg.edu.pl](mailto:malszcze@pg.edu.pl)

Original content from this work may be used under the terms of the [Creative Commons Attribution 4.0 licence](https://creativecommons.org/licenses/by/4.0/).

Any further distribution of this work must maintain attribution to the author(s) and the title of the work, journal citation and DOI.



## Abstract

Black phosphorus is a 2D material, which properties are still being discovered. In this paper, the sensitivity to the temperature of a few-layer black phosphorus coating deposited, on the surface of a microsphere-based fiber-optic sensor, by a dip-coating method is presented. The coating was investigated after 2, 3, and 5 deposition cycles and during temperature growth from 50 °C to 300 °C in an interferometric setup. The intensity of the reflected signal increases with each applied layer. During the investigation of the thermal properties, in the range of 50 °C–200 °C, the polynomial growth rate of the reflected signal can be observed, whereas, for the temperatures over 200 °C, the measured peak intensity of the reflected signal stabilizes at a nearly constant level.

## Introduction

From 2010, the year when Andre Geim and Kostya Novoselov were awarded the Nobel Prize in Physics ‘for groundbreaking experiments regarding the two-dimensional material graphene’, there has been intensive work on the development of new 2D materials [1]. From that time on, the group has enriched with many new representatives such as boron nitride (BN) [2], graphitic carbon nitride (g-C<sub>3</sub>N<sub>4</sub>), metal oxides (e.g. ZnO, TiO<sub>2</sub>) [3], metal-organic frameworks (MOFs), molybdenum disulfide (MoS<sub>2</sub>) [4], transition metal dichalcogenides (TMDCs) [5] and a single layer of black phosphorus (BP) [6]. On the other hand, the further development of fiber-optic technology - elements as well as entire measurement and imaging systems—is possible only with the use of the latest achievements of material engineering.

Various possibilities of using 2D materials in photonic structures as protective coatings [7], reflective layers, or sensing media were presented [8]. These materials are interesting because of their unique optical properties, as well as geometrical dimensions, which makes the 2D materials the optimal solution for integration with photonic microstructures, e.g., tapers, microrings, microcavities, microdiscs [9–12]. One of the basic problems related to the integration of 2D materials with photonic structures is its effectiveness. So far, thin metal oxides produced by the ALD technique have been used most often in optical fiber technology. Thin carbon-based films were also used by attaching them to optical fiber elements with the use of Van der Waals forces.

The isolation of a thin layer of black phosphorus (in 2013) similarly to graphite by exfoliation using scotch tape began an interest in a new 2D material research field [13]. Phosphorene distinguishes itself from the other two-dimensional materials by a unique puckered honeycomb network and as a result of strong in-plane anisotropy [14]. Thanks to this structure, phosphorene has anisotropic electronic and optical properties. One of the most interesting behaviors of layered black phosphorus is a strong dependence of its properties on layer numbers. For example, a single phosphorene has a bandgap of ca. 2 eV and 0.3 eV in bulk, which provides a wide range of tunability for the band gap [15]. Part of the growing interest in phosphorene can be attributed to the high carrier mobility up to 103 cm<sup>2</sup>V<sup>-1</sup>s<sup>-1</sup> [16] and moderate on/off ratios 104–105 as well as to the much larger direct bandgap demonstrated in few-layer BP [17]. These properties open a platform to manipulate anisotropic interactions and they enable using phosphorene in electronic and optoelectronic devices as well as sensors, catalysts, capacitors, and batteries [18–22].

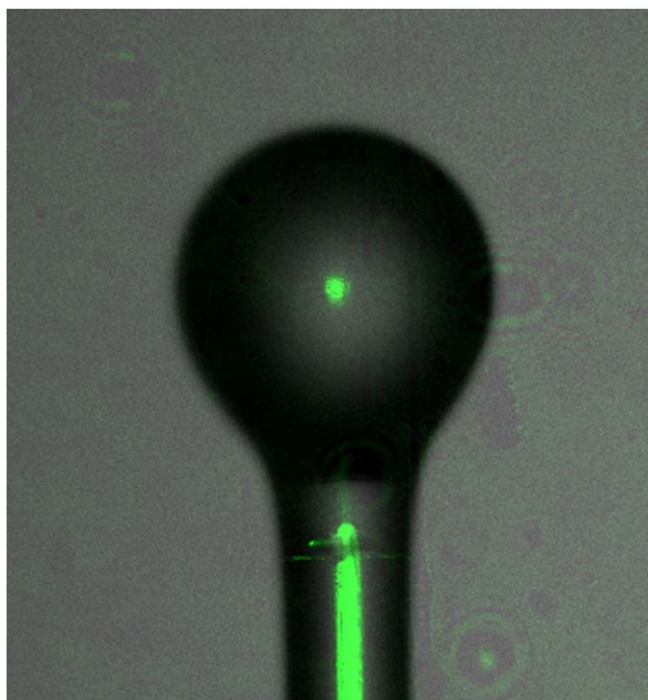


**Figure 1.** Picture of a microsphere-based fiber-optic sensor fabricated by optical fiber fusion splicer.

In this article, we present the fabrication process of the 2D coating of black phosphorous on the fiber-optic microsphere. The measurements in the low-coherent interferometry set-up allow us to determine how the optical properties of the 2D black phosphorous coating can change while depositing subsequent layers of the material on the surface of a sensor. Furthermore, the thermal properties of the material were investigated in the temperature range from 50 °C to 200 °C.

## Materials and methods

The black phosphorus crystals were purchased from Smart Elements. N, N-Dimethylformamide (DMF) was obtained from Sigma Aldrich. All reagents were analytical grade and were used without further purification. The highest purity class argon was collected from Air Liquid.

Few-layer black phosphorus (FLBP) was synthesized via liquid exfoliation from pre-crushed black phosphorus (BP) (30 mg) dispersed in anhydrous, oxygen-free dimethylformamide (7 ml). The process of liquid exfoliation was realized in an ice-cooled bath, in the temperature range of 0 °C–3 °C, under a stream of argon using a horn probe ultrasonicator (Bandelin Sonopuls HD2200, 20 kHz). The sonication tip was set to a power of 40 W with a 0.5/0.5 s ON/OFF time. The exfoliation process took 4 h. Subsequently, the resulting suspension was centrifugated at 11,000 rpm for 45 min to remove the residual unexfoliated particles, yielding blackish-yellow supernatant.

The fiber-optic sensor was manufactured from a standard single-mode telecommunications fiber. To form a microsphere, a fusion splicer (FSU 975, Ericsson Network Technologies AB, Stockholm, Sweden) was used. The splicer incites an electric arc, which causes the fiber to heat up. Simultaneous pulling, at the time, allows obtaining fiber-optic microsphere, due to surface tension occurring at the tip of a fiber. The diameter of the microsphere used for this investigation equals 250 μm. Figure 1. shows a picture of the designed structure obtained by a Stimulated Emission Depletion microscopy (Leica TCS SP8 STED, Germany).

The FLBP was deposited on the surface of a microsphere by the dip-coating technique, in several iterations. Before the beginning of the process, the microstructure was thoroughly cleared of any residual impurities, using isopropanol. Subsequently, the fiber-optic microsphere was immersed in the synthesized supernatant for 1 min, then the sample was left for 24 h to ensure the evaporation of the remaining liquid. The process was repeated five times in an inert environment to prevent oxidation and provide proper deposition of the coating. A schematic of the deposition process is presented in figure 2.

The FLBP coating was characterized by a Raman spectrometer. The Raman spectra were recorded on a micro-Raman spectrometer (InVia, Renishaw, United Kingdom) with a 532 excitation laser (Ar ion laser), and the Raman shift was in the range of 300–600 cm<sup>-1</sup> (figure 3).

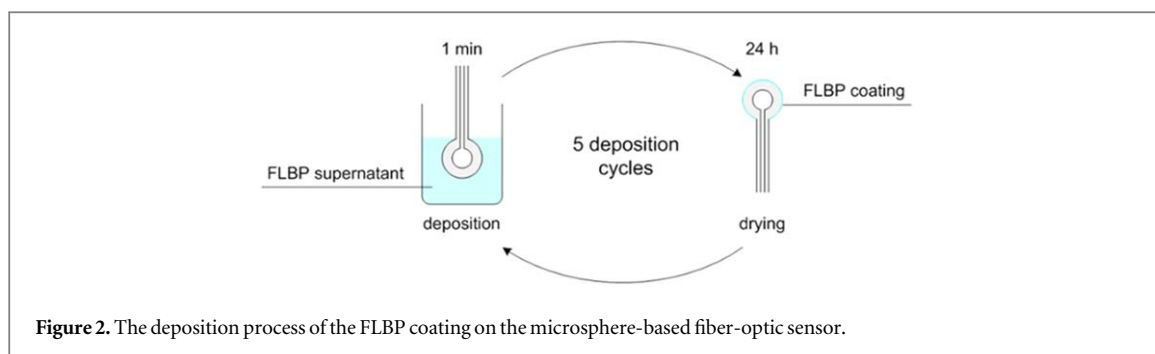


Figure 2. The deposition process of the FLBP coating on the microsphere-based fiber-optic sensor.

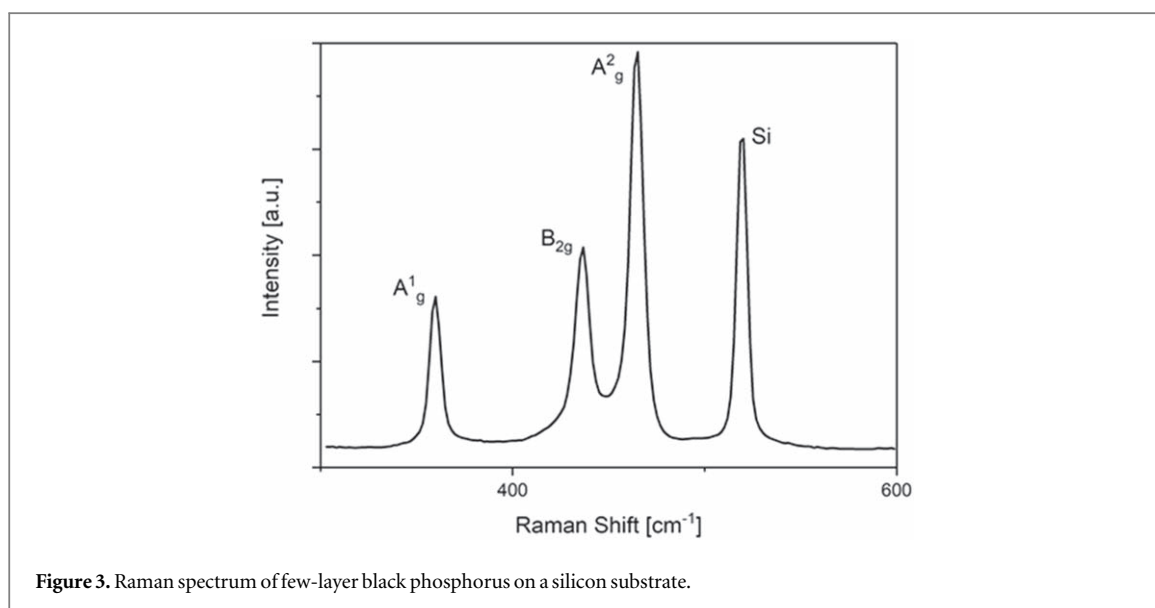


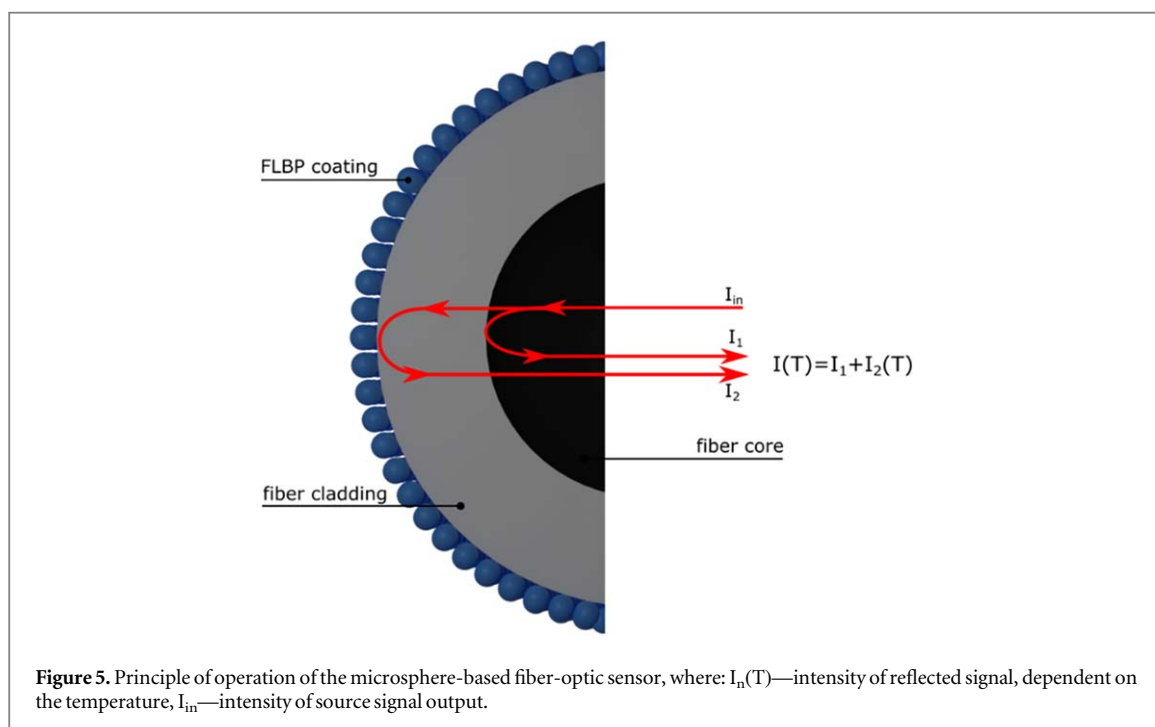
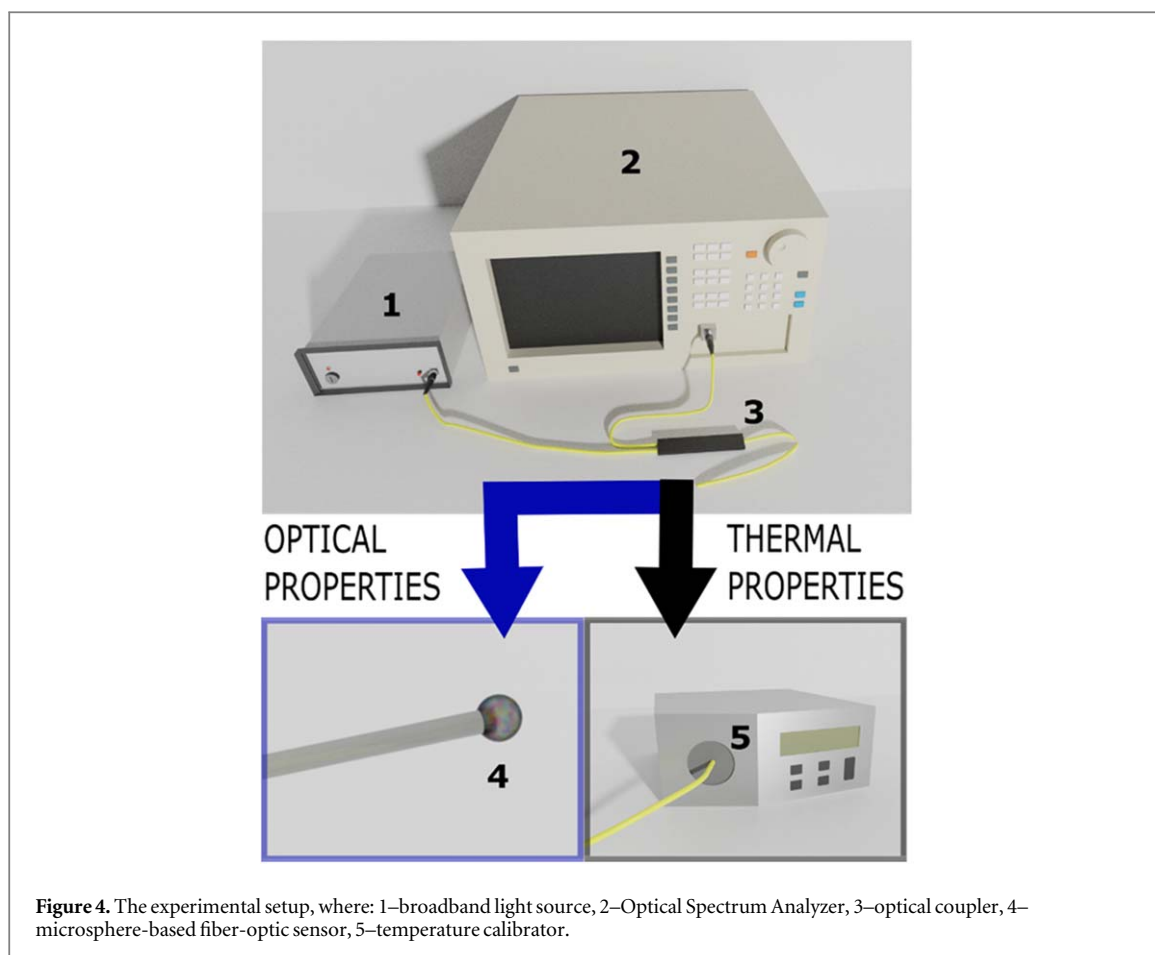
Figure 3. Raman spectrum of few-layer black phosphorus on a silicon substrate.

The phosphorus atoms in phosphorene are covalently linked by  $sp^3$  hybridization and form a quadrangular pyramid structure. Based on the principle of momentum conservation and group theory, Raman spectra should exhibit the six active vibration modes of the 12 lattice vibrational modes [23], but only the three vibration modes  $A_1^g$ ,  $A_2^g$  and  $B_{2g}$  are visible when the laser beam is perpendicular to the phosphorene surface [24]. In figure 3, there are three Raman peaks at  $359.3\text{ cm}^{-1}$ ,  $437.0\text{ cm}^{-1}$ , and  $464.7\text{ cm}^{-1}$  of a few layer black phosphorus corresponding to the  $A_1^g$ ,  $A_2^g$  and  $B_{2g}$  modes, respectively [25]. The peak for the  $518.5\text{ cm}^{-1}$  of Raman shift is derived from the silicon substrate. The peak of silicon is clearly visible due to the small and thin phosphorus flakes.

The FLBP coatings of different thicknesses were investigated after the 2nd, 3rd and 5th deposition cycle. The experimental interferometric setup consisted of a light source, fiber-optic devices, an optical analyzer and a sensor head. As the sources, a Compact Laser Diode Driver (CLD1015, Thorlabs Inc., Newton, NJ, USA) with mounted butterfly light source (SLD830S-A20, Thorlabs Inc., Newton, NJ, USA) with a central wavelength of  $830 \pm 10\text{ nm}$ , and a light source with a central wavelength of  $1310 \pm 20\text{ nm}$  (SLD-1310-18-W, FiberLabs Inc., Fujimi) were used. The visualization of the experimental setup used during the investigation of the optical and thermal properties of the FLBP coating is shown in figure 4.

The source signal output propagated through the  $2 \times 150/50\%$  optical coupler (780 HP, Cellco Communications, Kobylanka, Poland) to the sensor head. A part of the signal was reflected on the boundary created between the core and the cladding of an optical fiber, whereas the rest transmitted through and was reflected on the surface of the sensor, placed directly in the measured medium. Reflected waves superposed, which resulted in interference. An obtained signal was then acquired using Optical Spectrum Analyzer (OSA, Ando AQ6319, Yokohama, Japan) and the data was analyzed.

The principle of operation of a microsphere-based fiber optic sensor is presented in figure 5.



## Results and discussion

This section discusses the results obtained for the microsphere-based fiber-optic sensors coated with few-layer black phosphorus (FLBP). Figure 5 shows changes in the intensity of the reflected signal measured before the deposition process and after the deposition of 2, 3, and 5 cycles of FLBP coating. Figure 5(a) shows the spectra of

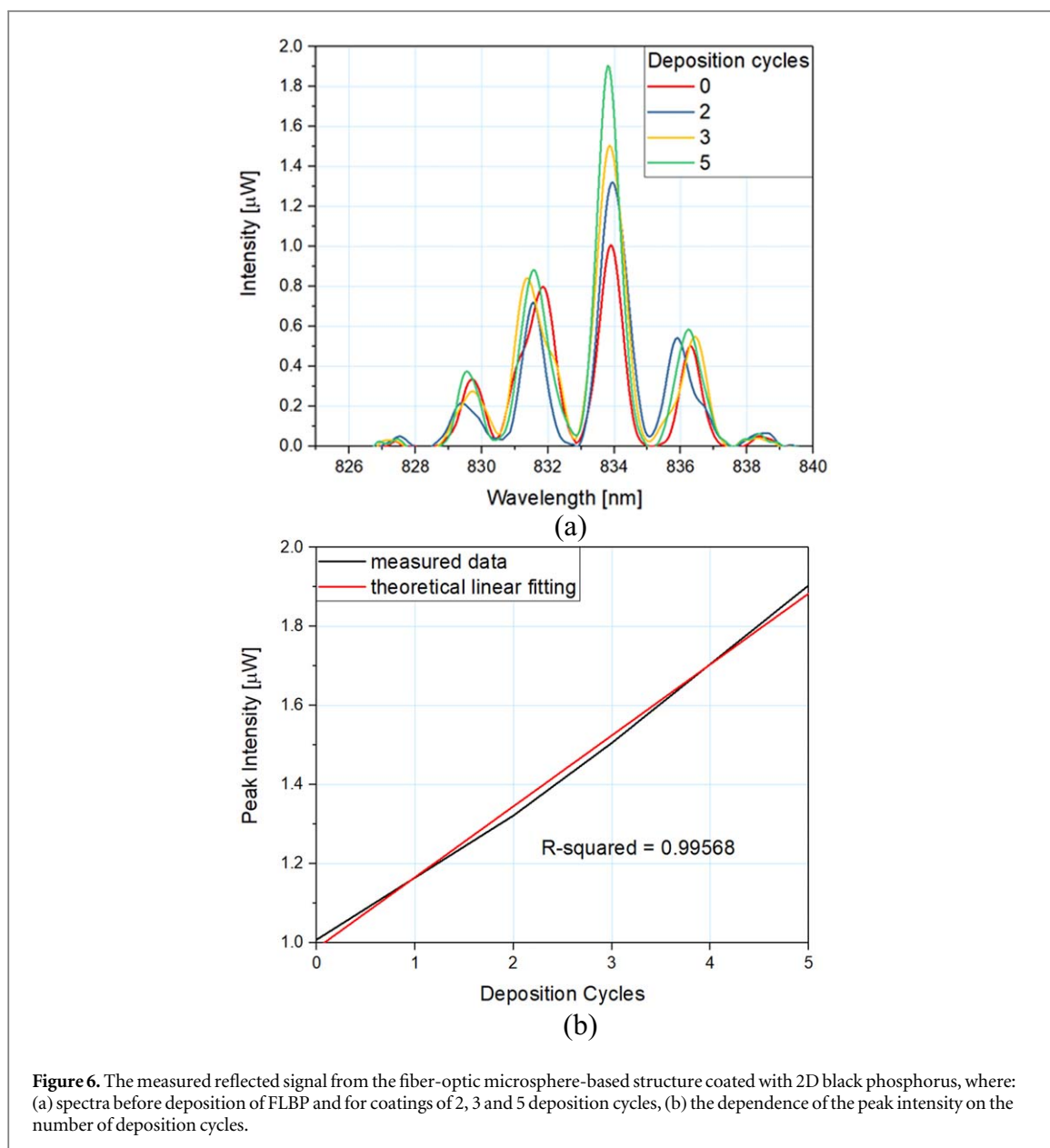


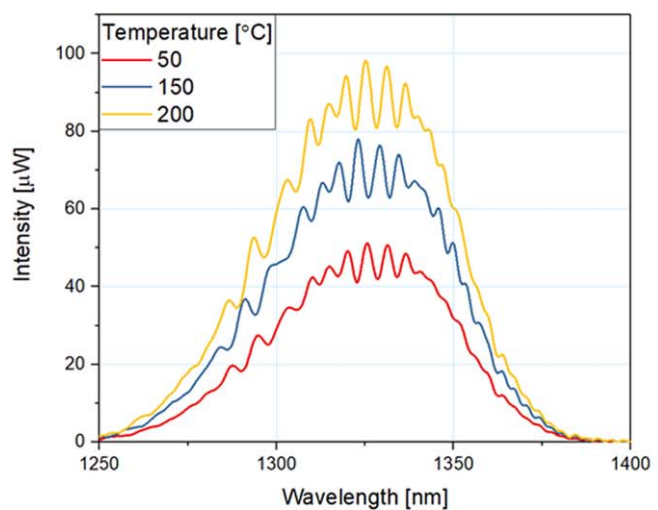
**Figure 6.** The measured reflected signal from the fiber-optic microsphere-based structure coated with 2D black phosphorus, where: (a) spectra before deposition of FLBP and for coatings of 2, 3 and 5 deposition cycles, (b) the dependence of the peak intensity on the number of deposition cycles.

the measured signal for the sensor without a coating and with coatings of 2, 3 and 5 deposition cycles, while in figure 5(b) magnification of the central fringe is presented in order to emphasize the increase of the reflected signal's intensity with a growth of an FLBP coating. The increase in the intensity of the reflected light after successive cycles was caused by a tighter layer forming on the sphere of the optical fiber. The produced FLBP layer acted as a mirror reflecting the light that falls on it. However, the envelope of the spectrum remains similar, after each deposition cycle.

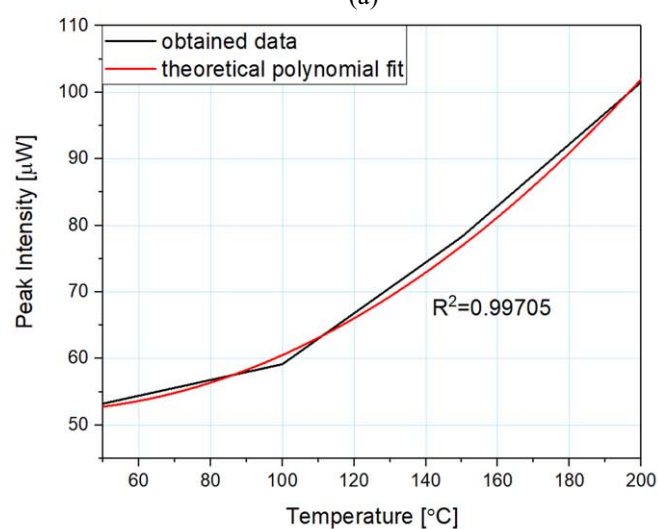
The peak intensity of the reflected signal depends on the number of cycles, in which the coating was deposited, increasing with the increase of the number of coating cycles, as is presented in figure 6(b). It can be observed, the intensity of a reflected signal increases, the thicker the deposited coating. The intensity steadily rises with the number of deposition cycles. Additionally, figure 6(b). Contains a theoretical linear fitting. It proves a close fit to the data obtained from performed measurements. The convergence of the plots is also confirmed by coefficient  $R^2$ , which equals over 0.995.

The temperature measurements were performed to evaluate the coating's sensitivity to alternating temperature. The coating was investigated in a range of  $50\text{ }^\circ\text{C}$ – $300\text{ }^\circ\text{C}$  with a step of  $50\text{ }^\circ\text{C}$ . The obtained results are shown in figure 7. Presented measurements contain data registered for the coating of 5 deposition cycles. Figure 7(a) consists of the spectra measured at  $50\text{ }^\circ\text{C}$ ,  $100\text{ }^\circ\text{C}$  and  $200\text{ }^\circ\text{C}$ , figure 7(b) presents the dependence of changing peak intensity of the reflected signal on the altering temperature in the range of  $50\text{ }^\circ\text{C}$ – $200\text{ }^\circ\text{C}$ , including theoretical polynomial fitting, whereas figure 7(c) shows the measurements in a range  $50\text{ }^\circ\text{C}$ – $350\text{ }^\circ\text{C}$ .

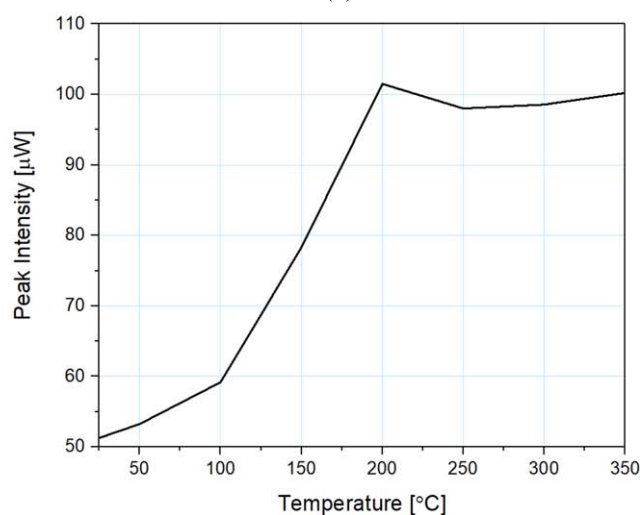




(a)



(b)



(c)

**Figure 7.** The measured reflected signal from the fiber-optic microsphere-based sensor during the temperature measurements, where: (a) representative spectra measured at 50, 100, 200 °C for the sensor with a coating of 5 deposition cycles; and reflected signal peak intensity dependence on changing temperature, measured for a coating of 5 deposition cycles, where: (b) range of 50 °C–200 °C with theoretical fitting, (c) range of 50 °C–350 °C.

As shown in figure 7(b), the intensity of the reflected signal increases nearly twice, as the temperature rises. Growth of the reflected signal intensity, depending on temperature setting is closer presented in figures 7(b), (c). The increase in temperature leads to softened atomic bonds and higher phonon velocity, resulting in a higher refractive index and thus in a higher intensity of the reflected signal (figure 7(b)). Such the temperature-dependence of intensity peak proves the FLBP coating is sensitive to the temperature in a range of 50 °C–200 °C. A further increase in temperature above 200 °C does not increase the intensity of the reflected signal peak, which may be related to the anharmonicity of phonons and further the phonon-phonon scattering. A similar dependence on temperature is in the case of thermal conductivity of phosphorene [26, 27]. It can be observed, from polynomial regression, that the obtained data accurately matches the calculated one. Coefficient  $R^2$  equals over 0.997, which proves, the acquired results only slightly vary from the theoretical model.

## Conclusion

The successful coating of a few-layer black phosphorous on the surface of the fiber-optic microsphere is reported. This structure was combined with a light source and an optical spectrum analyzer via fiber link to investigate the spectrum of the signal reflected of the black phosphorous layer.

The spectrum of reflected signal from 2, 3 and 5 deposition cycles coating was observed and it was concluded that the reflected signal increases with the increase of the number of layers.

Furthermore, the thermal properties of the few-layer black phosphorous coating in the range of 50 °C to 300 °C was investigated. The increase of the reflected signal from 50 to 200 °C was observed and stabilization of the intensity of the reflected signal at the constant level after 200 °C.

The study has revealed that this is possible to effectively coat the fiber optic structure with few-layers black phosphorus. It can suggest that this 2D material can be used in the fiber optic sensor technology as a reflection layer, which parameters can be tuned by the temperature.

## Acknowledgments

Financial support of these studies from Gdańsk University of Technology by the 11/2020/IDUB/I.3/CC grant under the Curium Combating Coronavirus - EIRU program is gratefully acknowledged. The authors acknowledge the financial support DS Programs of the Faculty of Electronics, Telecommunications, and Informatics of the Gdańsk University of Technology and the Polish National Science Centre [2016/22/E/ST7/00102].

## Data availability statement

The data that support the findings of this study are available upon reasonable request from the authors.

## ORCID iDs

Paulina Listewnik  <https://orcid.org/0000-0002-4857-1019>

Małgorzata Szczerska  <https://orcid.org/0000-0003-4628-6158>

Paweł Jakóbczyk  <https://orcid.org/0000-0002-6528-3713>

## References

- [1] Anon 2011 It's still all about graphene *Nature Mater* **10** 1–1
- [2] Gonzalez-Ortiz D, Salameh C, Bechelany M and Miele P 2020 Nanostructured boron nitride-based materials: synthesis and applications *Materials Today Advances* **8** 100107
- [3] Marichy C, Bechelany M and Pinna N 2012 Atomic layer deposition of nanostructured materials for energy and environmental applications *Adv. Mater.* **24** 1017–32
- [4] Li X and Zhu H 2015 Two-dimensional  $\text{MoS}_2$ : properties, preparation, and applications *Journal of Materiomics* **1** 33–44
- [5] Manzeli S, Ovchinnikov D, Pasquier D, Yazyev O V and Kis A 2017 2D transition metal dichalcogenides *Nat. Rev. Mater* **2** 17033
- [6] Zhang M, Wu Q, Chen H, Zheng Z and Zhang H 2020 Fiber-based all-optical modulation based on two-dimensional materials *2D Mater.* **8** 012003
- [7] Kosowska M, Listewnik P, Majchrowicz D, Rycewicz M, Bechelany M, Flegler Y, Chen M, Fixler D, Dholakia K and Szczerska M 2020 Microscale diamond protection for a ZnO coated fiber optic sensor *Sci. Rep.* **10** 19141
- [8] Hirsch M, Listewnik P, Struk P, Weber M, Bechelany M and Szczerska M 2019 ZnO coated fiber optic microsphere sensor for the enhanced refractive index sensing *Sens. Actuators, A* **298** 111594
- [9] Kou J, Feng J, Ye L, Xu F and Lu Y 2010 Miniaturized fiber taper reflective interferometer for high temperature measurement *Opt. Express* **18** 14245



- [10] Arumona A E, Garhwal A, Youplao P, Amiri I S, Ray K, Punthawanunt S and Yupapin P 2020 Electron cloud spectroscopy using Micro-Ring Fabry–Perot sensor embedded gold grating *IEEE Sensors J.* **20** 10564–71
- [11] Ma J, Ju J, Jin L, Jin W and Wang D 2011 Fiber-tip micro-cavity for temperature and transverse load sensing *Opt. Express* **19** 12418
- [12] Shankar R and Lončar M 2014 Silicon photonic devices for mid-infrared applications *Nanophotonics* **3** 329–41
- [13] Xu Y, Yan B, Zhang H-J, Wang J, Xu G, Tang P, Duan W and Zhang S-C 2013 Large-Gap Quantum Spin Hall Insulators in Tin Films *Phys. Rev. Lett.* **111** 136804
- [14] Eswaraiyah V, Zeng Q, Long Y and Liu Z 2016 Black phosphorus nanosheets: synthesis, characterization and applications *Small* **12** 3480–502
- [15] Tran V, Soklaski R, Liang Y and Yang L 2014 Layer-controlled band gap and anisotropic excitons in few-layer black phosphorus *Phys. Rev. B* **89** 235319
- [16] Xia F, Wang H and Jia Y 2014 Rediscovering black phosphorus as an anisotropic layered material for optoelectronics and electronics *Nat. Commun.* **5** 4458
- [17] Huang Y C, Chen X, Wang C, Peng L, Qian Q and Wang S F 2017 Layer-dependent electronic properties of phosphorene-like materials and phosphorene-based van der Waals heterostructures *Nanoscale* **9** 8616–22
- [18] Irshad R, Tahir K, Li B, Sher Z, Ali J and Nazir S 2018 A revival of 2D materials, phosphorene: Its application as sensors *J. Ind. Eng. Chem.* **64** 60–9
- [19] Jakóbczyk P, Kowalski M, Brodowski M, Dettlaff A, Dec B, Nidzworski D, Ryl J, Ossowski T and Bogdanowicz R 2021 Low-power microwave-induced fabrication of functionalised few-layer black phosphorus electrodes: a novel route towards Haemophilus Influenzae pathogen biosensing devices *Appl. Surf. Sci.* **539** 148286
- [20] Sajedi-Moghaddam A, Mayorga-Martinez C C, Sofer Z, Bouša D, Saievar-Iranizad E and Pumera M 2017 Black phosphorus Nanoflakes/Polyaniline hybrid material for high-performance pseudocapacitors *J. Phys. Chem. C* **121** 20532–8
- [21] Park C-M and Sohn H-J 2007 Black phosphorus and its composite for lithium rechargeable batteries *Adv. Mater.* **19** 2465–8
- [22] Ding K, Wen L, Huang S, Li Y, Zhang Y and Lu Y 2016 Electronic properties of red and black phosphorous and their potential application as photocatalysts *RSC Adv.* **6** 80872–84
- [23] Guo Z et al 2015 From black phosphorus to phosphorene: basic solvent exfoliation, evolution of Raman scattering, and applications to ultrafast photonics *Adv. Funct. Mater.* **25** 6996–7002
- [24] Ribeiro H B, Pimenta M A and de Matos C J S 2018 Raman spectroscopy in black phosphorus *J. Raman Spectrosc.* **49** 76–90
- [25] Dettlaff A, Skowierzak G, Macewicz Ł, Sobaszek M, Karczewski J, Sawczak M, Ryl J, Ossowski T and Bogdanowicz R 2019 Electrochemical stability of few-layered phosphorene flakes on boron-doped diamond: a wide potential range of studies in aqueous solutions *J. Phys. Chem. C* **123** 20233–40
- [26] Qin G and Hu M 2018 Thermal transport in phosphorene *Small* **14** 1702465
- [27] Ong Z-Y, Cai Y, Zhang G and Zhang Y-W 2014 Strong thermal transport anisotropy and strain modulation in single-layer phosphorene *J. Phys. Chem. C* **118** 25272–7



## Contribution Statements



Tel-Aviv, 10/5/2021

.....  
Place and date

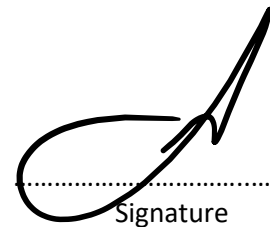
Prof. Dror Fixler  
Faculty of Engineering,  
Head of the Institute for Nanotechnology  
And Advanced Materials  
Bar-Ilan University  
Israel

## **Statement on my contribution to joint publication with Paulina Listewnik**

Referencing to the below publication:

1. Kosowska, M.; Listewnik, P.; Majchrowicz, D.; Rycewicz, M.; Bechelany, M.; Fleger, Y.; Chen, M.; Fixler, D.; Dholakia, K.; Szczerska, M. Microscale diamond protection for a ZnO coated fiber optic sensor. Sci. Rep. 2020, 10, doi:10.1038/s41598-020-76253-5.

I declare, that my contribution to the publication is:  
- checking and reviewing the manuscript.

  
.....  
Signature

Gdańsk, 19.05.2021

Place and date

Daria Majchrowicz, PhD EE  
Department of Metrology and Optoelectronics  
Faculty of Electronics, Telecommunications and Informatics  
Gdansk University of Technology  
Poland

## Statement on my contribution to joint publication with Paulina Listewnik

Referencing to the below publication:

1. Kosowska, M.; Listewnik, P.; Majchrowicz, D.; Rycewicz, M.; Bechelany, M.; Fleger, Y.; Chen, M.; Fixler, D.; Dholakia, K.; Szczerska, M. Microscale diamond protection for a ZnO coated fiber optic sensor. Sci. Rep. 2020, 10, doi:10.1038/s41598-020-76253-5.

I declare, that my contribution to the publication is:

- performing the experiments,
- performing and analyzing data from Raman Spectroscopy,
- preparing selected figures (fig. 3).

  
Signature



Louisville / May 11, 2021  
.....  
Place and date

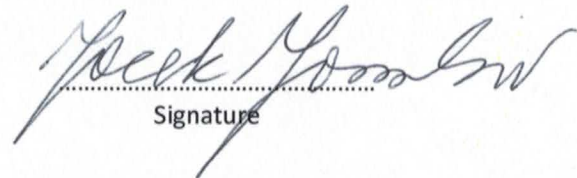
Jacek B. Jasinski, PhD  
Conn Center for Renewable Energy Research  
University of Louisville  
Louisville, KY 20292, USA

### Statement on my contribution to joint publication with Paulina Listewnik

Referencing to the below publication:

1. Listewnik, P.; Bechelany, M.; Jasinski, J.B.; Szczerska, M. ZnO ald-coated microsphere-based sensors for temperature measurements. *Sensors (Switzerland)* 2020, 20, 1–8, doi:10.3390/s20174689.

I declare, that my contribution to the publication is:  
- checking and reviewing the manuscript.

  
.....  
Signature



Montpellier May 20<sup>th</sup> 2021

**Statement on my contribution to joint publications  
with Paulina Listewnik**

Referencing to the below publications:

1. Listewnik, P.; Bechelany, M.; Jasinski, J.B.; Szczerska, M. ZnO ald-coated microsphere-based sensors for temperature measurements. *Sensors (Switzerland)* 2020, 20, 1–8, doi:10.3390/s20174689.
2. Kosowska, M.; Listewnik, P.; Majchrowicz, D.; Ryciewicz, M.; Bechelany, M.; Fleger, Y.; Chen, M.; Fixler, D.; Dholakia, K.; Szczerska, M. Microscale diamond protection for a ZnO coated fiber optic sensor. *Sci. Rep.* 2020, 10, doi:10.1038/s41598-020-76253-5.
3. Hirsch, M.; Listewnik, P.; Struk, P.; Weber, M.; Bechelany, M.; Szczerska, M. ZnO coated fiber optic microsphere sensor for the enhanced refractive index sensing. *Sensors Actuators, A Phys.* 2019, 298, doi:10.1016/j.sna.2019.111594.
4. Listewnik, P.; Hirsch, M.; Struk, P.; Weber, M.; Bechelany, M.; Jędrzejewska-Szczerska, M. Preparation and characterization of microsphere ZnO ALD coating dedicated for the fiber-optic refractive index sensor. *Nanomaterials* 2019, 9, doi:10.3390/nano9020306.

I declare, that my contribution to the publications is:

- depositing the ZnO thin coating,
- performing ZnO thin coating characterization,
- writing selected parts of the manuscripts.

Mikhael Bechelany  
Senior Scientist



24.05.2021 GDAŃSK

Place and date

Marzena Hirsch, PhD EE  
Department of Metrology and Optoelectronics  
Faculty of Electronics, Telecommunications and Informatics  
Gdansk University of Technology  
Poland

## Statement on my contribution to joint publications with Paulina Listewnik

Referencing to the below publication:

1. Hirsch, M.; Listewnik, P.; Struk, P.; Weber, M.; Bechelany, M.; Szczerska, M. ZnO coated fiber optic microsphere sensor for the enhanced refractive index sensing. *Sensors Actuators, A Phys.* 2019, 298, doi:10.1016/j.sna.2019.111594.
2. Listewnik, P.; Hirsch, M.; Struk, P.; Weber, M.; Bechelany, M.; Jędrzejewska-Szczerska, M. Preparation and characterization of microsphere ZnO ALD coating dedicated for the fiber-optic refractive index sensor. *Nanomaterials* 2019, 9, doi:10.3390/nano9020306.

I declare, that my contribution to the publication is:

- performing theoretical modelling,
- preparing selected figures,
- writing selected parts of the manuscript.

Marzena Hirsch

Signature

Gdańsk, 18.05.21

Place and date

Monika Kosowska, MSc EE  
Department of Metrology and Optoelectronics  
Faculty of Electronics, Telecommunications and Informatics  
Gdansk University of Technology  
Poland

## Statement on my contribution to joint publication with Paulina Listewnik

Referencing to the below publication:

1. Kosowska, M.; Listewnik, P.; Majchrowicz, D.; Rycewicz, M.; Bechelany, M.; Fleger, Y.; Chen, M.; Fixler, D.; Dholakia, K.; Szczerska, M. Microscale diamond protection for a ZnO coated fiber optic sensor. Sci. Rep. 2020, 10, doi:10.1038/s41598-020-76253-5.

I declare, that my contribution to the publication is:

- performing the experiments,
- analyzing the data of the optical spectrum analyzer,
- performing imaging with SEM,
- preparing selected figures (Fig. 1a,b; 4; 5)
- writing selected parts of the manuscript.

  
Signature

Delft, 12.05.2021

Place and date

Michał Rycewicz, MSc EE  
Department of Metrology and Optoelectronics  
Faculty of Electronics, Telecommunications and Informatics  
Gdansk University of Technology  
Poland

## Statement on my contribution to joint publication with Paulina Listewnik

Referencing to the below publication:

1. Kosowska, M.; Listewnik, P.; Majchrowicz, D.; Rycewicz, M.; Bechelany, M.; Fleger, Y.; Chen, M.; Fixler, D.; Dholakia, K.; Szczerska, M. Microscale diamond protection for a ZnO coated fiber optic sensor. Sci. Rep. 2020, 10, doi:10.1038/s41598-020-76253-5.

I declare, that my contribution to the publication is:

- synthesis of the nanocrystalline diamond sheet with specific optical, morphological, and electrical parameters,
- analysis of the sample with an optical microscope,
- preparing selected figures (Fig. 2, 7),
- writing selected parts of the manuscript.

.....  
Rycewicz  
Signature



Małgorzata Szczerska, PhD, DSc EE  
Gdańsk University of Technology  
Poland

Gdańsk 25/05/2021

Place and date

## Statement on my contribution to joint publications with Paulina Listewnik

Referencing to the below listed publications:

1. Listewnik, P.; Hirsch, M.; Struk, P.; Weber, M.; Bechelany, M.; Jędrzejewska-Szczerska, M. Preparation and characterization of microsphere ZnO ALD coating dedicated for the fiber-optic refractive index sensor. *Nanomaterials* 2019, 9, doi:10.3390/nano9020306.
2. Hirsch, M.; Listewnik, P.; Struk, P.; Weber, M.; Bechelany, M.; Szczerska, M. ZnO coated fiber optic microsphere sensor for the enhanced refractive index sensing. *Sensors Actuators, A Phys.* 2019, 298, doi:10.1016/j.sna.2019.111594.
3. Listewnik, P.; Bechelany, M.; Jasinski, J.B.; Szczerska, M. ZnO ALD-coated microsphere-based sensors for temperature measurements. *Sensors (Switzerland)* 2020, 20, 1–8, doi:10.3390/s20174689.
4. Kosowska, M.; Listewnik, P.; Majchrowicz, D.; Rycewicz, M.; Bechelany, M.; Flegler, Y.; Chen, M.; Fixler, D.; Dholakia, K.; Szczerska, M. Microscale diamond protection for a ZnO coated fiber optic sensor. *Sci. Rep.* 2020, 10, doi:10.1038/s41598-020-76253-5.
5. Listewnik, P.; Szczerska, M.; Jakóbczyk P. Measurements of the optical and thermal properties of the 2D black phosphorus coating. *Mater. Res. Express.* 2021, 8, doi: 10.1088/2053-1591/ac07e2.

I declare, that my contribution to these publications are:

- conceiving and designing experiments,
- analysing and interpreting the data from optical spectrum analyzer,
- reviewing of literature,
- writing selected parts of the manuscripts,
- editorial check-up and article improvements.

M. Szczerska

Signature

25.05.2021, Gdansk

Place and date

Paweł Jakóbczyk, PhD  
Department of Metrology and Optoelectronics  
Faculty of Electronics, Telecommunications and Informatics  
Gdansk University of Technology  
Poland

## Statement on my contribution to joint publications with Paulina Listewnik

Referencing to the below publication:

1. Listewnik, P.; Szczerska, M.; Jakóbczyk P. Measurements of the optical and thermal properties of the 2D black phosphorus coating. Mater. Res. Express. 2021, 8, doi: 10.1088/2053-1591/ac07e2.

I declare, that my contribution to the publication is:

- phosphorene fabrication
- depositing the coating,
- writing and reviewing the paper.

  
Signature

Gliwice, 22.03.2021

Przemysław Struk, PhD EE  
Silesian University of Technology  
Poland

## Statement on my contribution to joint publications with Paulina Listewnik

Referencing to the below listed publications:

1. P. Listewnik, M. Hirsch, P. Struk, M. Weber, M. Bechelany, and M. Jędrzejewska-Szczerska, "Preparation and Characterization of Microsphere ZnO ALD Coating Dedicated for the Fiber-Optic Refractive Index Sensor," *Nanomaterials*, 2019, 9(2), 306.
2. M. Hirsch, P. Listewnik, P. Struk, M. Weber, M. Bechelany, M. Jędrzejewska-Szczerska, "ZnO coated fiber optic microsphere sensor for the enhanced refractive index sensing", *Sensors and Actuators A: Physical*, 2019, 298, 111594.

I declare, that my contribution to these publications are:

Manuscript 1.

Carrying out research and analysis of the results obtained by: scanning electron microscopy and Raman spectroscopy for ZnO layers, literature review, creating selected drawings, writing part of the manuscript, editing and improving of the manuscript.

Manuscript 2.

Performing sample characterization by scanning electron microscopy, providing description of characterization results.



.....  
Signature



30/5/2021

Yafit Fleger, PhD  
Institute for Nanotechnology and Advanced Materials  
Bar-Ilan University  
Israel

## Statement on my contribution to joint publication with Paulina Listewnik

Referencing to the below publication:

1. Kosowska, M.; Listewnik, P.; Majchrowicz, D.; Rycewicz, M.; Bechelany, M.; Fleger, Y.; Chen, M.; Fixler, D.; Dholakia, K.; Szczerska, M. Microscale diamond protection for a ZnO coated fiber optic sensor. *Sci. Rep.* 2020, 10, doi:10.1038/s41598-020-76253-5.

I declare, that my contribution to the publication is:

- performing HR-SEM images,
- Cutting the sample using FIB (Figure 1c)



.....  
Signature